Copyright Warning & Restrictions

The copyright law of the United States (Title 17, United States Code) governs the making of photocopies or other reproductions of copyrighted material.

Under certain conditions specified in the law, libraries and archives are authorized to furnish a photocopy or other reproduction. One of these specified conditions is that the photocopy or reproduction is not to be "used for any purpose other than private study, scholarship, or research." If a, user makes a request for, or later uses, a photocopy or reproduction for purposes in excess of "fair use" that user may be liable for copyright infringement,

This institution reserves the right to refuse to accept a copying order if, in its judgment, fulfillment of the order would involve violation of copyright law.

Please Note: The author retains the copyright while the New Jersey Institute of Technology reserves the right to distribute this thesis or dissertation

Printing note: If you do not wish to print this page, then select "Pages from: first page # to: last page #" on the print dialog screen

BRAGG REFLECTION GRATING WAVEGUIDE

by

Wei Zhong

A Thesis
Submitted to the Faculty of New Jersey
Institute of Technology
in Partial Fulfillment of the Requirements for
the Degree of Master of Science
Department of Electrical and Computer Engineering
October, 1992

APPROVAL PAGE

Bragg Reflection Grating Waveguide

by

Wei Zhong

Aug 7, 1992

Dr. Haim Grebel, Thesis Adviser
Associate Professor of Electrical Engineering, NJIT

Aug 6, 1992

Dr. M. Sosnowski, Thesis Adviser
Associate Professor of Electrical Engineering, NJIT

8/5/92

Dr. K. Sohn, Committee Member
Professor of Electrical Engineering and
Assistant Chairperson of the Department, NJIT

BIOGRAPHICAL SKETCH

Author: Wei Zhong

Degree: Master of Science in Electrical Engineering

Date: October, 1992

Date of Birth:

Place of Birth:

Undergraduate and Graduate Education:

- Master of Science in Electrical Engineering, New Jersey Institute of Technology, Newark, NJ, 1992
- Bachelor of Science in Electronic Engineering, Fudan University, Shanghai, P. R. China, 1985

Major: Electric Engineering

ABSTRACT

Bragg Reflection Grating Waveguide

by

Wei Zhong

Bragg reflection waveguides (BRW) are non-conventional optical guides in which optical confinement is achieved via periodic set of grooves or stratified media along the guiding path. BRW may also serve as optical filters, because of spectral discrimination of the guiding process. A novel UV laser ablation technique was used in this thesis to fabricate periodic metal-clad polymeric waveguides. Spin-on technique was applied to fabricate the waveguide core on glass substrates, evaporation of metal film and selective ablation process defined the optical guides. Various periodicities have been fabricated and the near field patterns have been measured to compare the different guiding confinement properties. Two techniques for deposition of the polymeric layer have been assessed: spin-on and plasma polymerization. The latter, though being very promising, did not produce a satisfactory yield. Finally, a bend in the waveguide has been fabricated and measured. Good optical confinement has been achieved in the waveguide with the near field patterns becoming narrower when the number of confining structures was increased from two to ten.

This thesis is dedicated to

my lovely family.

ACKNOWLEDGMENT

The author wishes to express his sincere gratitude to his supervisors, Professor H. Grebel and Professor M. Sosnowski, for their guidance, friendship, and moral support throughout this research.

Special thanks to Professor k. Sohn for serving as a member of committee.

The author appreciates the timely help from the MBE laboratory members, including: Professor G. H. Feng, Mr. G. M. Qin.

And finally, a thank you to Mike Berry and Mike Grieco for their help.

TABLE OF CONTENTS

Page

LIST OF TABLE

Table **Page**

LIST OF FIGURES

Figure **Page**

CHAPTER 1

INTRODUCTION

The transmission and processing of signals carried by optical beams rather than by electrical current or radio wave has been a topic of great interest ever since early 1960's, when the development of the laser first provided a stable source of coherent light for such application. In the late 1960's, the concept of "integrated optics" emerged, in which wired and radio links are replaced by light-waveguiding optical fibers rather than by through-the-air optical paths, and conventional electrical integrated circuits are replaced by miniaturized optical integrated circuits (OIC's). The optical waveguide is the fundamental element that literally ties the OIC together. Without effective, low-loss optical waveguides one cannot even contemplate an OIC.

The general requirement for a guide for electromagnetic radiation is that there be a flow of energy only along the guiding structure and not perpendicular to it. This means that field will be appreciable only in the immediate neighborhood of the guiding structure. For conventional optical waves this means that the core of the guide must have a higher refractive index than its surroundings as a beam propagating in a transversely inhomogeneous medium tends to bend toward the high-refractive-index region.

Bragg reflection waveguides (BRW'S), were proposed, analyzed, and demonstrated more than ten years ago [1.1]-[1.3]. The BRW is a waveguide which uses the Bragg reflection mechanism (rather than total internal reflection as in conventional guides) in order to achieve waveguiding. Bragg reflection is created by the use of the periodic multilayered media as the bounding section of the waveguide (Fig. 1.1). As is well known in thin-film optics, periodic stratified media act as highly efficient bandpass reflectors, in certain wavelength regions (at normal incidence), which are called high reflectance zones, or alternatively, stopbands. When the incidence is oblique, there are also stopbands in the incidence angle. These stopbands correspond to "allowed" and "forbidden" bands for propagation constant ß (which is a function of the incidence angle), and the wavelength, arising from the translational symmetry of the structure. Unlike in ordinary dielectric waveguides, confined guiding with arbitrarily low loss is possible in BRW's even when the guiding layer index of refraction is lower than that of the periodic layers. On the basis of these properties, some of the potential applications of BRW's were already identified in their early studies [1.2]-[1.3]. However, apart from some laboratory demonstrations [1.4], these structures were not further studied in relation to practical integrated optical devices. One reason for that may have been that multilayered structures with tight control of the refraction indexes and

thickness were difficult to fabricate, and integrated optic technology was devoted to the design and control of simpler structures.

In the last few years, the desire to integrate active device (e.g., lasers, detectors) with passive ones (e.g., waveguides, modulators) motivated intensive research in semiconductor integrated optics. Periodic layered heterostructures acting as Bragg reflectors, with very tight control of the layer indexes and thicknesses were grown. As a result of these advances, BRW's can now not only be fabricated but also incorporated in an optical integrated circuits as a narrow-band transmission filter and modulator.

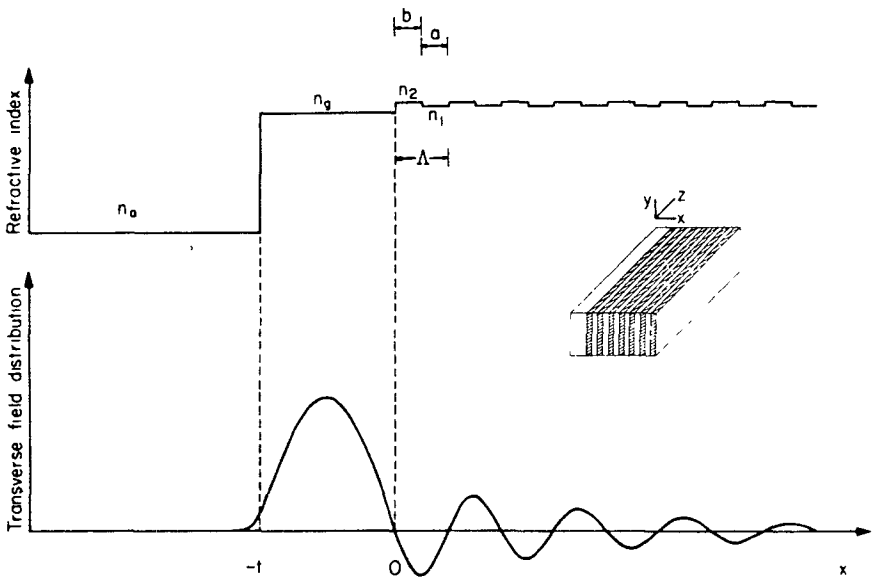

Figure 1.1 Transverse field distribution of the fundamental modes of a typical Bragg reflection (slab) waveguide. [1.7]

The grating guide has been proposed [1.5] as a useful alternative to the usual form of slab waveguide currently used in integrated optics. In its simplest form the grating guide consists of a stack of layers of two different material with refractive indexes n_1, n_2 and widths d_1, d_2. A useful form of the grating guide is obtained if we use a transverse grating in conjunction with a guiding film (Fig. 1.2). The grating action then serves to confine the wave laterally, and the film provides confinement in the vertical direction. Several possibilities are available for constructing such a guide, e.g., ion implantations, optical damage effects, eletrooptic effect, and perturbation by a metallic cladding. All the effects are small and at best offer a change in index 10^{-2}. The last two effects are attractive and are compatible with photolithographic techniques. For instance, the transverse eletrooptic effect could be used with a high-reflectivity metal like silver. Preliminary calculations indicate that a fractional change in phase velocity of the TM1 mode of $5*10^{-3}$ could be produced by a silver cladding [1.6].

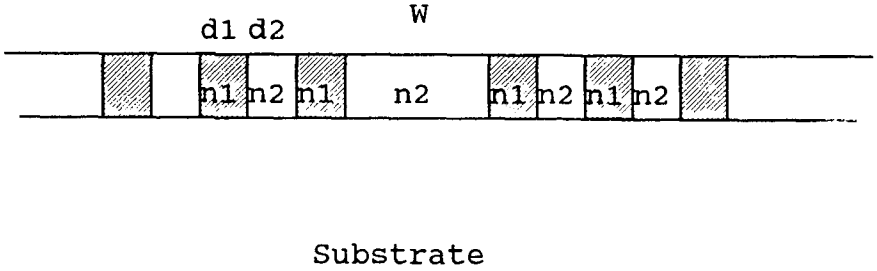

Figure 1.2 Thin-film grating guide.

In our experiments we tried new fabrication technique for making grating waveguide based on the effect of periodic metal loading perturbations. Our waveguides were made of polymer on glass substrates. The metal films of thickness ranging between 20 A to 500 A were deposited using evaporation technique. The metal film is between the glass substrate and the polymeric film, and patterned by using UV laser ablation process. In this way we have achieved effective spatial periodicity for the refractive index in the transverse direction.

The thesis is organized as following: the theory of slab and grating waveguides is given in chapter 2. Most of the theory for slab, channel and strip loaded waveguides is taken from the book of Hunsperger, "Integrated Optics: Theory and Technology", 2nd ed., Springer-Verlag, 1985. The general techniques to make polymeric, Bragg optical waveguide are given in chapter 3. We devoted this chapter to only successful polymeric deposition technique (spin-on technique). A detailed description of the other deposition technique, the plasma polymerization technique, is given in Appendix B. The description of the measurement systems and experiments is given in chapter 4 while results and discussion are given in chapter 5. In chapter 6 we concluded our work and suggested further work to be done in this field.

CHAPTER 2

THEORY OF OPTICAL WAVEGUIDE

The optical waveguide is the fundamental element that interconnects the various devices of an optical integrated circuit, just as a metallic strip does in an electrical integrated circuit. However, unlike electrical current that flows through a metal strip according to Ohm's law, optical waves travel in the waveguide in distinct optical modes. A mode, in this sense, is a spatial distribution of optical energy in one or more dimensions.

2.1 The Slab Dielectric Waveguides

To begin the discussion of optical mode, consider the basic three-layer waveguide structure shown in Fig. 2.1. The light confining layers, with indices of refraction n_1 and n_3 are assumed to extend to infinity in the +x and -x directions.

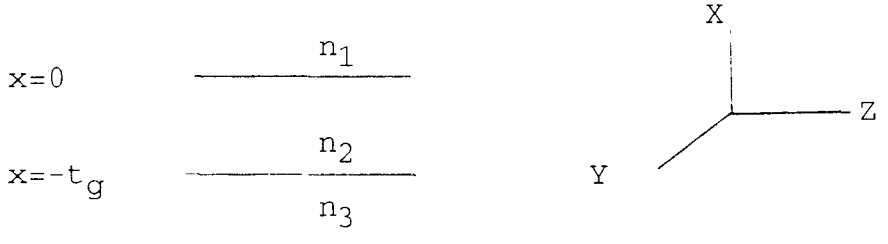

Figure 2.1 Basic three-layer planar waveguide structure.

2.1.1 TE and TM Modes in an Asymmetric Waveguides

A. TE Modes

For the case of TE plane wave traveling in the z direction, with propagation constant ß, Maxwell's wave equation reduces to

$$\nabla^2 E_y = \frac{n_i^2}{c^2}\frac{\partial^2 E_y}{\partial t^2} \quad i = 1,2,3,\ldots \tag{2.1}$$

with solution of the form

$$E_y(x,z,t) = \mathcal{E}_y(x)e^{i(\omega t - \beta z)} \tag{2.2}$$

The transverse function $\mathcal{E}_y(x)$ has the general form

$$\mathcal{E}_y(x) = \begin{cases} A\exp(-qx) & 0 \le x \le \infty \\ B\cos(hx) + C\sin(hx) & -t_g \le x \le 0 \\ D\exp[p(x+t_g)] & -\infty \le x \le -t_g \end{cases} \tag{2.3}$$

where A, B, C, D, q, h, and p are all constants that can be determined by matching the boundary conditions, which requires the continuity of $\mathcal{E}_y$ and $\mathcal{H}_z = (i/\omega\mu)\partial E_y/\partial x$. So that the solution for $\mathcal{E}_y$ can be expressed:

$$\mathcal{E}_y(x) = \begin{cases} C'\exp(-qx) & 0 \le x \le \infty \\ C'[\cos(hx) - (q/h)\sin(hx)] & -t_g \le x \le 0 \\ C'[\cos(ht_g) + (q/h)\sin(ht_g)]\exp[p(x+t_g)] & -\infty \le x \le -t_g \end{cases} \tag{2.4}$$

To determine q, h, and p substitute (2.4) into (2.2), then using (2.1) for each of the three regions, obtaining:

$$\begin{aligned} q &= (\beta^2 - n_1^2k^2)^{1/2} \\ h &= (n_2^2k^2 - \beta^2)^{1/2} \\ p &= (\beta^2 - n_3^2k^2)^{1/2} \\ k &\equiv \omega/c \end{aligned} \tag{2.5}$$

Note in (2.5) that q, h and p are all given in terms of the single unknown ß, which is the propagation constant in the Z direction. By making $\partial E_y/\partial x$ continuous at x=-t_g, as required, a condition on ß is derived. It yields the condition

$$-h\sin(-ht_g) - h(q/h)\cos(-ht_g) = p[\cos(ht_g) + (q/h)\sin(ht_g)]$$

or, after simplification,

$$\tan(ht_g) = \frac{p+q}{h(1-pq/h^2)} \qquad (2.6)$$

The transcendental equation (2.6), in conjunction with (2.5), can be solved either graphically, or numerically on computer. Given a set of refractive indices n_1, n_2, and n_3 of a plane waveguide. (2.6) in general yield a finite number of solutions for ß provided the thickness t_g is large enough. The result is a set of discrete allowed values of ß, corresponding to the allowed modes.

Let us assume that $n_2 > n_3 > n_1$ For $kn_3 < ß < kn_2$, it follows from Eq.(2.3) that the solution is sinusoidal in region 2, but is exponential in region 1 and 3. The confined modes are possible only when inner layer posses the highest index of refraction.

B. TM Mode

For the case of TM modes, the development exactly parallels that which has just been performed for the TE case, except the non-zero components are H_y, E_x, and E_z rather than E_y, H_x and H_z.

$$H_y(x,z,t) = \mathcal{H}_y(x)e^{i(\omega t - \beta z)}$$

$$E_x(x.z.t) = \frac{\imath}{\omega\epsilon}\frac{\partial H_y}{\partial z} = \frac{\beta}{\omega\epsilon}\mathcal{H}_y(x)\epsilon^{\imath(\omega t-\beta z)} \qquad (2.7)$$

$$E_z(x.z.t) = -\frac{\imath}{\omega\epsilon}\frac{\partial H_y}{\partial x}$$

The transverse magnetic component $\mathcal{H}_y(x)$ is given by

$$\mathcal{H}_y(x) = \begin{cases} -C'\frac{h}{q'}\epsilon xp(-qx) & 0 \le x \le \infty \\ C'[-\frac{h}{q'}cos(hx) - sin(hx)] & -t_g \le x \le 0 \\ -C'[\frac{h}{q'}cos(ht_g) + sin(ht_g)]\epsilon xp[p(x+t_g)] & -\infty \le \imath \le -t_g \end{cases} \qquad (2.8)$$

where h, q and p are again defined by (2.5), and where

$$q' = \frac{n_2^2}{n_1^2}q \qquad (2.9)$$

When boundary conditions are matched in a manner that is analogous to the TE case, it is found that only those value of ß are allowed for which

$$tan(ht_g) = \frac{h(p'+q')}{h^2 - p'q'} \qquad (2.10)$$

where

$$p' = \frac{n_2^2}{n_3^2}p \qquad (2.11)$$

The solutions of the TE- and TM-modes for the core of a polystyrene film on a glass are illustrated in Fig. 2.2. In general, a mode becomes confined above a certain (cutoff) value of t_g/λ . At cutoff value p=0 and ß=n_3k_o, and the mode extends to x= $-\infty$. According to the mode condition, cutoff

values of t_g/λ for TE and TM modes are given, respectively, by

$$\left(\frac{t_g}{\lambda}\right)_{TE} = \frac{1}{2\pi\sqrt{n_2^2 - n_3^2}}\left[m\pi + \tan^{-1}\sqrt{\frac{n_3^2 - n_1^2}{n_2^2 - n_3^2}}\right]$$

$$\left(\frac{t_g}{\lambda}\right)_{TM} = \frac{1}{2\pi\sqrt{n_2^2 - n_3^2}}\left[m\pi + \tan^{-1}\frac{n_2^2}{n_1^2}\sqrt{\frac{n_3^2 - n_1^2}{n_2^2 - n_3^2}}\right] \qquad (2.12)$$

where m is an integer (m=0,1,2,3,...) which refers to the mth confined TE (or TM) mode. Note that the cutoff thickness of TM_m mode is always larger than that of the TE_m mode, because $n_1 < n_2$. For value if t_g/λ slightly above the cutoff value, $p \approx 0$ and the mode is poorly confined. The selective excitation of waveguide mode by means of prism couplers and determination of their propagation constants β_m will be described in 2.4.

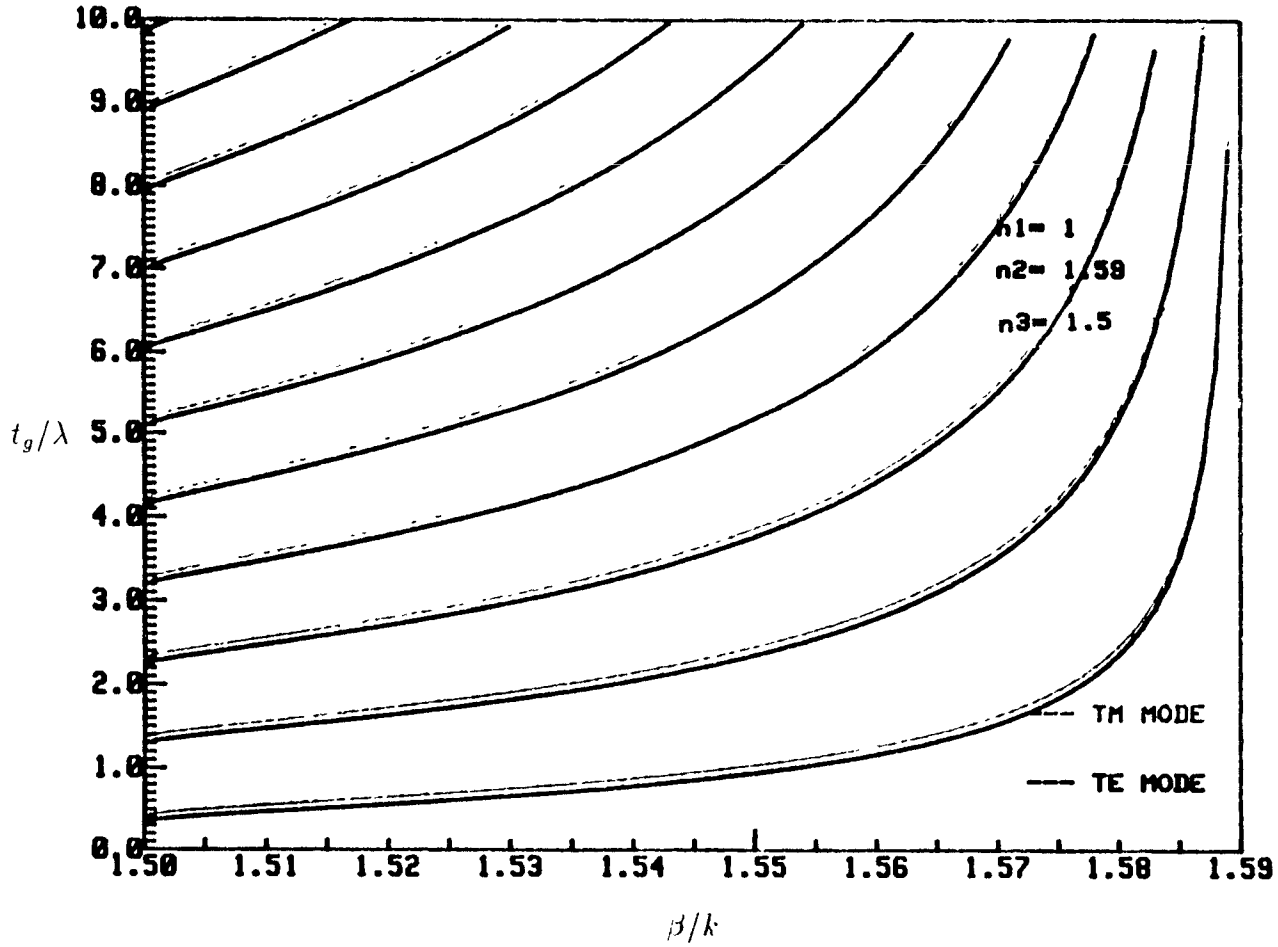

Figure 2.2 Dispersion curves for the confined modes of polystyrene film on a glass substrate.

2.1.2 Metal-Clad Waveguides

Consider a slab waveguide structure as shown in Fig. 2.1 with the substrate (medium III) being metal silver. The refractive index n_3 of silver is a complex number, n_3=0.067-i4.05 at λ = 6328A. Reflectivities from Silver surface are extremely high (almost 100%), especially at grazing incidence ($\theta \approx 90^\circ$), because of the large extinction coefficient (imaginary part) and the small real part of n_3.

For metal-clad waveguides with silver as substrate, the mode characteristics may be derived approximately by neglecting the real part of the refractive index n_3 (or the imaginary part of n_3^2). In this approximation, all the mode functions (2.2),(2.8) and mode conditions (2.6),(2.10) for TE and TM modes, respectively, can also be applied to the modes of silver metal-clad waveguide. Fig. 2.3 shows the dispersion curves for the confined modes of polystyrene film on an Silver substrate. Since the metal substrate has a negative dielectric constant (i.e, n_3^2 <0), total reflection always occurs at the interface between the guiding layer and the metal substrate, regardless of the value of n_2. Therefore, the refractive index of the guiding layer can be arbitrarily low, as long as $n_2 > n_1$. The propagation constant of the mode may have any value between $n_1 k_0$ and $n_2 k_0$. This range is much wider than with the usual dielectric waveguide. Thus metal-clad waveguides usually accommodate a large number of confined modes. In metal-clad waveguides TM

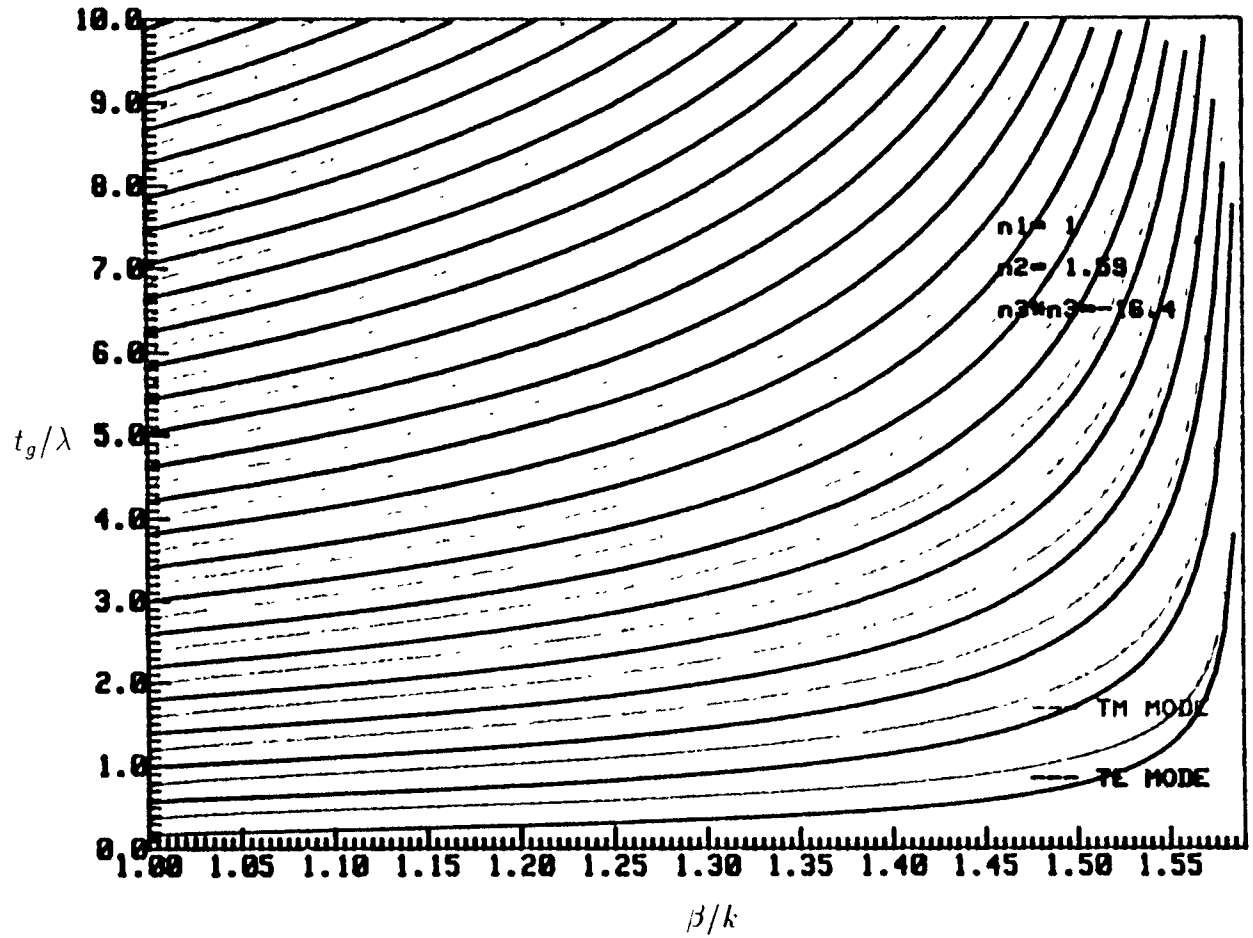

Figure 2.3 Dispersion curves for the confined modes of polystyrene film on a silver substrate.

modes are more lossy than TE modes, higher-order modes are more lossy than low-order modes [2.1].

In our experiment we deposited polystyrene on glass substrate with silver film of 500 A as a cladding layer. Since the reflectance of this Silver film is larger than 98% (see table 3.1), we may treat this planar waveguide as metal-clad waveguide according to the model described above.

2.2 THE RECTANGULAR WAVEGUIDE

The planar waveguides discussed in the previous section are useful in integrated optical applications where confinement of the optical field is in one transverse dimension. However, most applications require optical confinement in two dimensions. One example is a waveguide with a gain medium, the semiconductor laser [2.2]. Another example is a waveguide-type optical modulator [2.3]. Often two-dimensional confinement is required merely to guide light from one point on the surface of an OIC to another, to interconnect two circuit elements in a manner analogous to that of the metallic stripes used in an electrical integrated circuit.

2.2.1 Channel Waveguide

The basic rectangular waveguide structure consists of a waveguide region of index n_1 surrounded on all sides by a confining medium of lesser index n_2, as shown in Fig. 2.4. Such waveguides are often called channel guides, strip

guides, or 3-dimensional guides. It is not necessary that the index in the confining media be the same in all regions. A number of different materials, all with indices less than n_1, may be used to surround the guide. However, in that case, the modes in the waveguide will not be exactly symmetric. The exact solution of the wave equation for this general case is extremely complicated, and has not been obtained yet.

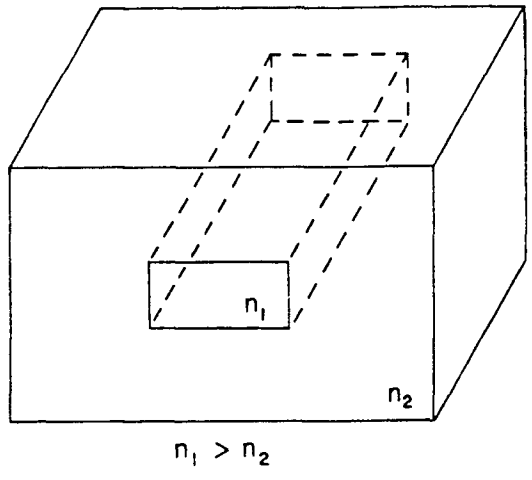

Figure 2.4 Basic rectangular dielectric waveguide structure.

Marcatilli [2.4] has derived an approximate solution to the rectangular channel waveguide problem, by analyzing the structure shown in Fig. 2.5, which is still fairly general. The key assumption made in Marcatili's analysis is that the modes are well guided, i.e., they are well above cutoff, so

that the field decays exponentially in Regions 2, 3, 4, and 5, with most of the power being confined to Region 1. The magnitudes of the fields in the shaded corner regions of Fig. 2.5 are small enough to be neglected. Hence, Maxwell's equations can be solved by assuming relatively simple sinusoidal and exponential field distributions, and by matching boundary conditions only along the four sides of Region 1. The waveguide is found to support a discrete number of guide modes that can be grouped into two families.

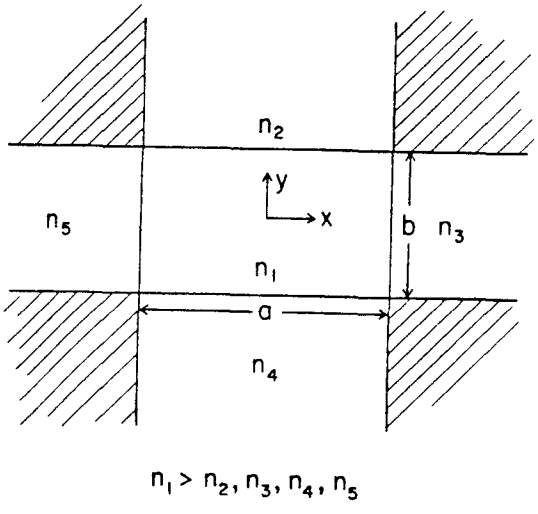

Figure 2.5 Cross-sectional view of a rectangular dielectric waveguide bounded by regions of smaller index of refraction.

2.2.2 Strip-Loaded Waveguide

It is possible to make a three-dimensional waveguide, in which there is confinement in both the x and y dimension, without actually surrounding the waveguide with materials of lesser index. This is done by forming a strip of dielectric materials of lesser index. n_3, on top of a planar waveguide, with index n_1, as shown in Fig. 2.6. Such a structure is usually called either a strip-loaded waveguide, or an optical stripline. The presence of the loading strip on top of the waveguiding layer makes the effective index in the region beneath it, n'_{eff} larger than the effective index, n_{eff1} in the adjacent regions. Thus there can be confinement in the *y* direction as well as in the *x* direction.

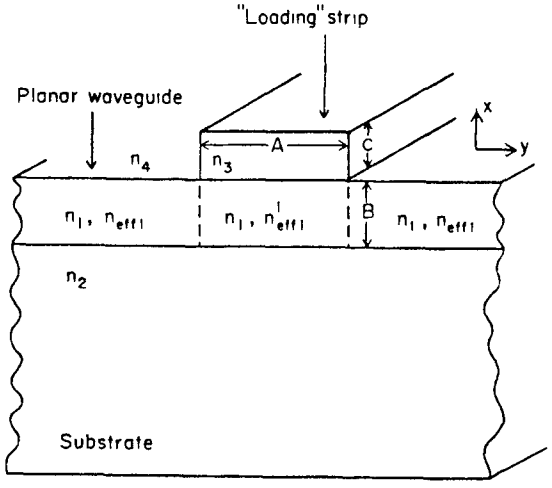

Figure 2.6 Diagram of dielectric strip-load waveguide.

Furuta et al.[2.5] have used the effective index of refraction method to analyze a strip-loaded guide like that

of Fig. 2.6 , and have shown that its waveguiding properties are equivalent to those of a dielectric waveguide like that shown in Fig. 2.7 , where the equivalent index in the side confining layer is given by

$$n_{eq} = \sqrt{n_1^2 - n_{eff1}^2 + n_{eff1}^2} \qquad (2.14)$$

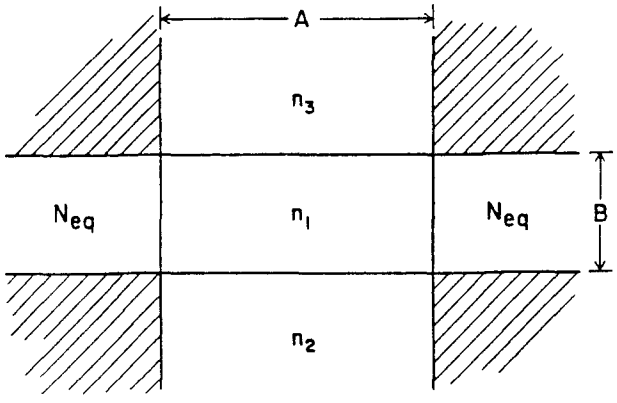

Figure 2.7 Cross-sectional view of rectangular dielectric waveguide equivalent to the strip-loaded waveguide of Fig. 2.5.

The propagation constants of the rectangular waveguide of Fig. 2.7 can be then determined by using Marcatili's method.

In principle, it is expected that strip-loaded waveguides should have less optical loss than rectangular channel dielectric waveguides, because scattering due to side-wall roughness is reduced.

2.3 Grating Guide

To discuss the propagation properties of the grating guide in Fig. 2.8. A. J. Fox[1.6] makes use of the result of multilayer theory [2.6] for the refraction of a plane-wave incident at an angle to the first layer of the stack. It can be shown that we need only consider the tangential components of the electric or magnetic field E_T, H_T and that the familiar transverse-electric (TE) or transverse-magnetic (TM) classification holds. Within the stack, the transformation of the tangential field takes place according to the matrix equation.

$$\begin{pmatrix} E_T(0) \\ H_T(0) \end{pmatrix} = [M]^N \begin{pmatrix} E_T(N) \\ H_T(N) \end{pmatrix} \qquad (2.15)$$

Where **M** is the characteristic matrix and the vector

$$\begin{pmatrix} E_T(N) \\ H_T(N) \end{pmatrix}$$

represents the exit tangential field at the **N** layer. If we assume that at the final boundary (medium 2) the wave radiates to infinity, we can approximate the exit vector by the impedance

$$\frac{E_T(N)}{H_T(N)} = \begin{cases} \dfrac{1}{n_2 \cos\theta_2} & \text{for TE waves} \\ \dfrac{\cos\theta_2}{n_2} & \text{for TM waves} \end{cases} \qquad (2.16)$$

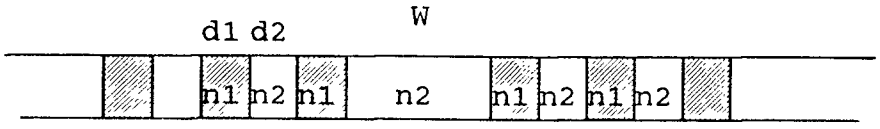

Figure 2.8 Thin-film grating guide.

The dependence of the modulus and phase of the reflection coefficient on the angle of incidence was calculated by Fox from (2.15). A typical result is shown in Fig. 2.9 (a). It can be seen that the reflectance peaks at an angle corresponding to the condition $o_1 = o_2 = \pi/2$ and decreases to zero on each side to form a well-defined stopband. Within the stopband the phase varies rapidly between.

Fox has established that a high-reflectivity wall can be made using periodic structures. To obtain a guide, he considers two such wall separated by a channel of width W. Rays will be successively reflected from each wall, and in order that constructive interference occurs, it must satisfy the following condition [2.7]:

$$2mo = 2\upsilon + 2\Gamma W \qquad (2.17)$$

Where m is an integer, the phase angle of the reflection coefficient, and is the transverse propagation constant is given by:

$$\Gamma = \frac{2\pi n_2 \cos o_2}{\lambda}$$

Equation (2.17) can be approximated by a series of straight lines on the phase plot where the intersection represents the operating point of the mode (see Fig. 2.9 (b)). For the case $w=2d_2$, the plot for m=1 passes through the center of the stopband where the phase is zero. Two other modes will also occur within the stopband, i.e., m=0,2. These additional modes occur at lower reflectivities than the m=1 mode and hence will be more lossy.

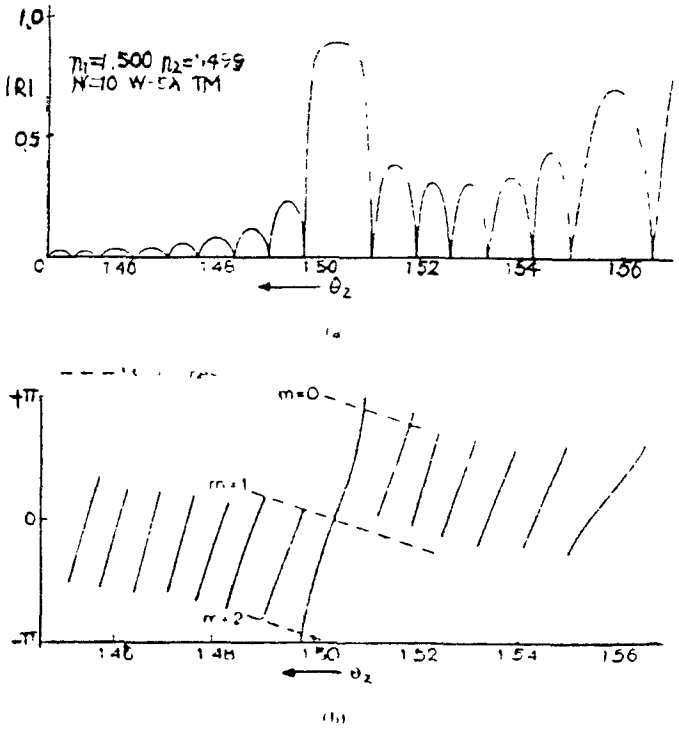

Figure 2.9 (a) Modulus of reflection coefficient.
(b) Phase of reflection coefficient.

By using the matrix transportation equation (2.15), Fox obtained the transverse field distribution in the grating guide at particular instant. Fig. 2.10 shows such a distribution for a first-order TM mode. The fractional difference in refractive index $(n_2-n_1)/n$ is 1% and only five periods are used on each side of the channel.

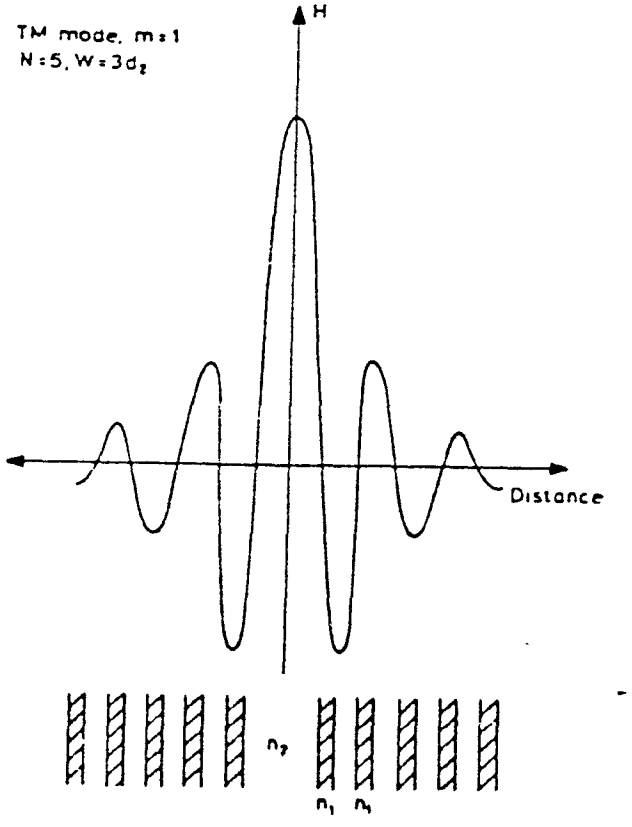

Figure 2.10 Field distribution in grating guide.

2.4 Waveguide Input and Output Coupling

2.4.1 Direct Focusing

The simplest method of transverse coupling of laser beam to a waveguide is the direct focusing or end-fire approach shown in Fig. 2.11. The waveguide may be of either the planar or channel type. The transfer of beam energy to a given waveguide mode is accomplished by matching the beam-field to the waveguide mode field. Care must be taken before each measurement to align the laser beam and the sample for optimum coupling, by maximizing the observed output power.

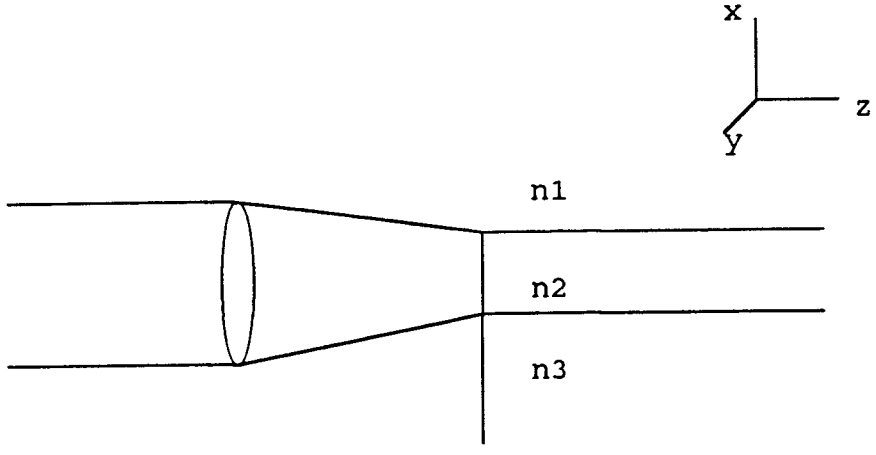

Figure 2.11 End-fire coupling method.

2.4.2 Prism Coupling

One of the primary diagnostic tools for evaluating the propagation characteristics of dielectric waveguides is the prism coupler. In this simplest form, the coupler makes use of a high-refractive-index prism placed in close proximity to a slab dielectric waveguide as shown in Fig. 2.12 . When

an optical beam passing through the prism is incident upon its bottom at an angle exceeding the critical angle, the evanescent fields that extend below the prism base penetrate into the waveguide. These fields are capable of transferring power between the incident beam and a waveguide mode. By appropriate choice of the angle of incidence and proper coupler design, a significant portion of the power in the incident beam may be transferred into a single chosen waveguide mode. Further, by reciprocity, if a second identical prism is placed in close proximity to the waveguide at some distance away from the input prism, each propagating mode will be coupled out of the guide at an angle that is characteristic of that particular mode. By measuring the output angle, a determination can be made of waveguide film refractive index and thickness.

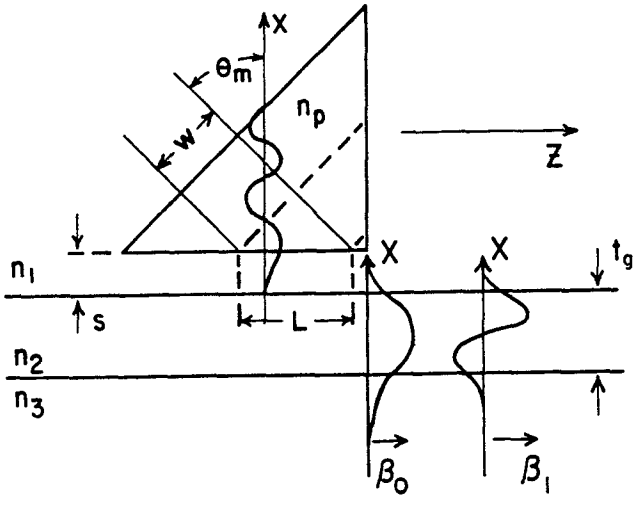

Figure 2.12 Diagram of a prism coupler.

CHAPTER 3

POLYMER FILM WAVEGUIDES FABRICATION TECHNIQUES

In Chapter 2, the theoretical consideration relevant to various types of waveguides were discussed. In every case, waveguiding depended on the difference in the index of refraction between the waveguiding region the surrounding media. A great many techniques have been devised for producing that required index difference. Each method has particular advantages and disadvantages, and no single method can be said to be clearly superior. The choice of a specific technique of waveguide fabrication depends on the desired application, and on the facilities available.

3.1 Solution-deposit Technique

Many materials can be used to form polymeric waveguides by applying a solution which dries to form a dielectric film and by spinning the substrate on a photoresist spinner to spread the layer evenly, or by dipping the substrate into the solution and slowly withdrawing it. Depending upon the polymer used, the films are subsequently air dried and baked at temperatures raging from 60 to 100°C for times varying between 5 min to 7 h. The solution-deposition technique offers several potential advantages including simplicity of fabrication and required equipment, low cost, and low optical attenuation (0.1-0.3 dB/cm). However, material purity is low and uniformity is relatively poor[3.1].

3.2 Plasma Polymerization

Another method for the deposition of polymer film involves a plasma polymerization process. In plasma polymerization, an electrical discharge is created in a vapor containing low-weight organic molecules called monomers. The discharge causes an ionization and fragmentation of the monomers and a subsequent rebounding of the fragments into a much larger two- or three- dimensional structure. When a substrate such as glass is introduced into the discharge, the polymer is deposited on its surface. Plasma polymerized organic films have several features distinct from conventional polymer films. In general, plasma polymerized polymer are highly crosslinked, insoluble, and pinhole free as well as heat resistant. In addition, no catalyst is required in this polymerization technique. For more detailed description and results see Appendix B.

3.3 Laser Ablation in Air

Upon impact of a laser beam on a material, electromagnetic energy is converted first into electronic excitation and then into thermal, chemical and mechanical energy.

3.3.1 Absorption of Laser Light

Laser light, in order to cause any lasting effect on a material, must first be absorbed. As trivial as this may sound, absorption very often turns out to be the most critical and cumbersome step in laser processing.

The absorption process can be thought of as a secondary "source" of energy inside the material. Whilst driven by the incident beam, it tends to develop its own dynamics and can behave in ways deviating from the laws of ordinary optics. It is this "secondary" source, rather than the beam issued by the laser device, which determines what happens to the irradiated material.

The optical response of a metal is dominated by the conduction electrons. Since the electron gas is degenerate, only electrons in states close to the Fermi level, referred to as "free electrons", contribute to the optical properties. There is no resonance frequency for a free electron, and its only interaction with lattice is by collisions. Some experimental valued of reflectance and absorption length for a number of metals are given in Table 3.1.

Table 3.1 Optical absorption lengths ($1/\alpha$) and reflectances (R) of evaporated metal films at room temperature for various wavelengths.[3.5]

Wavelength:	0.25 μm		0.5 μm		1.06 μm		10.6 μm	
	$1/\alpha$	R	$1/\alpha$	R	$1/\alpha$	R	$1/\alpha$	R
Ag	20 nm	0.30	14 nm	0.98	12 nm	0.99	12 nm	0.99
Al	8 nm	0.92	7 nm	0.92	10 nm	0.94	12 nm	0.98
Au	18 nm	0.33	22 nm	0.48	13 nm	0.98	14 nm	0.98
Cu		(0.1)	14 nm	0.62	13 nm	0.98	13 nm	0.99
Ni		(0.15)	12 nm	0.62	15 nm	0.67	37 nm	0.97
W	7 nm	0.51	13 nm	0.49	23 nm	0.58	20 nm	0.98

3.3.2 Ablation

Material evaporation is the most traditional branch of laser processing. By using short-pulsed, highly focused laser beam, the appropriate amount of energy may be introduced into the sample to melt and evaporate the desired quantity of material in order to achieve the required structure, without unnecessarily heating up the remainder of the sample. That is the aim of laser ablation in air.

At higher irradiation levels, extracted material leaves the hole as melt rather than as vapor. A simple model to help visualize this process is to think of the evaporating surface as a piston that exerts a pressure p_d onto the melt, squiring it out of the hole radially (Fig. 3.1).

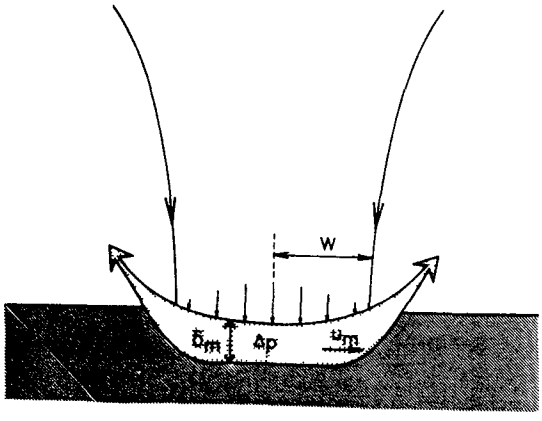

Figure 3.1 "Piston" mechanism of melt ejection by the evaporation recoil pressure. Small arrows symbolize the evaporation pressure distribution.

CHAPTER 4

EXPERIMENTS

Experiments included (1) waveguide fabrication, (2) optical measurement.

4.1 Waveguide Fabrication

The formation of our waveguides comprises only three main steps such as 1) metal film deposition, 2) laser ablation in air, 3) spin-on coating.

4.1.1 Substrate Preparation

The thin corning No. 2 cover glasses (25mm by 25mm by 0.2mm) were used as the substrate in our experiment. The contaminations on the specimen surface were removed by cleaning using ultrasonic cleaner:

5 min in Acetone;

5 min in Methanol;

10 min in deionized water, twice.

After the cleaning the samples were dried in oven of 120°C for 1 hour.

Prior to the plasma polymerization process, the cleaned glass substrates were weighed using analytical scale (0.1 mg accuracy).

4.1.2 Silver Layer Evaporation

The evaporation was done in a DENTON VACUUM CV-502 high vacuum evaporator (Fig. 4.1). The thickness of silver was

monitored by a crystal thickness monitor. The deposition rate can be changed from 1 A/sec to 12 A/sec by increasing the electrical current. After completing the evaporation the samples were cooled down to room temperature in the vacuum chamber to prevent oxidation. The operating procedure of evaporator as follows:

1. Open the bell jar of evaporator. Put the granular silver (99.99%) into the Tungsten boat and the cleaned glass substrates on the substrate holder. Turn off the shutter.
2. Close the bell jar, turn on the main switch and the mechanical pump of evaporator. Open valve 1 and 2 (valve 3 should be closed), using the thermocouple gauge 1 and 2 to monitor the vacuum.
3. When the vacuum pressure is better than 50 millitorr, open the tap of cooling water and turn on the diffusion pump.
4. After 30 min , when the vacuum is better than 0.001 Torr, use ionization gauge to monitor the vacuum pressure of chamber.
5. When vacuum reaches $2*10^{-5}$, turn on the power of thickness monitor and set the parameters.
6. Turn on the filament switch, increase the current until silver balls start to melt.
7. After the impurity clusters in silver disappear, open the shutter a little. Check the deposition rate using thickness monitor.

8. Adjust the current to get the satisfactory rate. Open the shutter completely to start the deposition.

9. When get enough thickness, close the shutter and turn off the current.

10. After complete the evaporation, turn off the diffusion pump, turn off the valve 1.

11. After 20 min vent the chamber, take the sample out. Pump the chamber again, keep the chamber in vacuum condition.

12. When diffusion pump is cooled down, close valve 2, close the tap of cooling water and turn off mechanical pump, main switch of evaporator, vent mechanical pump.

* See the manual for more details about how to load the chamber, how to rough the chamber, how to continue operation once the diffusion pump is hot.

In our experiment, we have made silver films of two thicknesses, 20 A and 500 A.

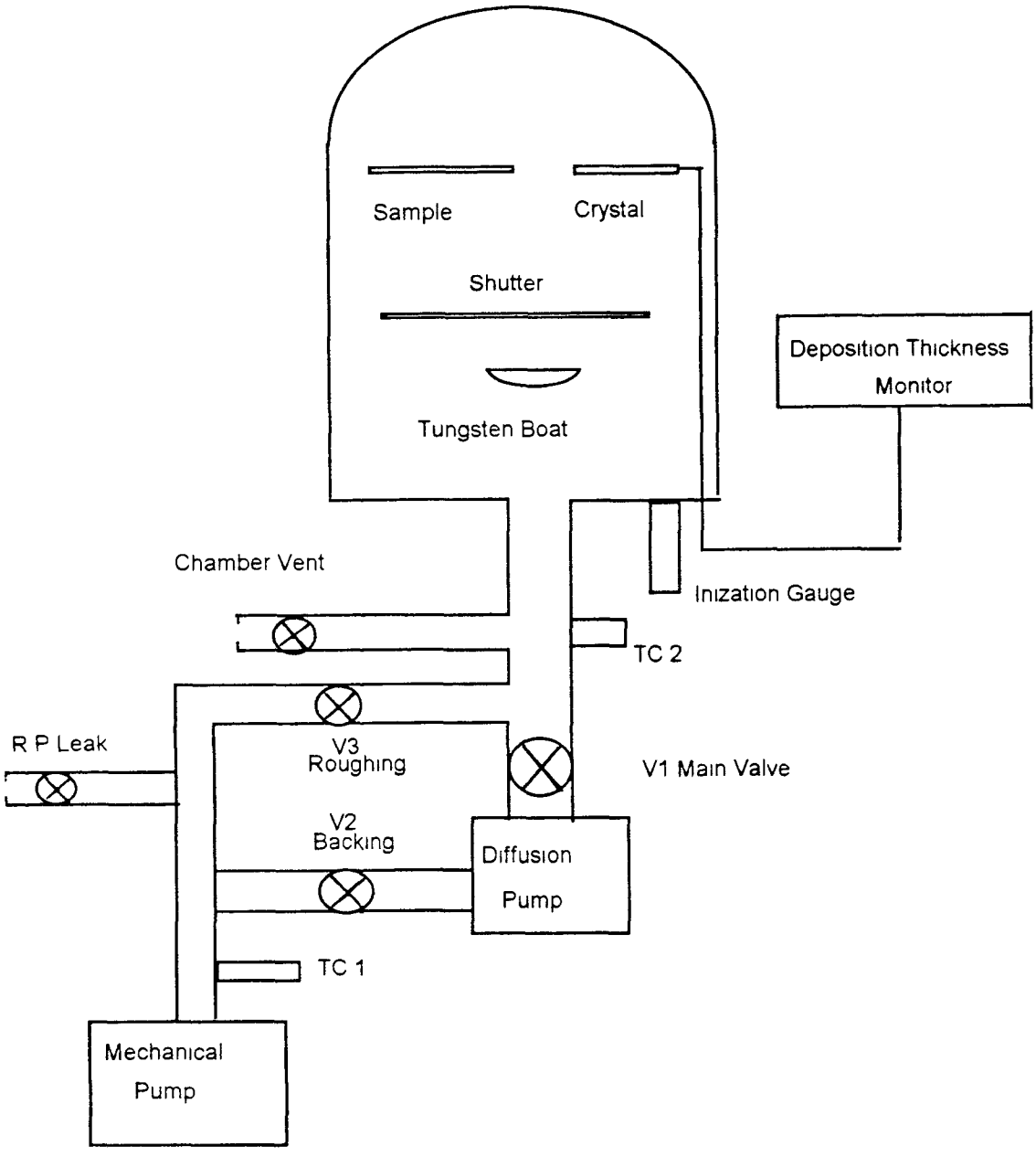

Figure 4.1 Schematic representation of high vacuum evaporator.

4.1.3 Laser Ablation

The laser used in our experiment is the KrF Excimer laser with wavelength of 248 nm, pulse duration of about 10 ns, and average output power of 300 millijoule/pulse. The optical system setup is shown in Fig. 4.2, which includes: 3 cylindrical lenses, 1 spherical lens, an adjustable slit, a mirror, and a three-dimention translation stage. Using this system we can get well focused, strong power, uniform, 2 inch long laser line, which will be used to pattern the sample surface.

The pattern of silver was formed by ablating the silver film with the laser beam. In order to achieve high resolution patterns, the power of laser should be well adjusted. By controlling the high voltage of laser plasma plus the width of slit (refer to the Fig. 4.2), we can achieve the needed power and line resolution. The power density around 20 millijoule/mm^2. Also, the laser beam should be well focused on the silver film. The sample is fixed on an x-y-z micropositioner, which is driven by stepper motor.

The periodic structure of grating is achieved by moving the substrate in a perpendicular direction to the evaporated line, one step a time. By changing the step distance we achieve different periodicity of grating. The final result is checked under an optical microscope of 400 times magnification.

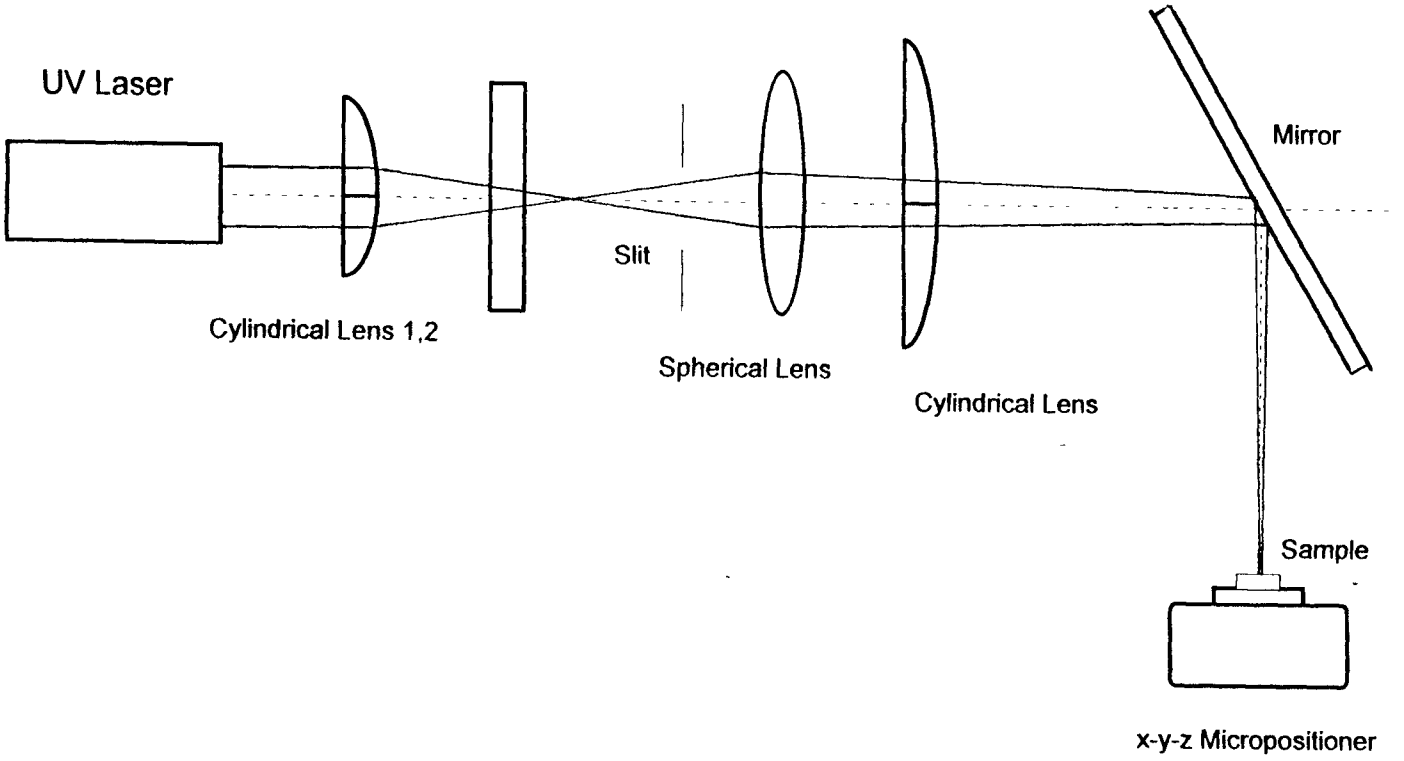

Figure 4.2 Schematic representation of the system for laser-induced patterning.

4.1.4 Polystyrene Film Spin-on Deposition

We chose thin corning No. 2 cover glass (25mm by 25mm by 0.2mm) as the substrate. The structures of the strip-buried waveguide and the grating waveguide are shown in Fig. 4.3. We made them both on same specimen.

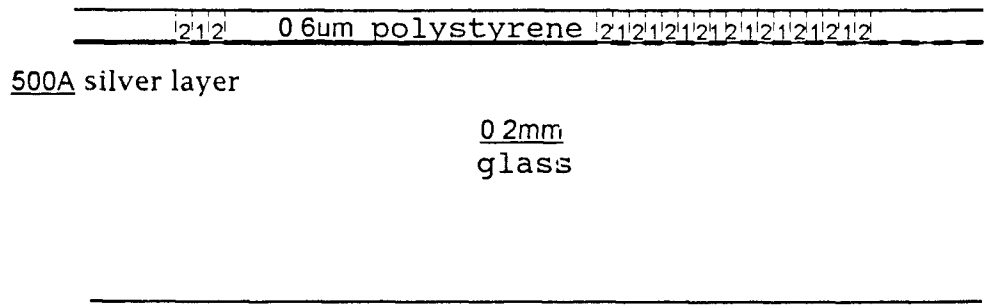

(a) (b)

Figure 4.3 The Cross-section View of the Novel Waveguides. (a) rectangular, (b) grating waveguides. (region 1--with metal layer area, region 2--metal ablated area.)

The solution which is used for spin-on coating is obtained by dissolving polystyrene pellets in Toluene solvent. The solution should be well stirred and the polystyrene should be completely dissolved in Toluene.

The substrate is placed on a photoresistor spinner and the polymer solution is metered onto the specimen. By spinning the substrate at a speed of 3500 RPM for 5 seconds we can get a very uniform coating. We let it dry in air overnight. By weighing the sample before and after coating, one may calculated the average thickness of waveguide. After

cutting the edges, we have completed our waveguides. Waveguides were 15 mm long and 25 mm in width (Fig. 4.4).

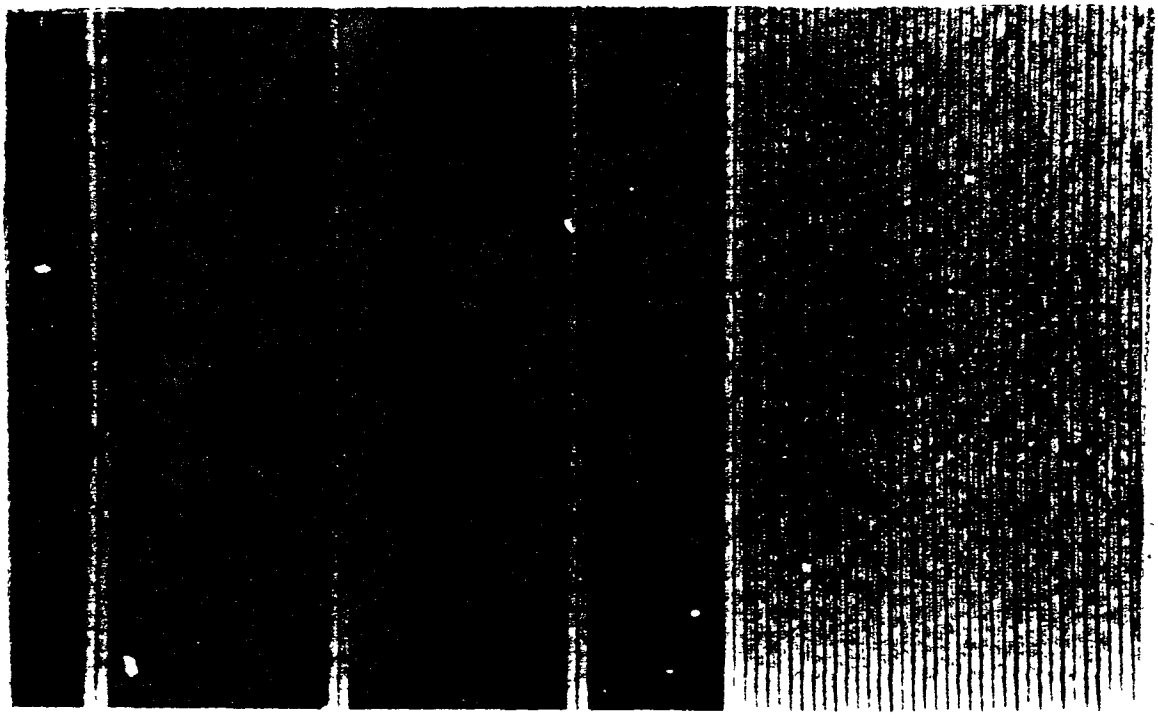

Figure 4.4 A magnified picture of our experimental waveguide. (top view, M=30)

4.2 Optical Measurement

4.2.1 Experimental System Setup

Since the optical waveguides are typically only a few micrometers thick, observation and measurement of the optical mode profile across a given dimension cannot be accomplished without a relatively elaborate experimental set-up, featuring at least several hundreds magnification. Our experimental setup is depicted in Fig. 4.5.

The sample, with its waveguide at the top surface, is fixed atop an x-y-z micropositioner. Microscope objective lenses, used for input beam coupling and output image magnification, are also mounted on micropositioners to facilitate the critical alignment that is required.

A chopper and a lock-in amplifier are used to increase the signal-to-noise ratio. The polarizer is used for selecting the polarization state of the propagating beam. An aperture of 70 um is mounted before the Si detector to increase the point resolution of the near-field measurements.

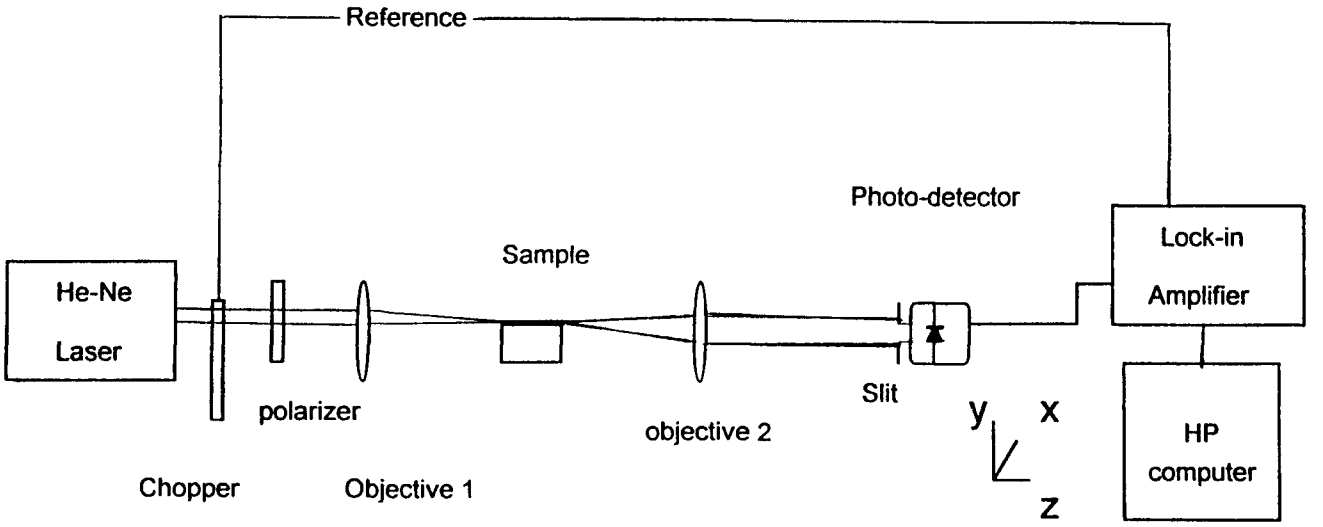

Figure 4.5 Diagram of an experimental setup which was used to measure optical mode shapes.

4.2.2 Computer Program for Data Collection and Treatment

The model SR510 lock-in amplifier has the GPIB interface. We connected it with HP 900 series 200/300 computer's I/O. The program (see appendix A) written in BASIC language was used to store the data from the lock-in amplifier in the computer.

4.2.3 Waveguide Mode Profile Observation and Measurement

One of the simplest, and also most accurate methods of measuring waveguides is to focus light of a desired wavelength directly onto a cleaved input face of a waveguide as shown in Fig. 4.6, and then measure the light output profile. Care must be take before measurement to align the laser beam and the sample for optimum coupling, by maximizing the observed output power. For visual observation of the waveguide mode profile, the output face of the waveguide can be imaged onto a white screen.

To obtain a quantitative display of the mode profile, i.e. optical power vs. distance across the waveguide, a photodetector with a tiny hole in its front is used. The photodetector is mounted on an x-y-z micropositioner, so it can scan the image in x and y directions. What is observed is optical power density at the waveguide output.

CHAPTER 5

EXPERIMENTAL RESULTS AND DISCUSSION

5.1 Confined Modes in Waveguides

5.1.1 Confined Modes in Planar Waveguides

The polystyrene film deposited by using spin-on technique (Fig. 5.1) is quite uniform and transparent. It is also well reproducible. By weighing the sample before and after spinning, we get the increase of 4.8 mg on 25 mm sq cover glass, which translates to a 6.8 um thick film. Thus,

$$d/\lambda = 10.8$$

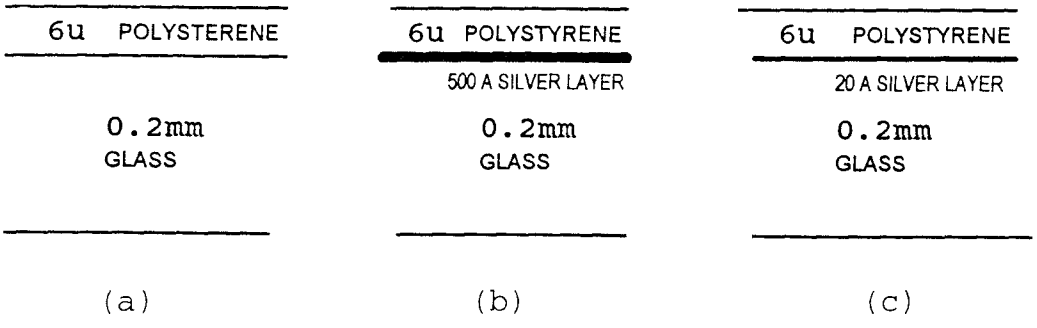

Figure 5.1 Cross-sectional view our planar waveguides. (a) regular (b) thick silver layer-clad (c) thin silver layer-clad.

From the dispersion curves of Fig. 2.2, we expect that our samples should be the multi-mode waveguides (m<10). For a ×60 objective lens the launching spot size is about 1 um, so the spot size is much smaller than the size of the waveguides (6 um). Therefore it can excite higher-order spatial modes. But caution should be taken to launch as many modes as possible in the waveguides.

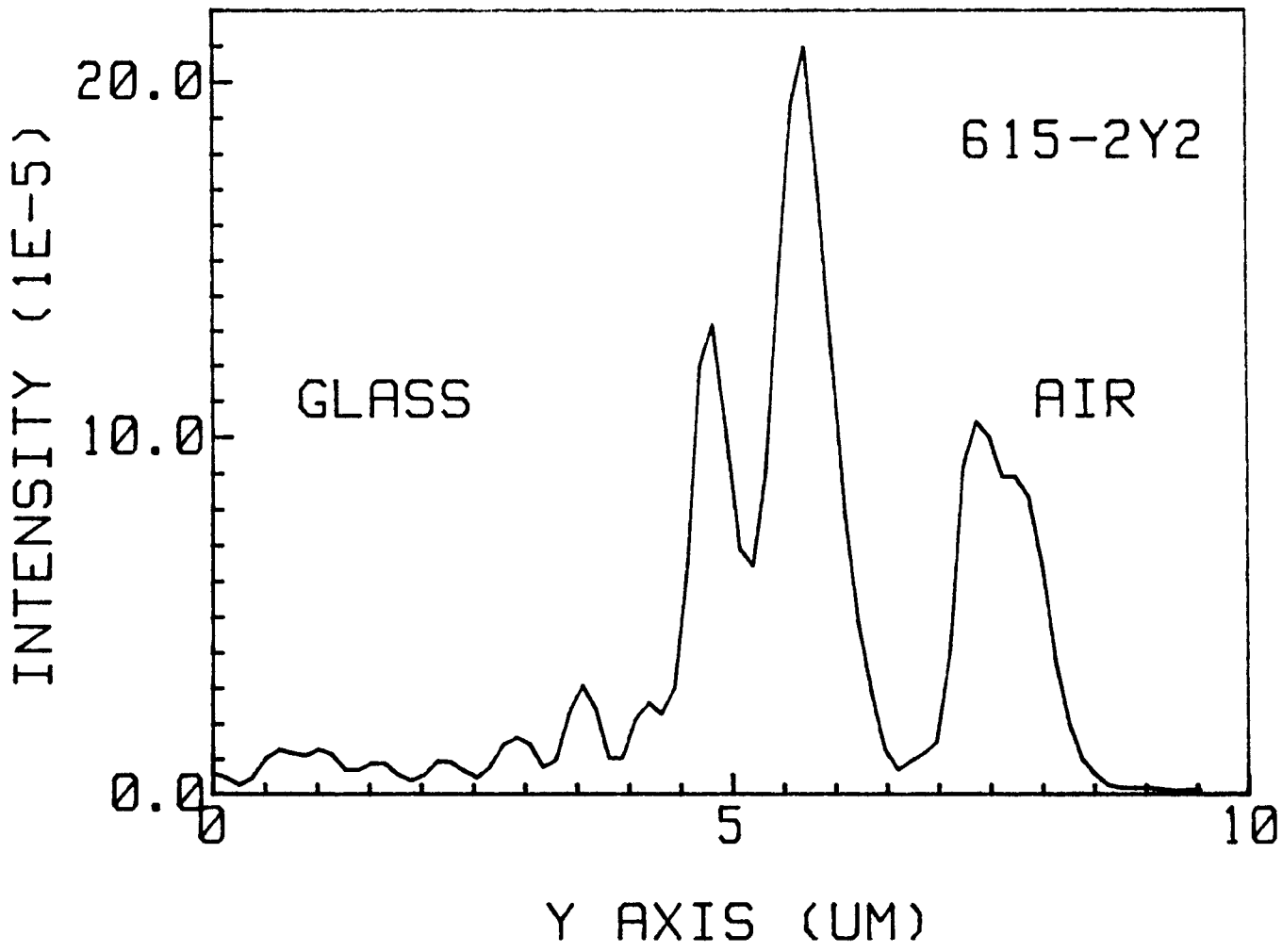

Figure 5.2 Near-field pattern of a regular polystyrene waveguide. (TE modes)

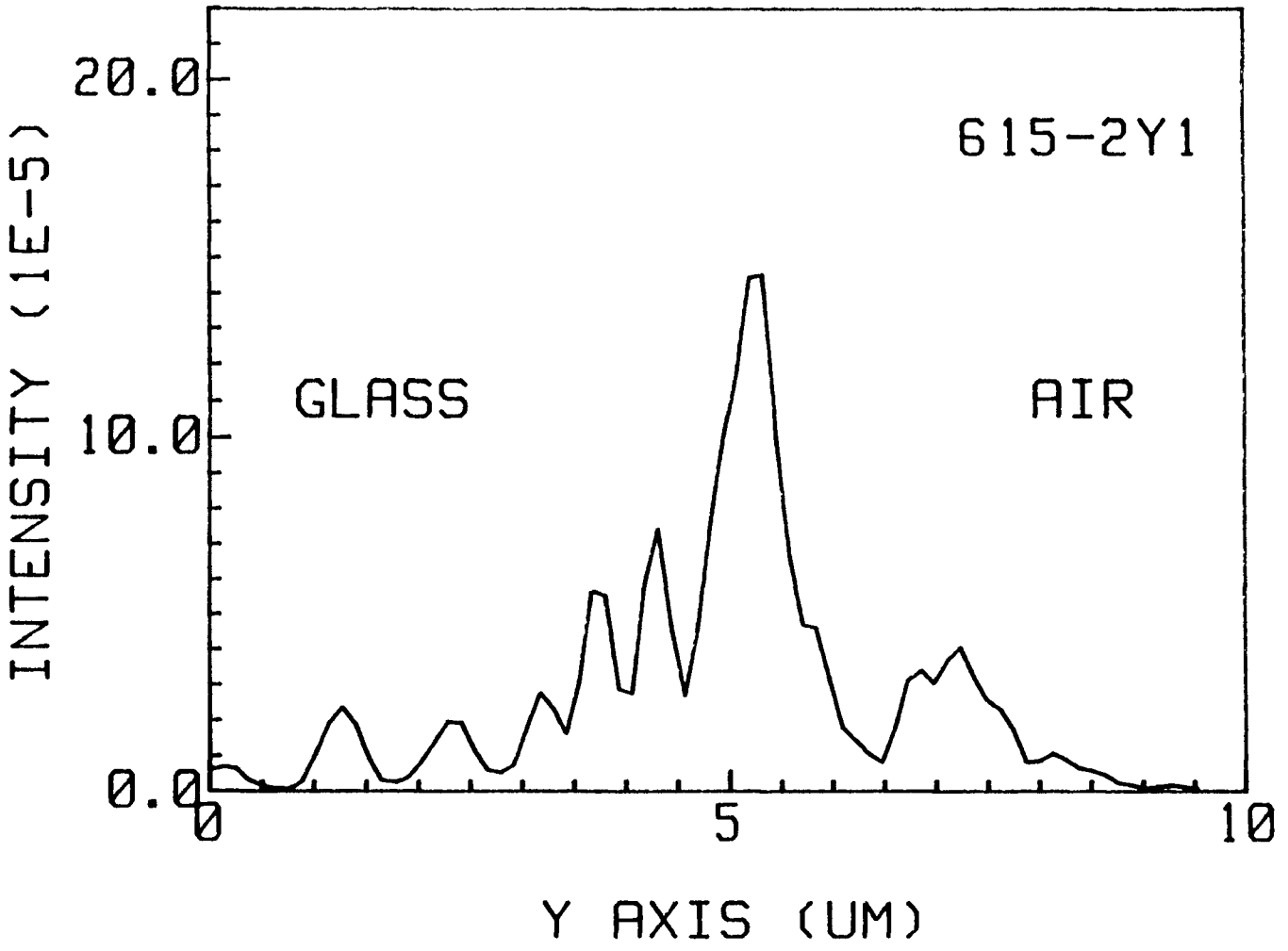

Figure 5.3 Near-field pattern of a regular polystyrene waveguide. (TM modes)

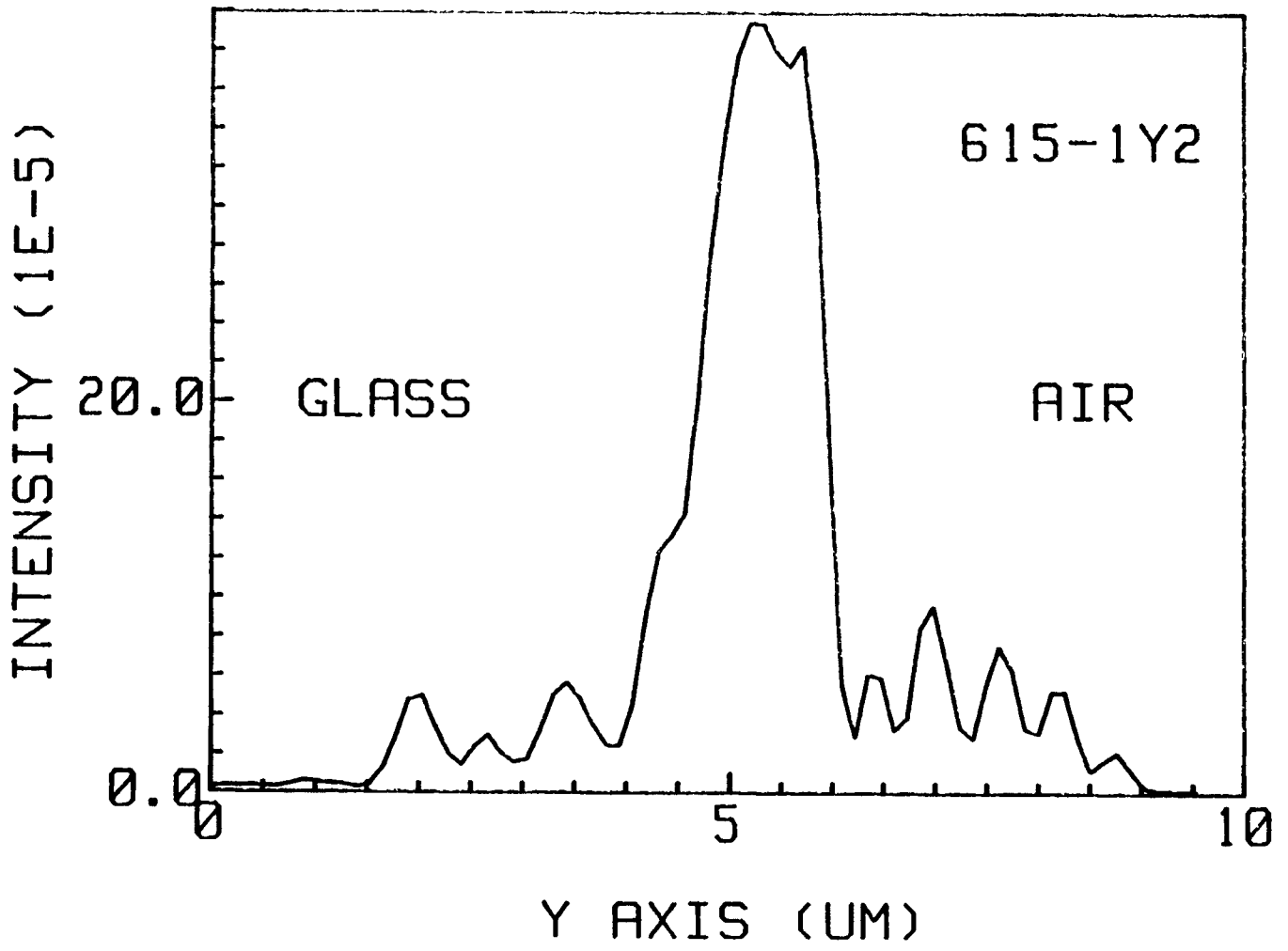

Figure 5.4 Near-field patter of thick silver film-clad waveguide. (TE modes)

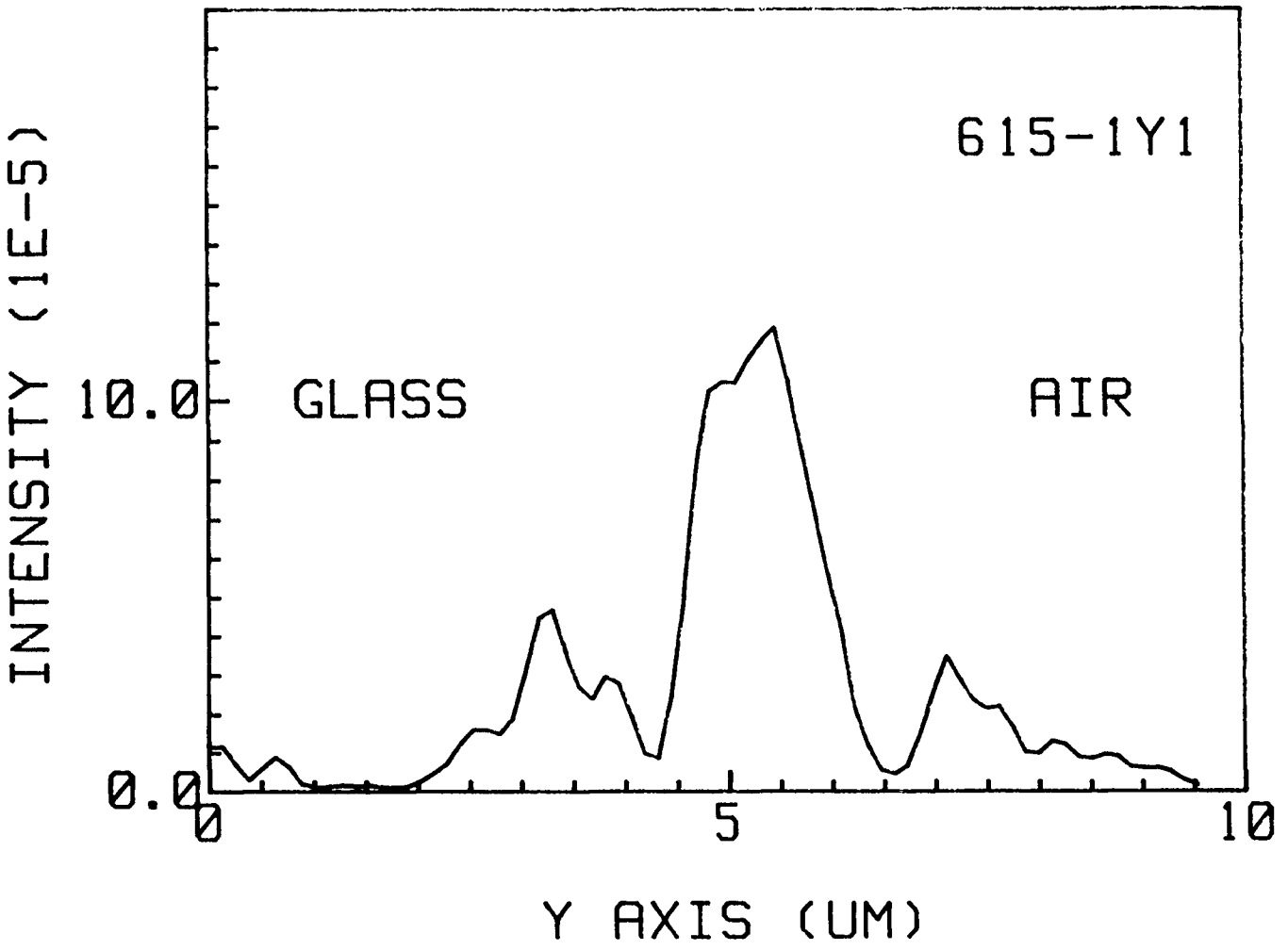

Figure 5.5 Near-field pattern of thick silver film-clad waveguide. (TM modes)

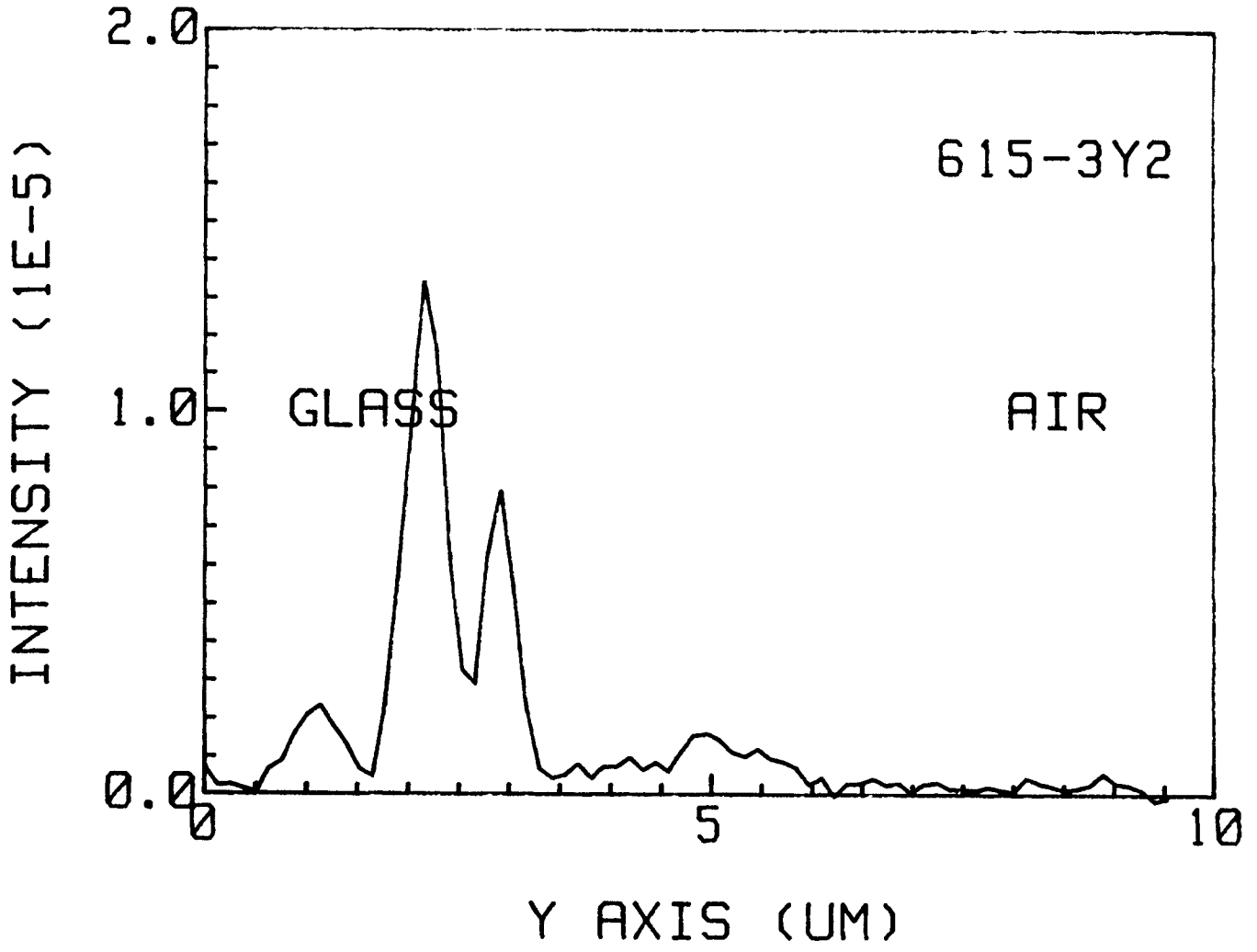

Figure 5.6 Near-field pattern of thin silver film-clad waveguide. (TE mode)

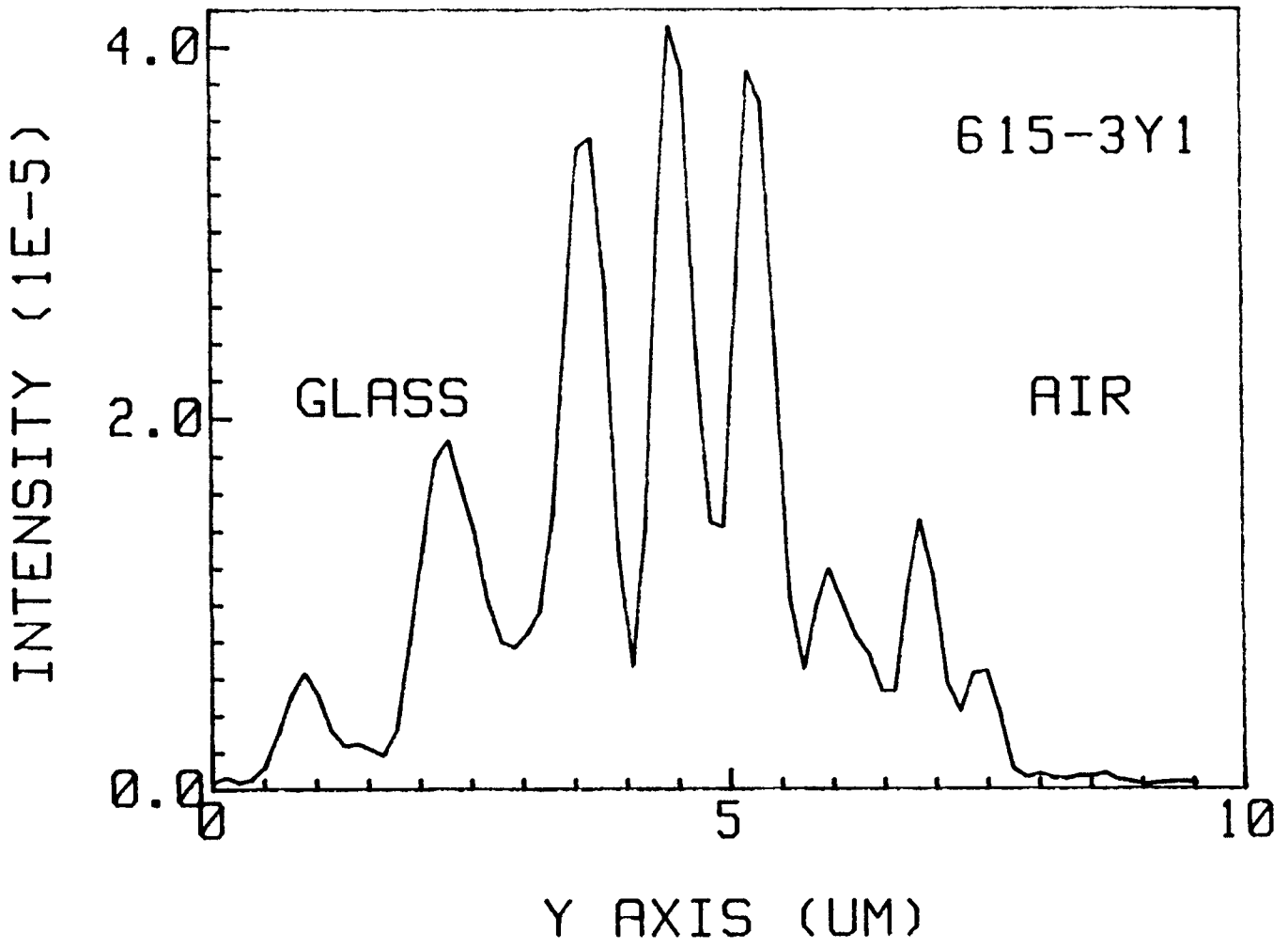

Figure 5.7 Near-field pattern of thin silver film-clad waveguide. (TM modes)

Fig. 5.2 - Fig. 5.7 show the modes profile for polystyrene waveguide on glass, polystyrene waveguide on glass with 500 A silver layer, and polystyrene waveguide on glass with 20 A silver layer. The experimental system used to measure these modes profile is shown in Fig. 4.6. The near field pattern of the waveguide's output has been magnified 200 times and recorded by moving a detector across the image. The pattern shown in the Figures are scaled down to their original size.

The near field image of a planar silver-clad waveguide is shown in Fig. 5.8.

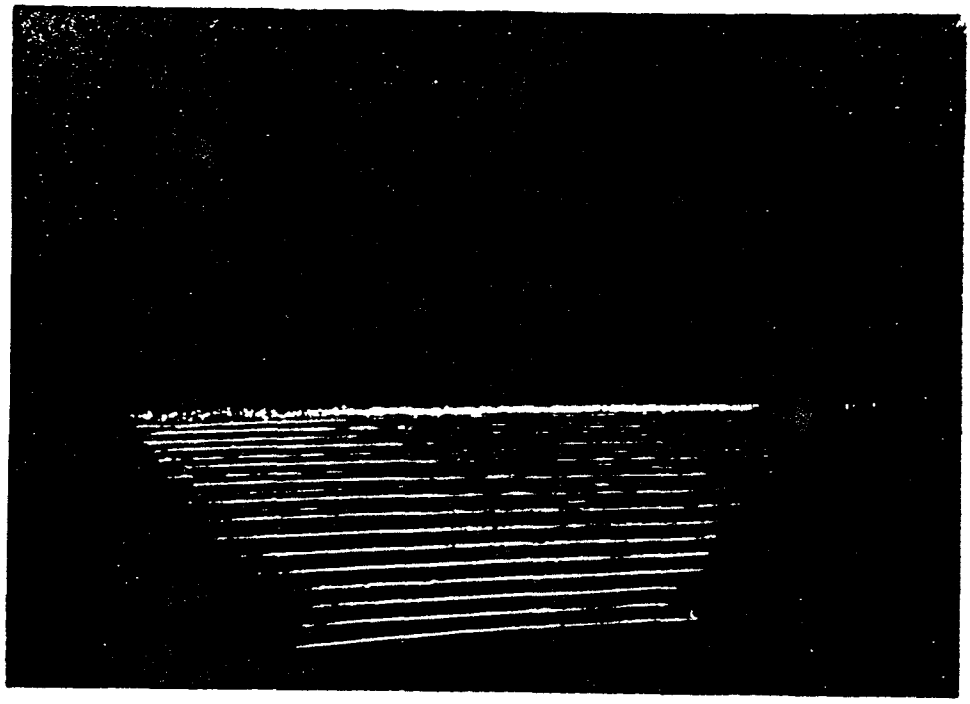

Figure 5.8 Near-field image of a planar thick silver layer-clad waveguide.

5.1.2 Rectangular Waveguides and Grating Waveguides

The structure of rectangular waveguide is shown in Fig. 5.9. We made rectangular waveguide and grating waveguide on same glass. For comparison, we made five samples which have different periodicity D (Table 5.1). We also made bent grating waveguide (Fig. 5.10).

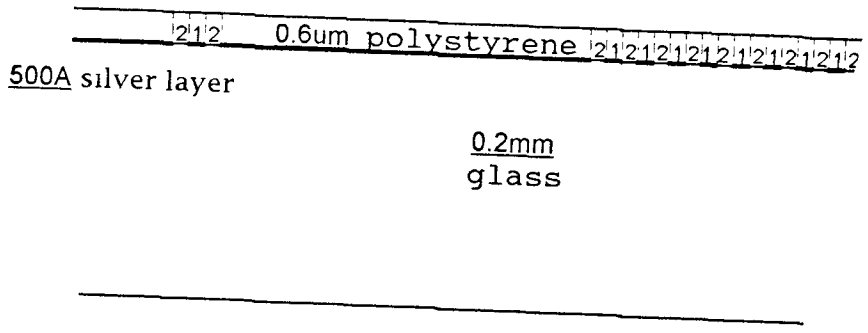

Figure 5.9 The cross-sectional view of our experimental waveguide. (region 2: silver ablated area)

Table 5.1 Periodicities of samples.

Sample No.	d1(um)	d2(um)	D(um)
1	20	30	50
2	22.6	30	52.6
3	28.8	30	58.8
4	36.7	30	66.7
5	41.4	30	71.4
6 (bent)	45	30	75

d1: width of region 1. d2: width of region 2.

D: periodicity (d1+d2)

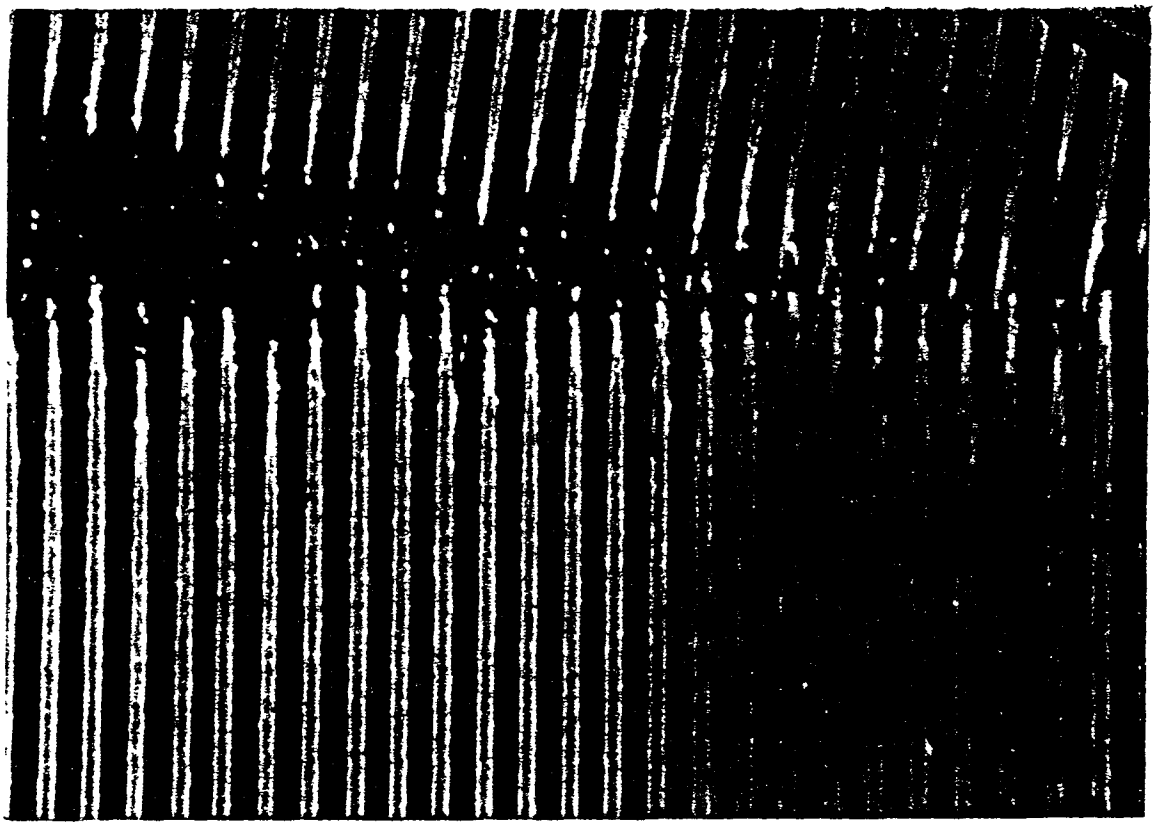

Figure 5.10 Picture of our experimental bent grating waveguide. (θ =9°)

For both the rectangular and grating waveguides we must launch the light beam on the region 1 (Fig. 5.9 and Fig. 5.11) to achieve the output profile.

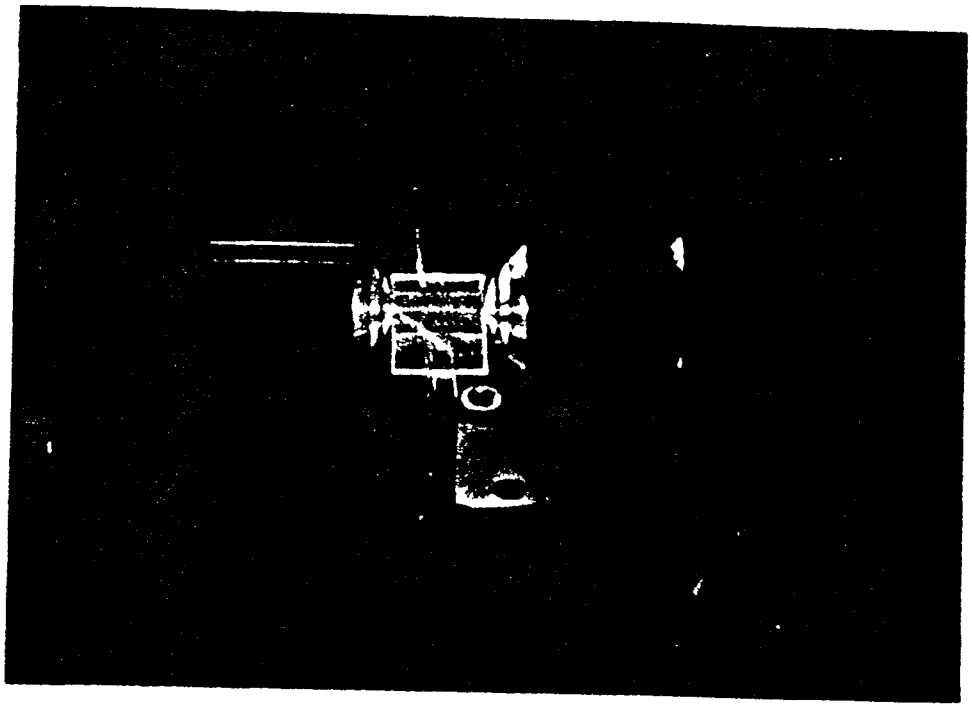

Figure 5.11 Top view of the light beam in grating waveguide. The Photograph shows a light beam which is fed into the grating waveguide by direct focusing at left. The light wave propagates inside the waveguide and is couple out at right.

The pictures of confined mode image of sample #4 are shown in Fig. 5.12.

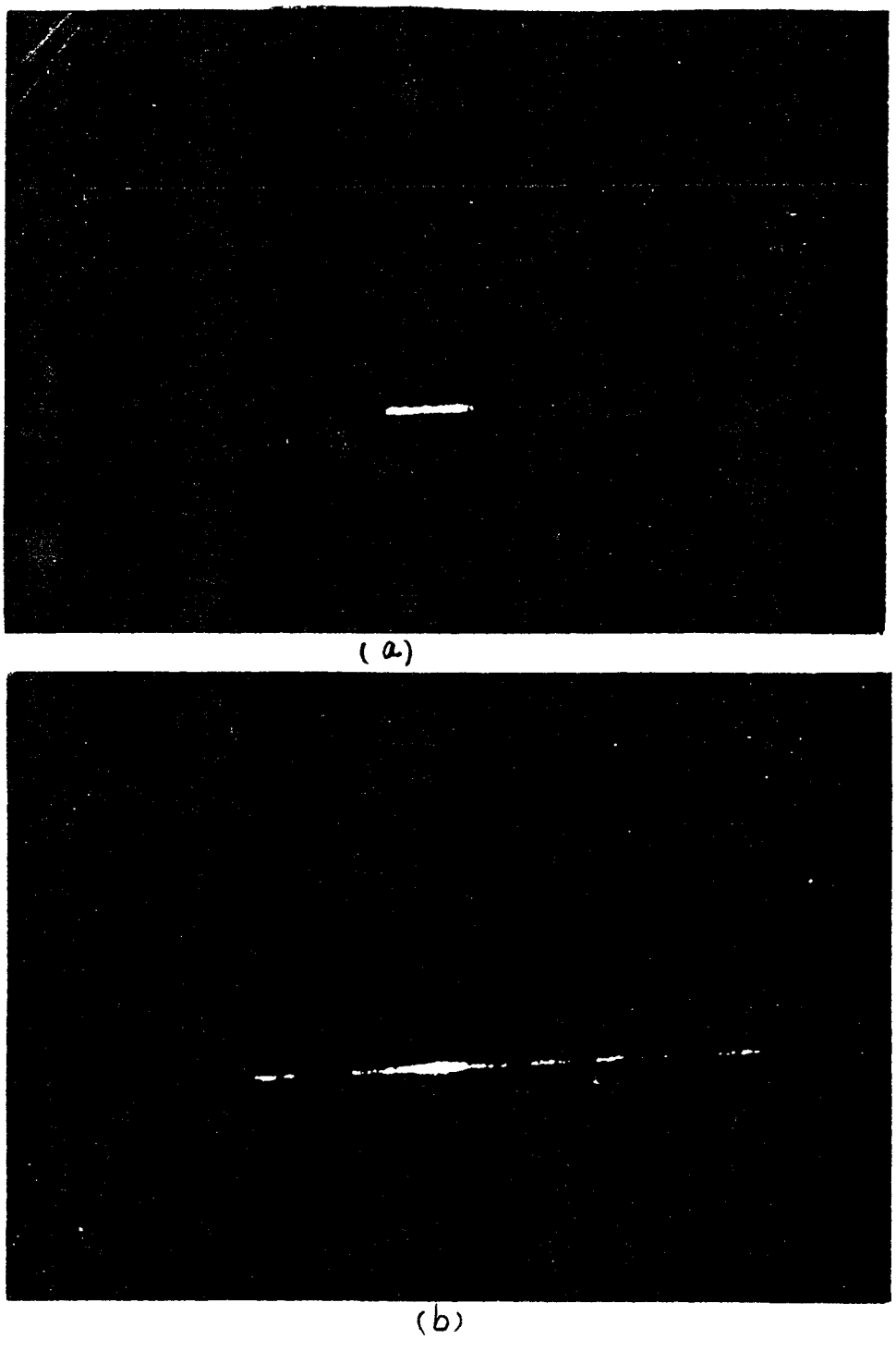

Figure 5.12 Near-field image of grating waveguide (sample #4). (a) well coupled at left lens. (b) poor coupled at left lens.

Their modes' profiles cross x axis (horizontal direction) and y axis (vertical direction) are shown in Fig. 4.13 - Fig. 4.36. We couldn't observe the output from sample 1.

The horizontal and vertical confinement sizes of rectangular and grating waveguides' output are summarized in Table 5.2 and Table 5.3. These are measured on the base of the intensity distribution of mode profiles (about 10 % of the peak value).

We have also taken photos of the waveguides' output. In Table 5.2 we give the comparison between the width of the waveguides' output as measured from the photos to the width of the waveguides' output as measured by the width of the mode profile.

Table 5.2 Horizontal confinement sizes of output pattern profiles and images of our experimental rectangular and grating waveguides.

		horizontal size (um) of output					
		" mode profile "				" photo image "	
Sample No.	D(um)	rectangular		grating		rect.	grating
		TE	TM	TE	TM		
2	52.6	25(14)*		20(12)			
3	58.8	33(21)	32(18)	24(13)	16(8)	22	20
4	66.7	28(14)		22(10)		28	22.4
5	71.4	39(24)	38(22)	39(21)	36(16)	44.8	39.2
6	75						50.4

* half-width values of profiles are given in parenthesis.

Table 5.3 The vertical confinement sizes of output pattern profiles and images of our experimental rectangular and grating waveguides.

Sample No.	d1(um)	D(um)	vertical size (um) of output profile rectangular		grating	
			TE	TM	TE	TM
2	22.6	52.6	7.5		6	
3	28.8	58.8	8	7.5	6.5	6.5
4	36.7	66.7	8.5		6	
5	41.4	71.4	7	6.5	6.75	6.5

5.2 DISCUSSION

By comparing the measured profiles (Fig. 5.4-Fig. 5.7), we can see that:

1) More modes exist in planar silver-clad waveguide than in regular planar polystyrene waveguide. This may be explained with the help of the calculated dispersion curves, Fig. 2.2 and Fig. 2.3, which show lager number of modes for a given thickness of the metal-clad waveguide.

2) In planar silver-clad waveguide, TM modes are more lossy than TE modes, and higher-order modes are more lossy than low-order modes. This was measured by comparing the output light power for each type of modes assuming identical launching conditions.

3) In thin silver-clad planar waveguide, TE modes are more lossy than TM modes, again measured by comparing the output power of light for both modes.

We found that a 20A-thick silver film was easily oxidized when exposed to air, even when covered later by a polystyrene film. The color of the film changes from purple to orange over night. This causes large light scattering losses for the TE modes in the waveguide. In certain cases the TE modes have been eliminated while propagating in the waveguide.

From figures Fig. 5.13 to Fig. 5.36 we can note the following:

1) The TE modes are stronger than the TM modes in both single rectangular and grating waveguide.

2) In general, grating waveguides confine more power than single rectangular waveguides.

3) The vertical confinement size of single rectangular waveguide is about 7-8 um, while the vertical confinement size of grating waveguide is about 6 um, even though the thickness of the confining polystyrene films was the same in both cases. We explain this by the higher degree of confinement achieved with the larger number of gratings.

Generally speaking, grating waveguides have better confinement than rectangular waveguides because of the reflection from the transverse gratings. On the other hand, because these waveguides are multi-mode waveguides, there must be some modes which satisfy the Bragg resonance requirement and some modes which do not. This means that we will achieve mode selectivity based on the Bragg confinement

condition. Each mode satisfies individual Bragg condition with the transverse periodic structure.

We have observed that thin metal-clad waveguides act as scatters in addition to their confining role. We attribute this not only to their possible granular structure but also to the fact that very thin metal layers incorporated in polymeric films exhibit high real index of refraction [4.2] which changes the mode profiles of the waveguide.

In most waveguide structures, a thick metal cladding results in a loaded waveguide with lower propagation constant. A two dimensional waveguide can be usually formed by two metal strips on both side of the guiding region. However, in our case no such confinement could be achieved. I our case 2-D confinement was achieved with one metal strip and two ablated metal strip claddings (Fig. 4.9). One may propose that by ablating the metal on the glass substrate, a higher index of refraction region is created leading to an effective mode structures that permits propagation only under the metal load.

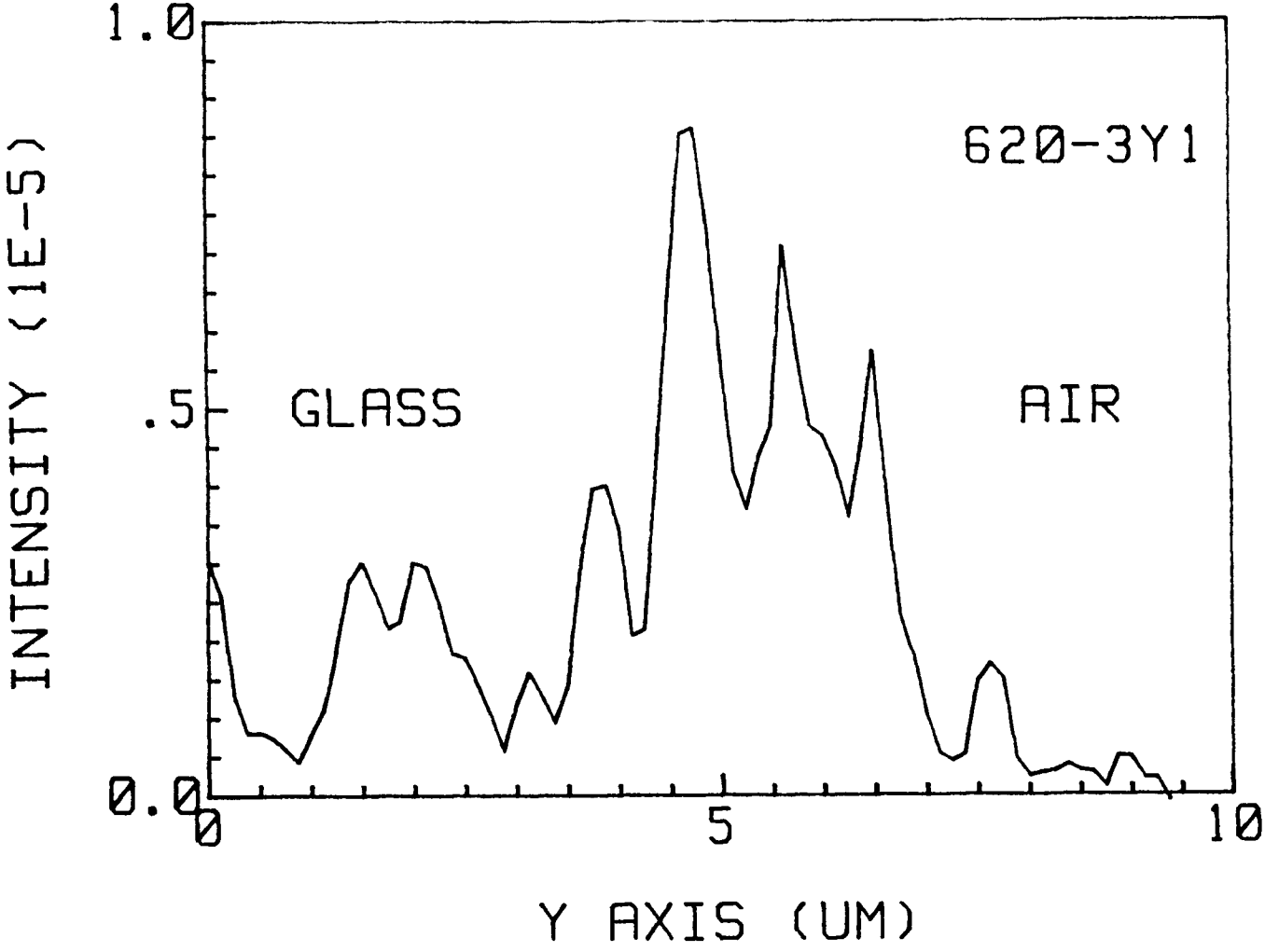

Figure 5.13 Near-field pattern of rectangular waveguide (sample 2) in vertical direction (TE).

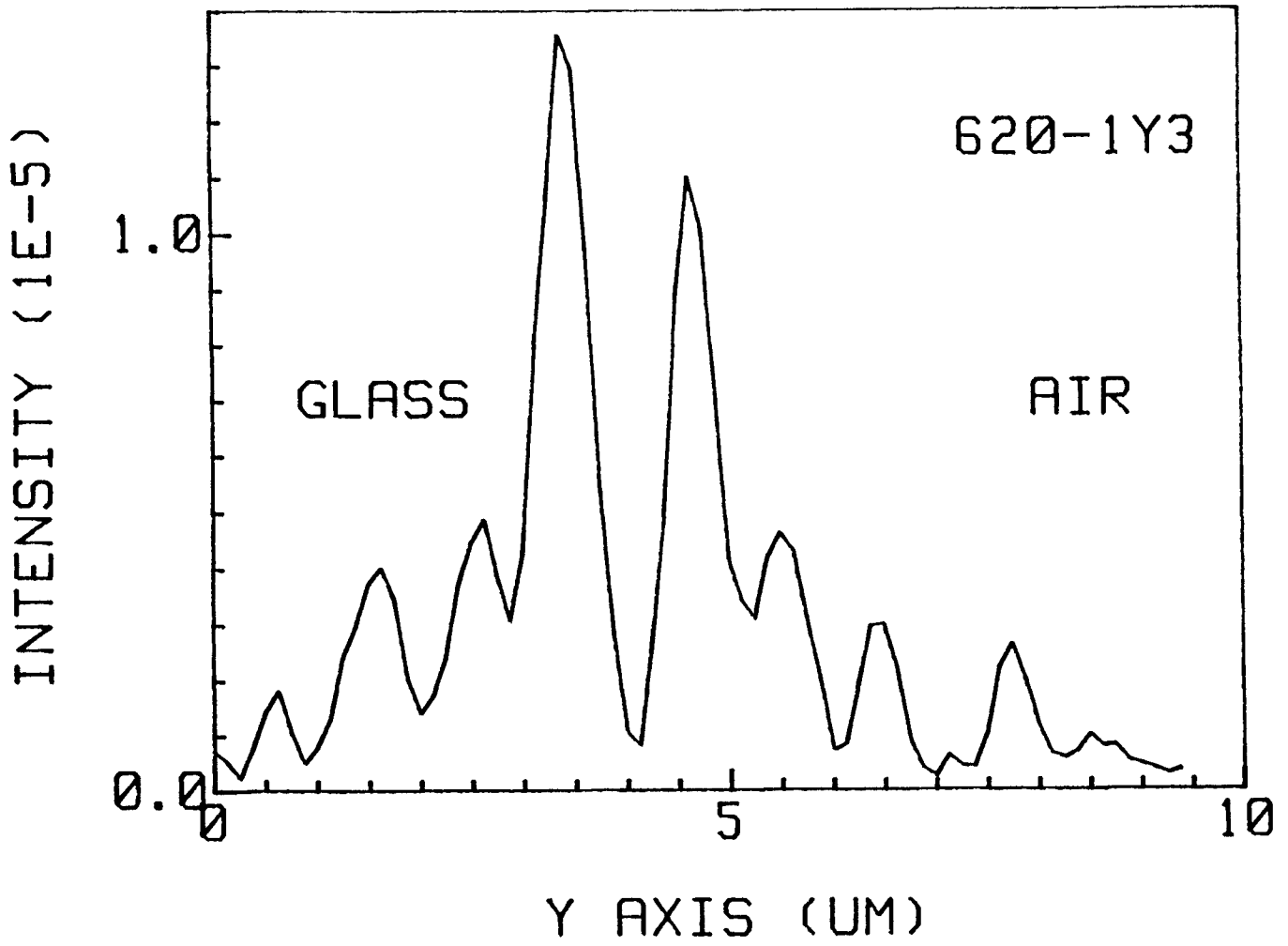

Figure 5.14 Near-field pattern of rectangular waveguide (sample 3) in vertical direction (TE).

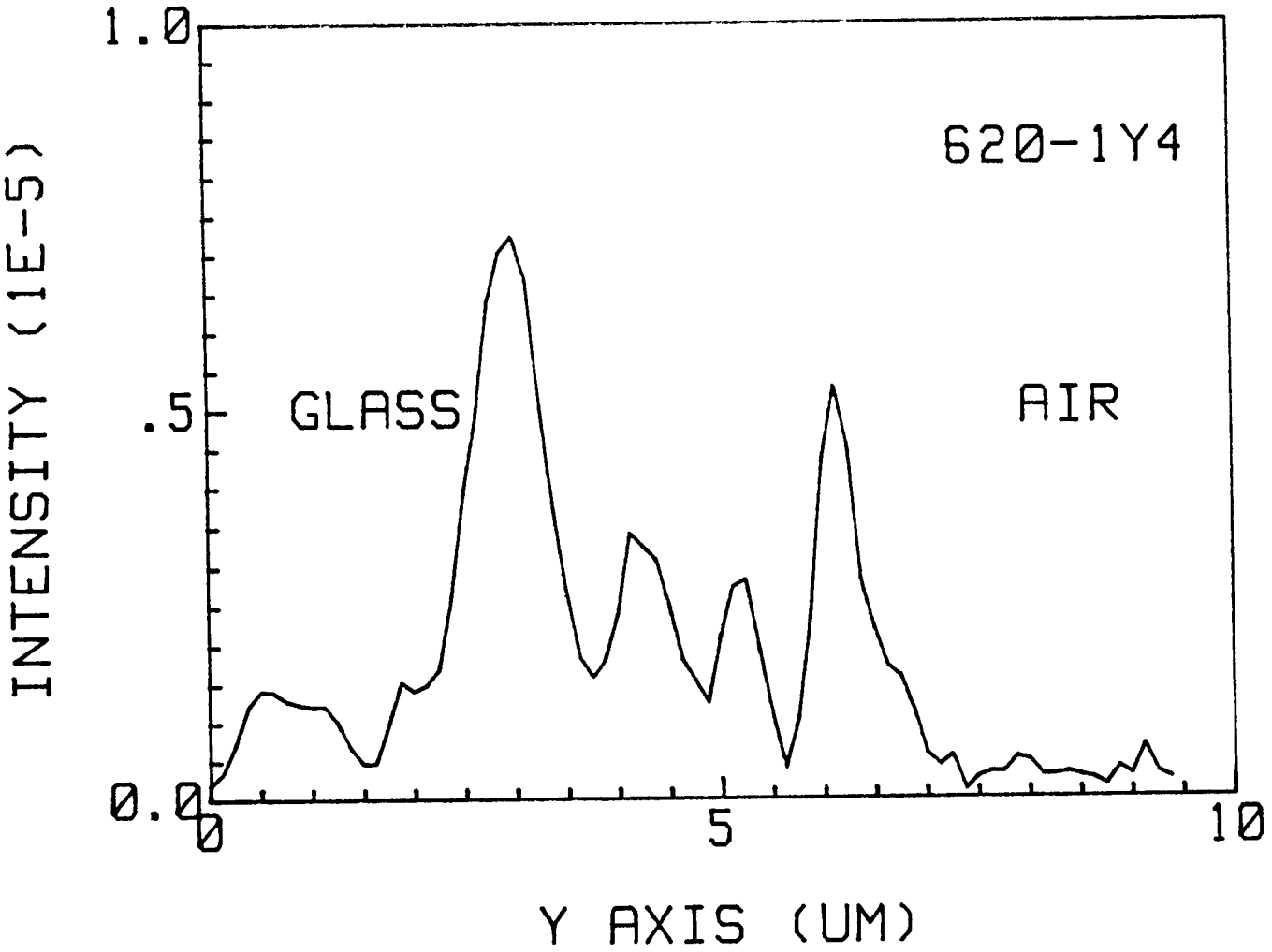

Figure 5.15 Near-field pattern of rectangular waveguide (sample 3) in vertical direction (TE).

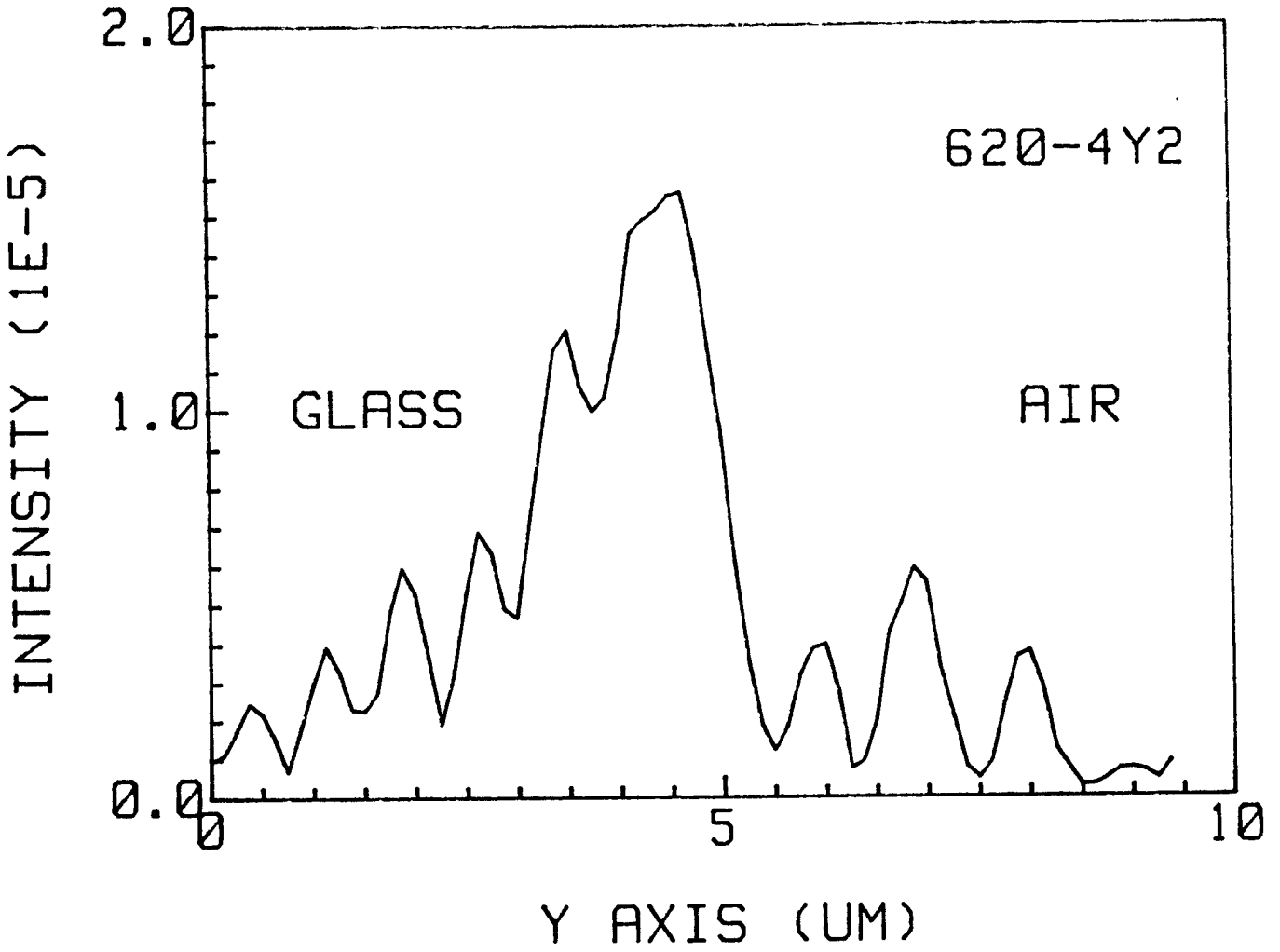

Figure 5.16 Near-field pattern of rectangular waveguide (sample 4) in vertical direction (TE).

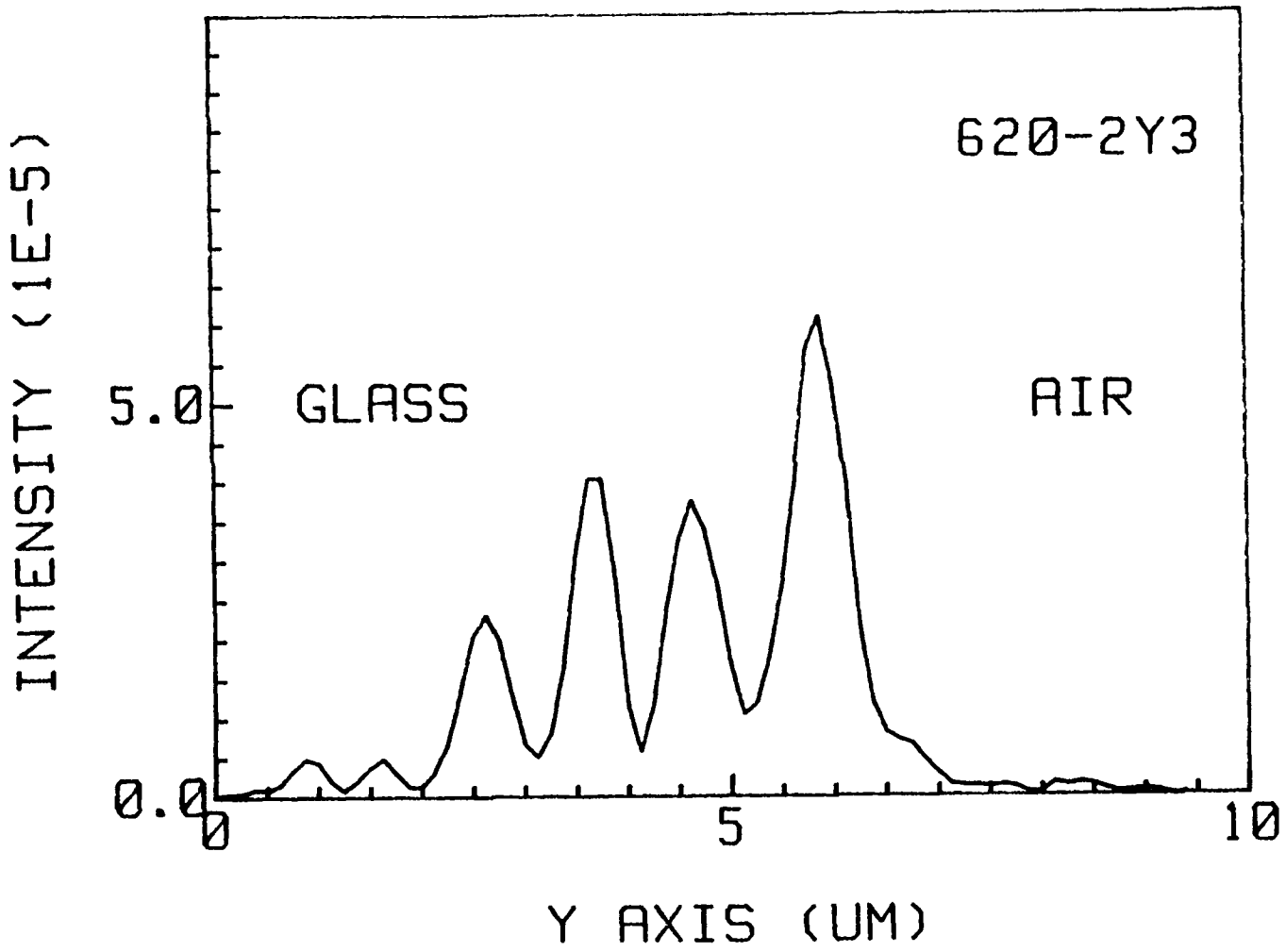

Figure 5.17 Near-field pattern of rectangular waveguide (sample 5) in vertical direction (TE).

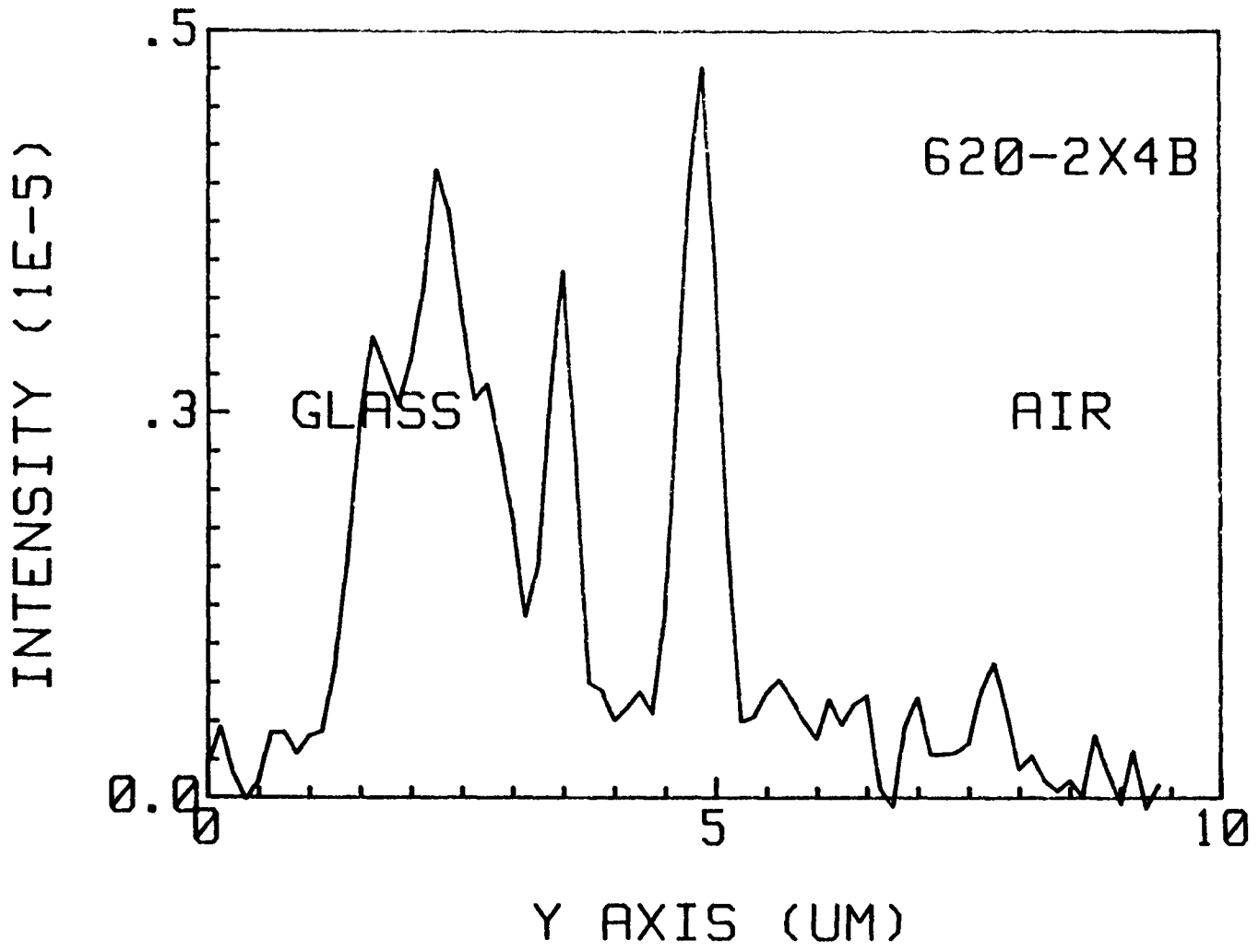

Figure 5.18 Near-field pattern of rectangular waveguide (sample 5) in vertical direction (TE).

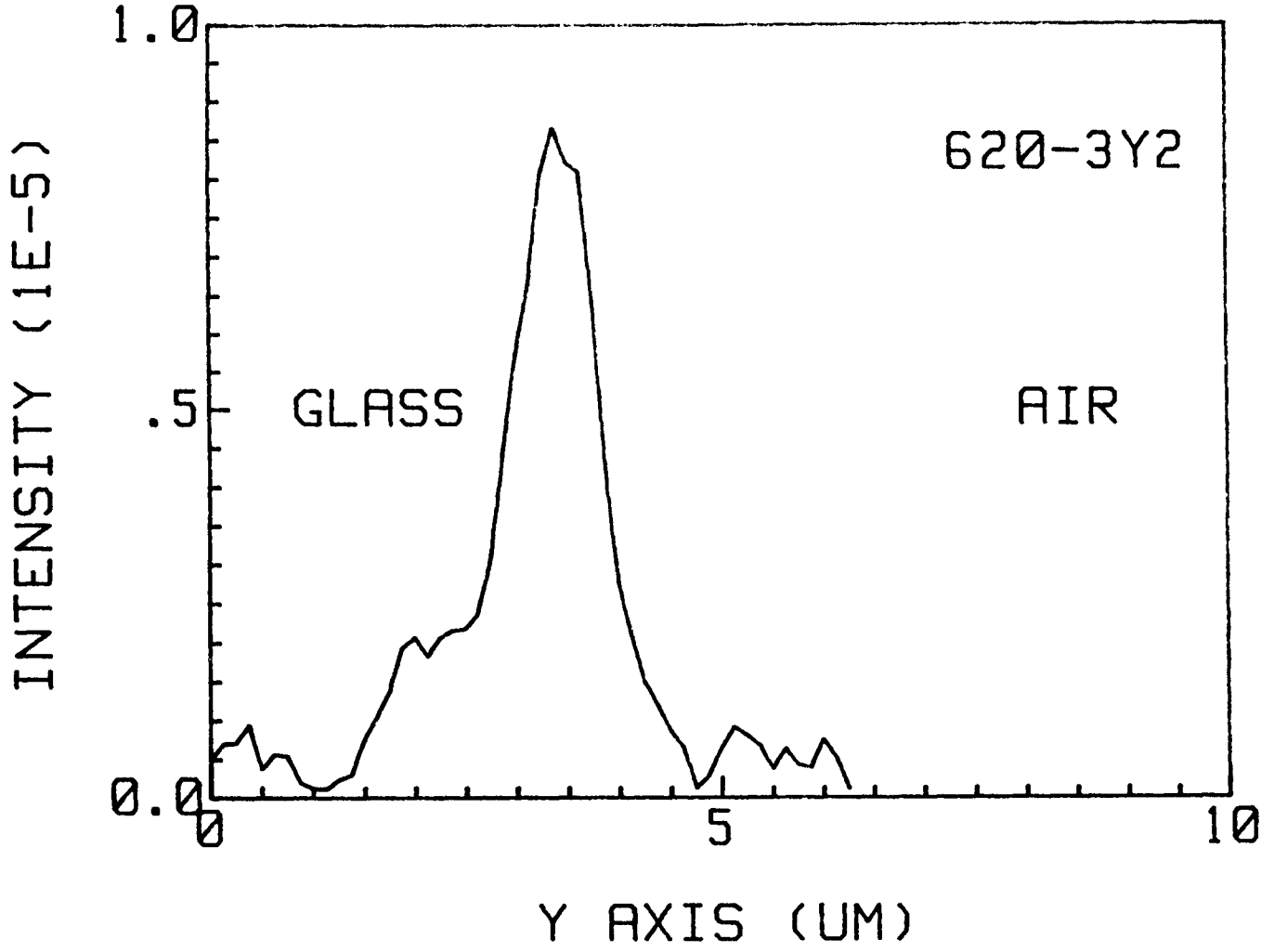

Figure 5.19 Near-field pattern of grating waveguide (sample 2) in vertical direction (TE).

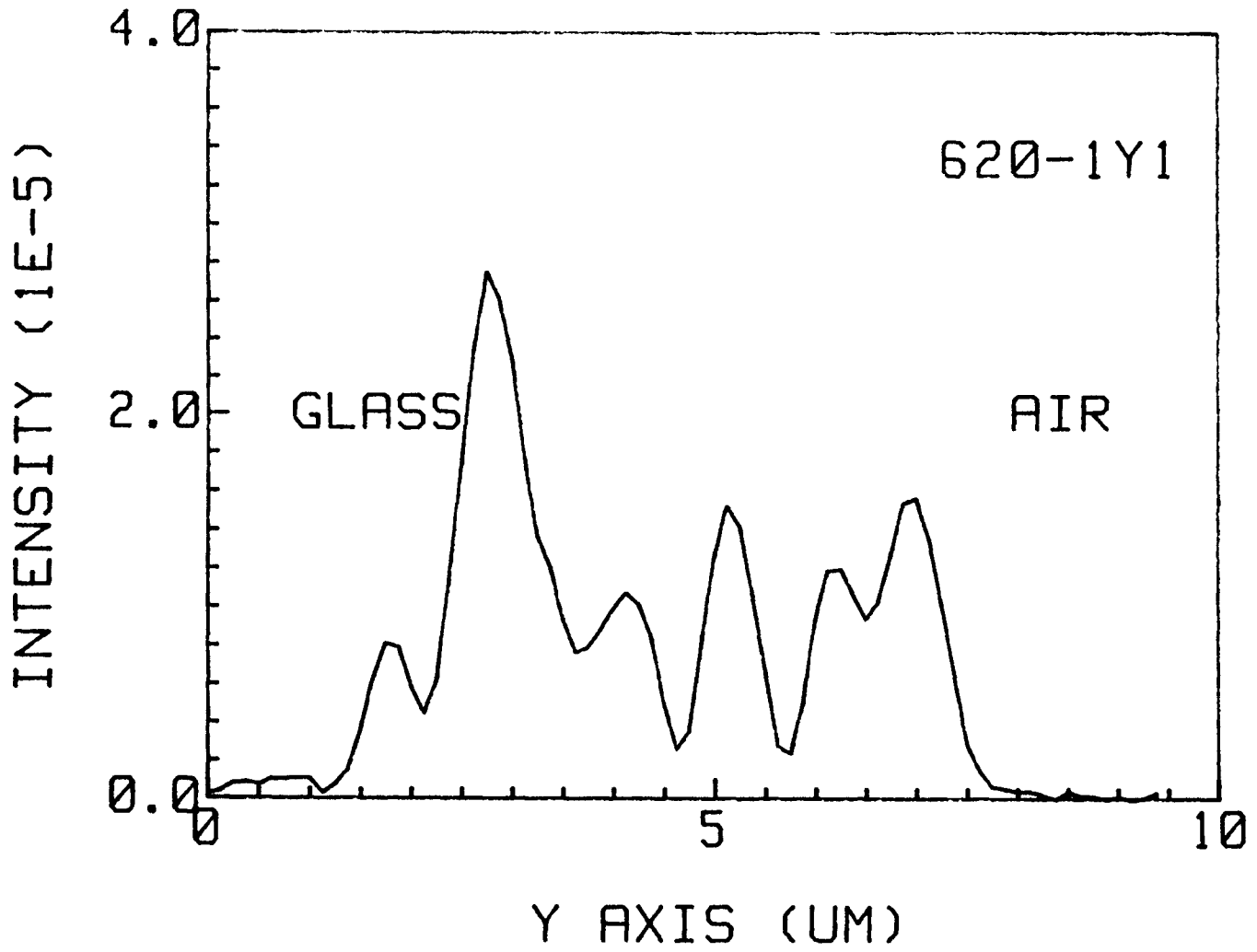

Figure 5.20 Near-field pattern of grating waveguide (sample 3) in vertical direction (TE).

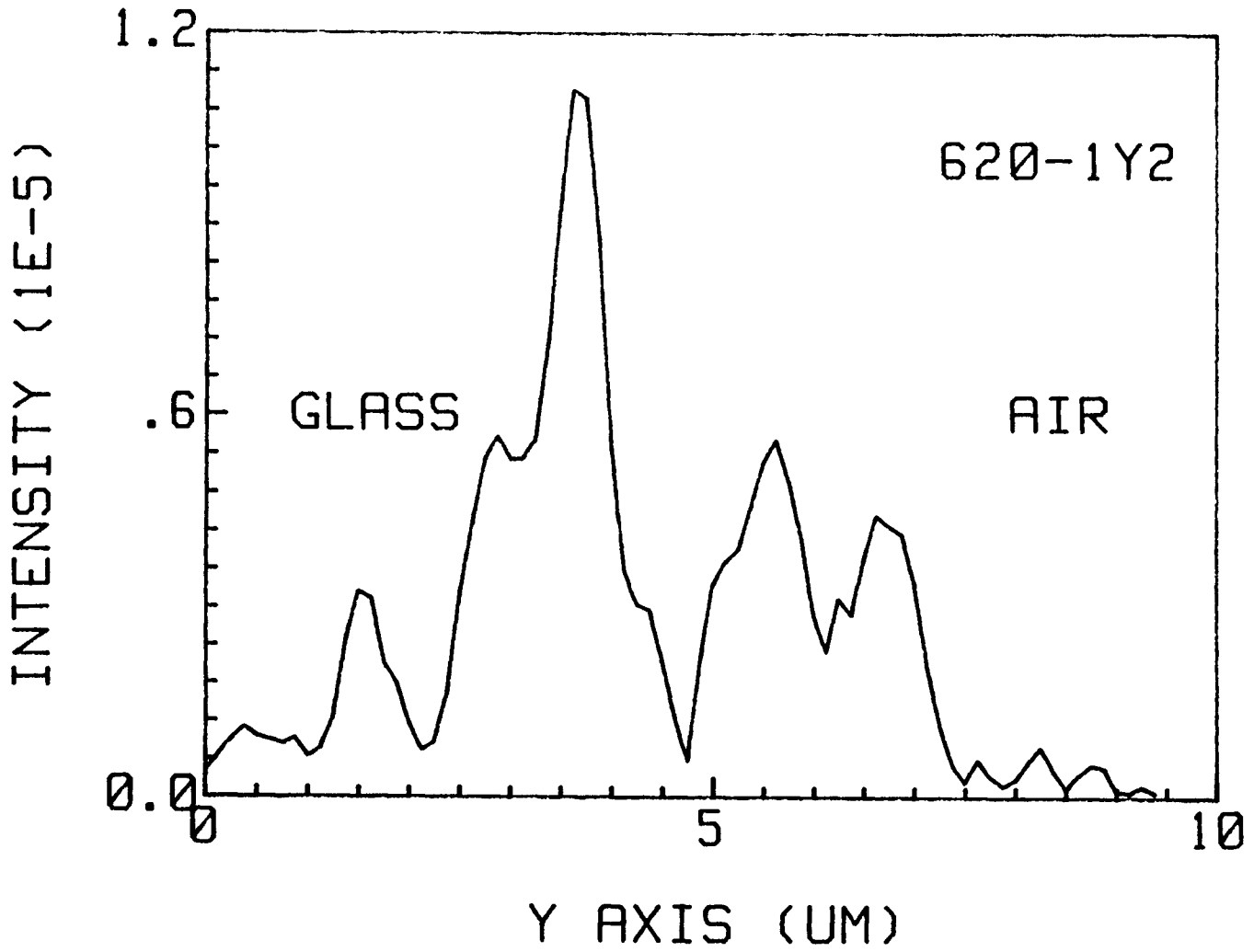

Figure 5.21 Near-field pattern of grating waveguide (sample 3) in vertical direction (TM).

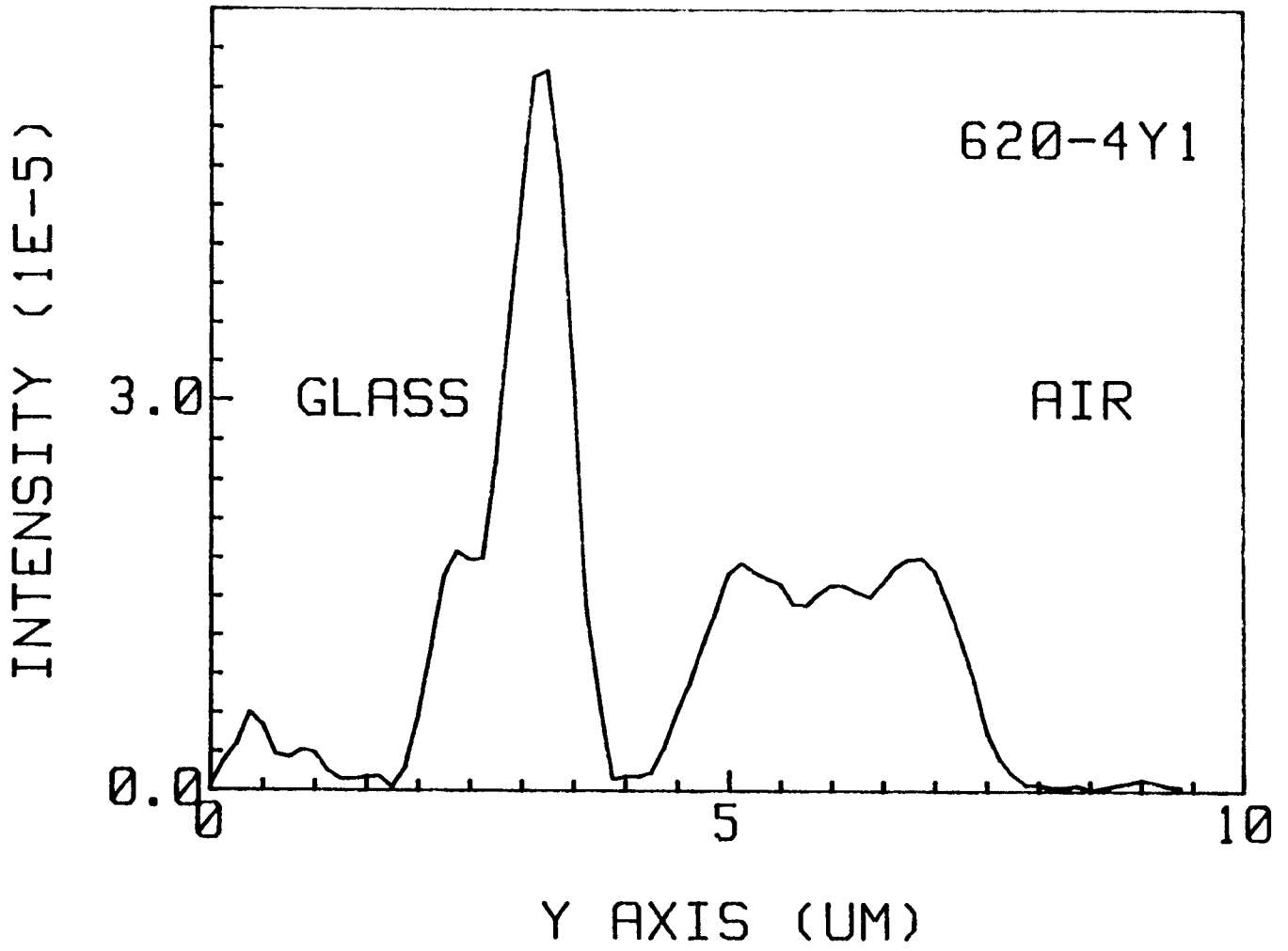

Figure 5.22 Near-field pattern of grating waveguide (sample 4) in vertical direction (TE).

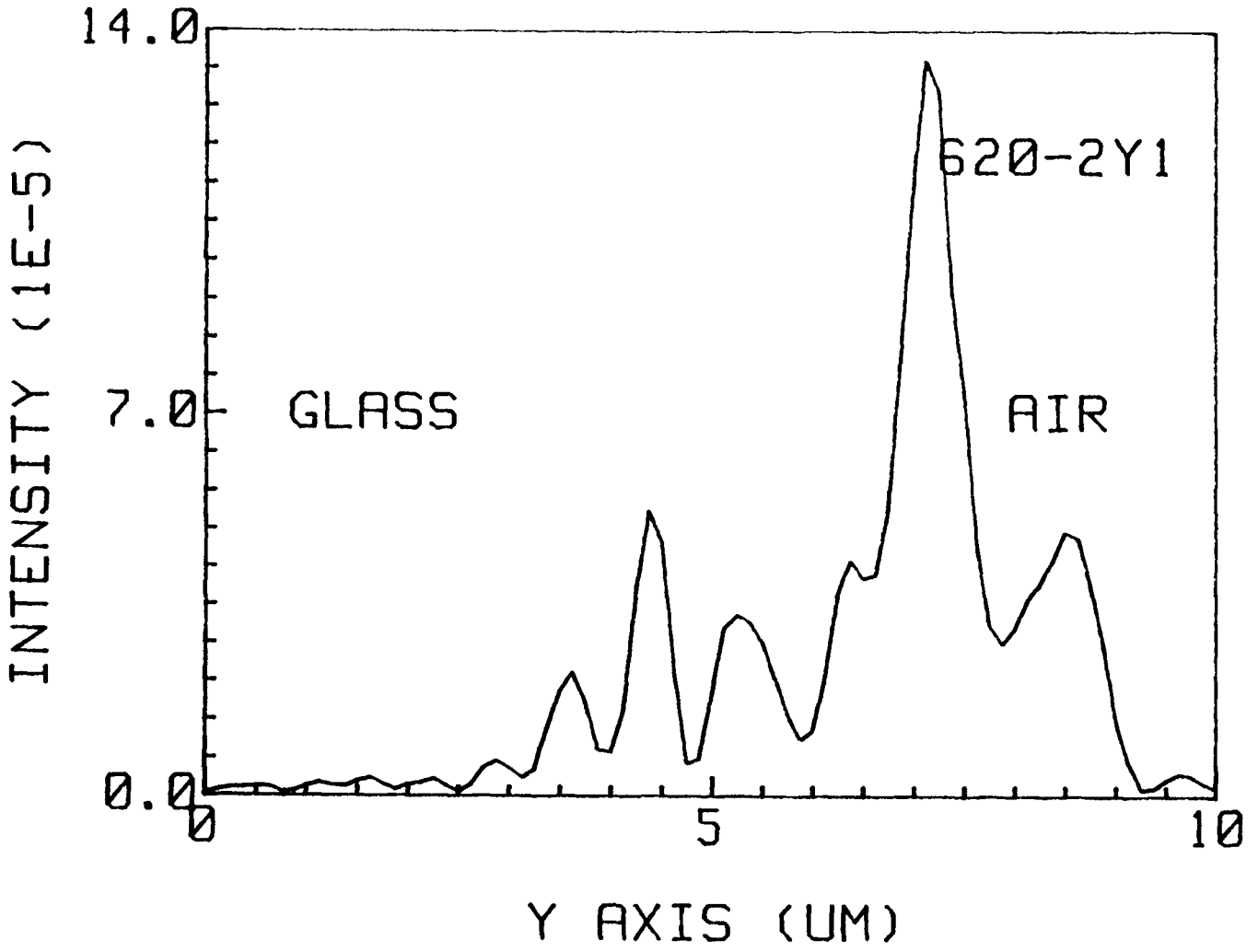

Figure 5.23 Near-field pattern of grating waveguide (sample 5) in vertical direction (TE).

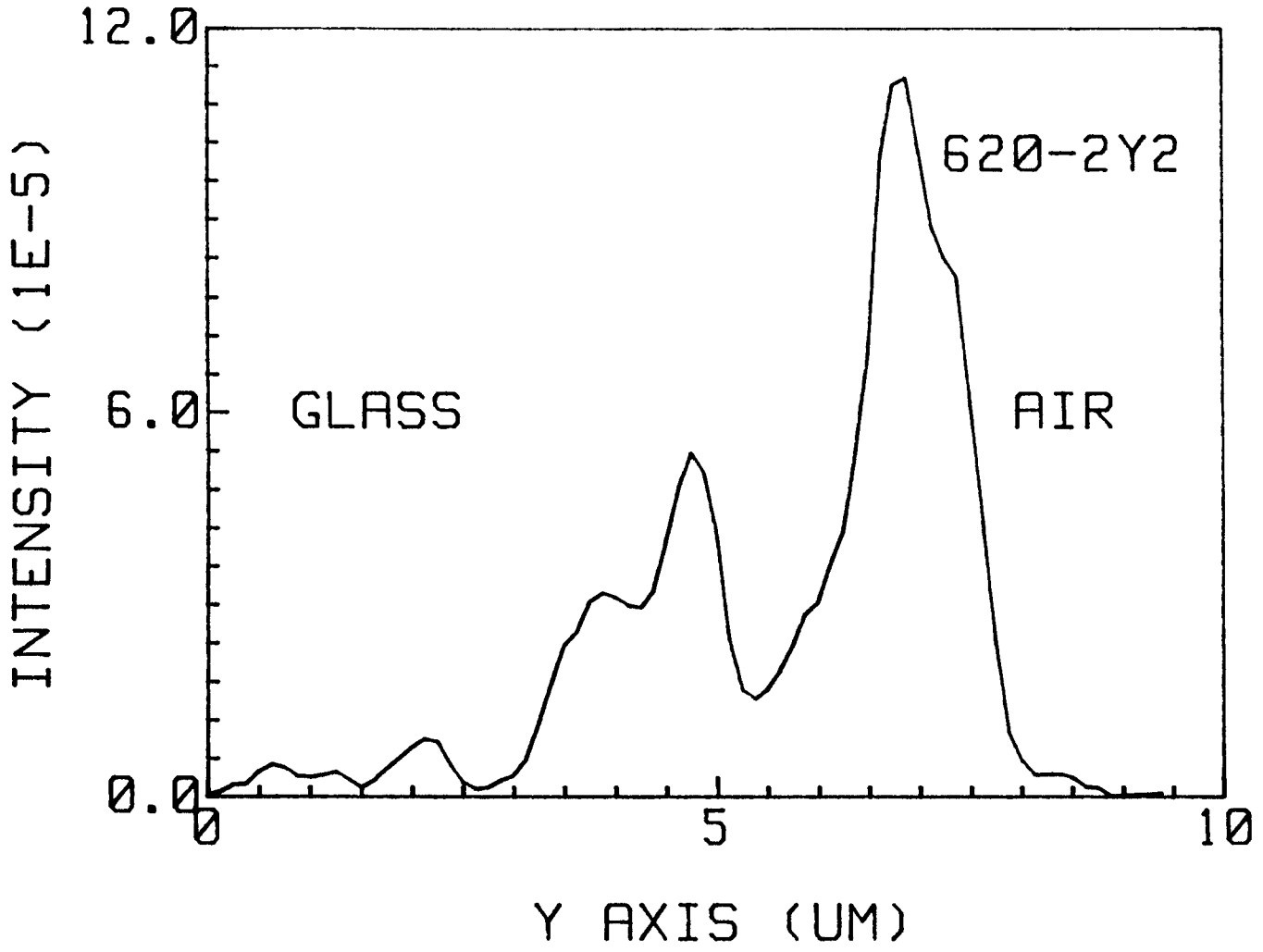

Figure 5.24 Near-field pattern of grating waveguide (sample 5) in vertical direction (TM).

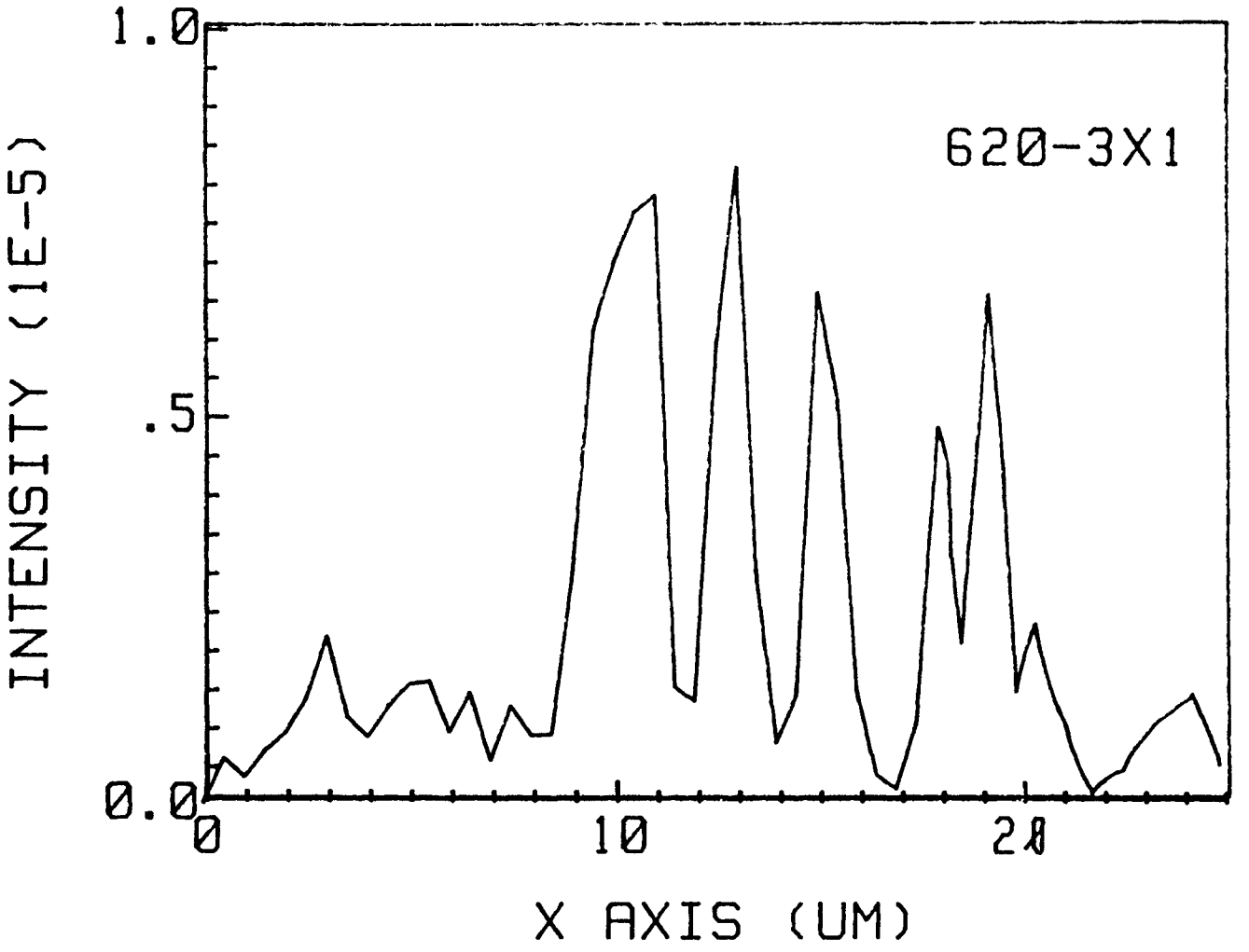

Figure 5.25 Near-field pattern of rectangular waveguide (sample 2) in horizontal direction (TE).

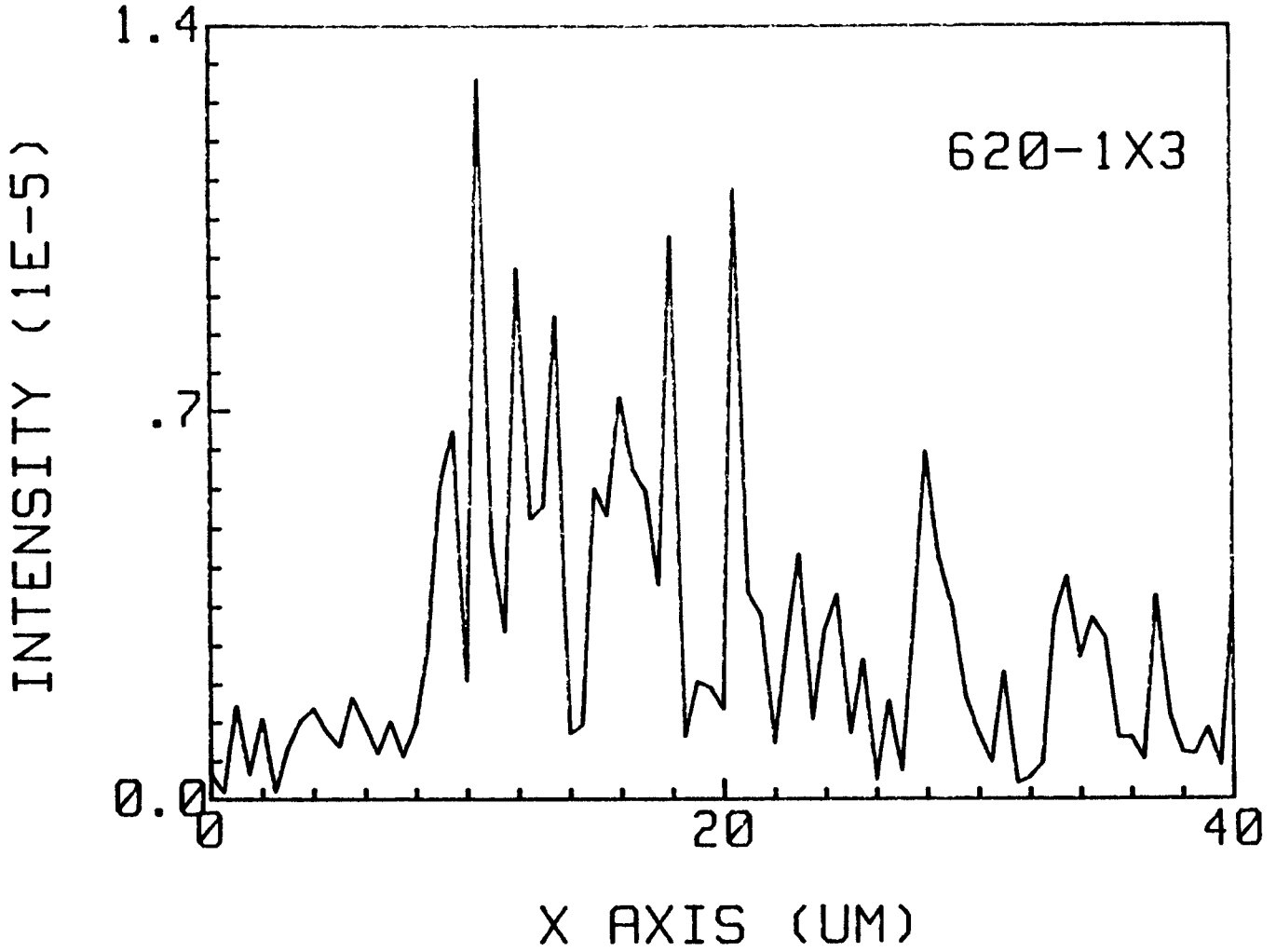

Figure 5.26 Near-field pattern of rectangular waveguide (sample 3) in horizontal direction (TE).

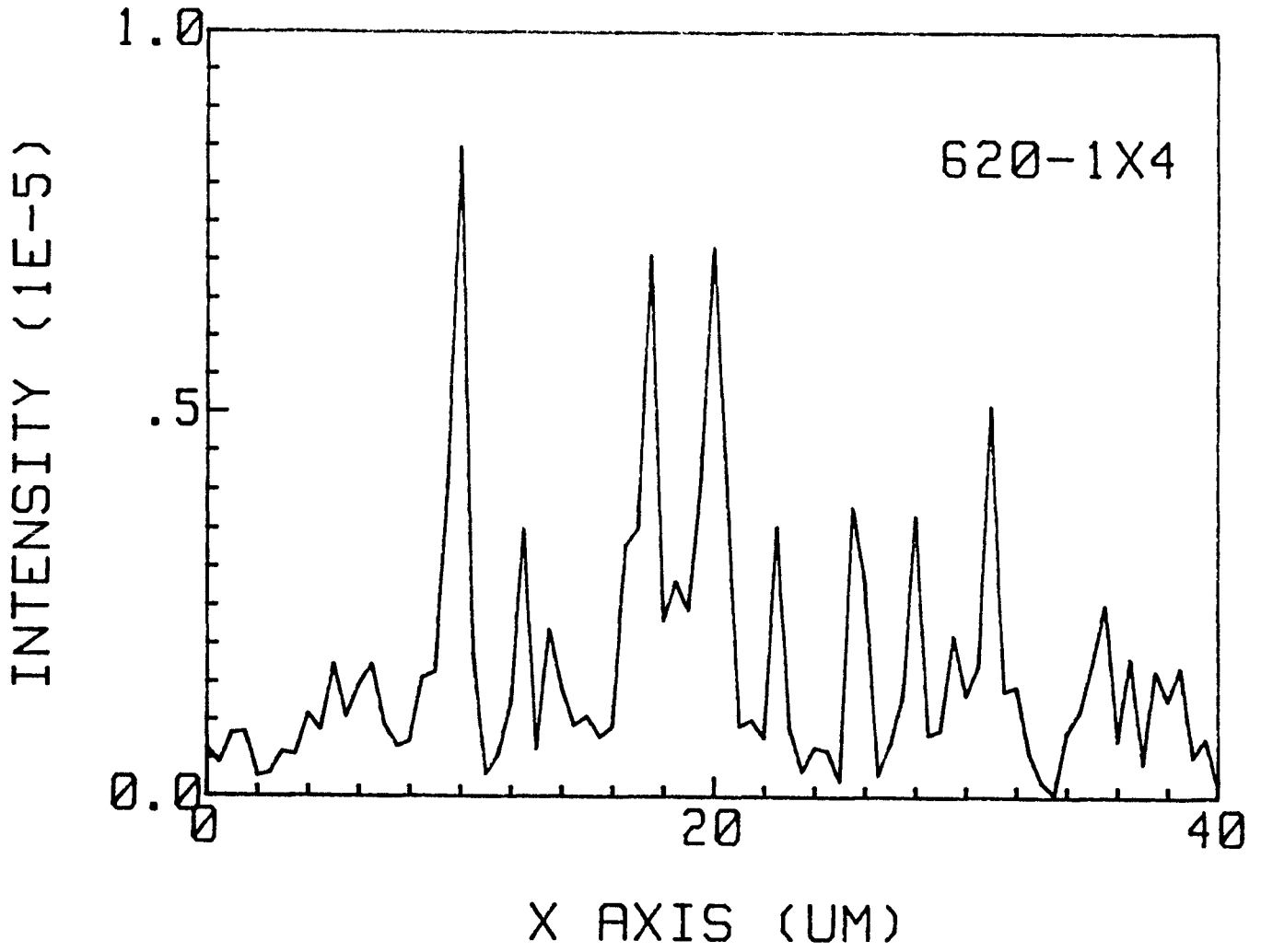

Figure 5.27 Near-field pattern of rectangular waveguide (sample 3) in horizontal direction (TM).

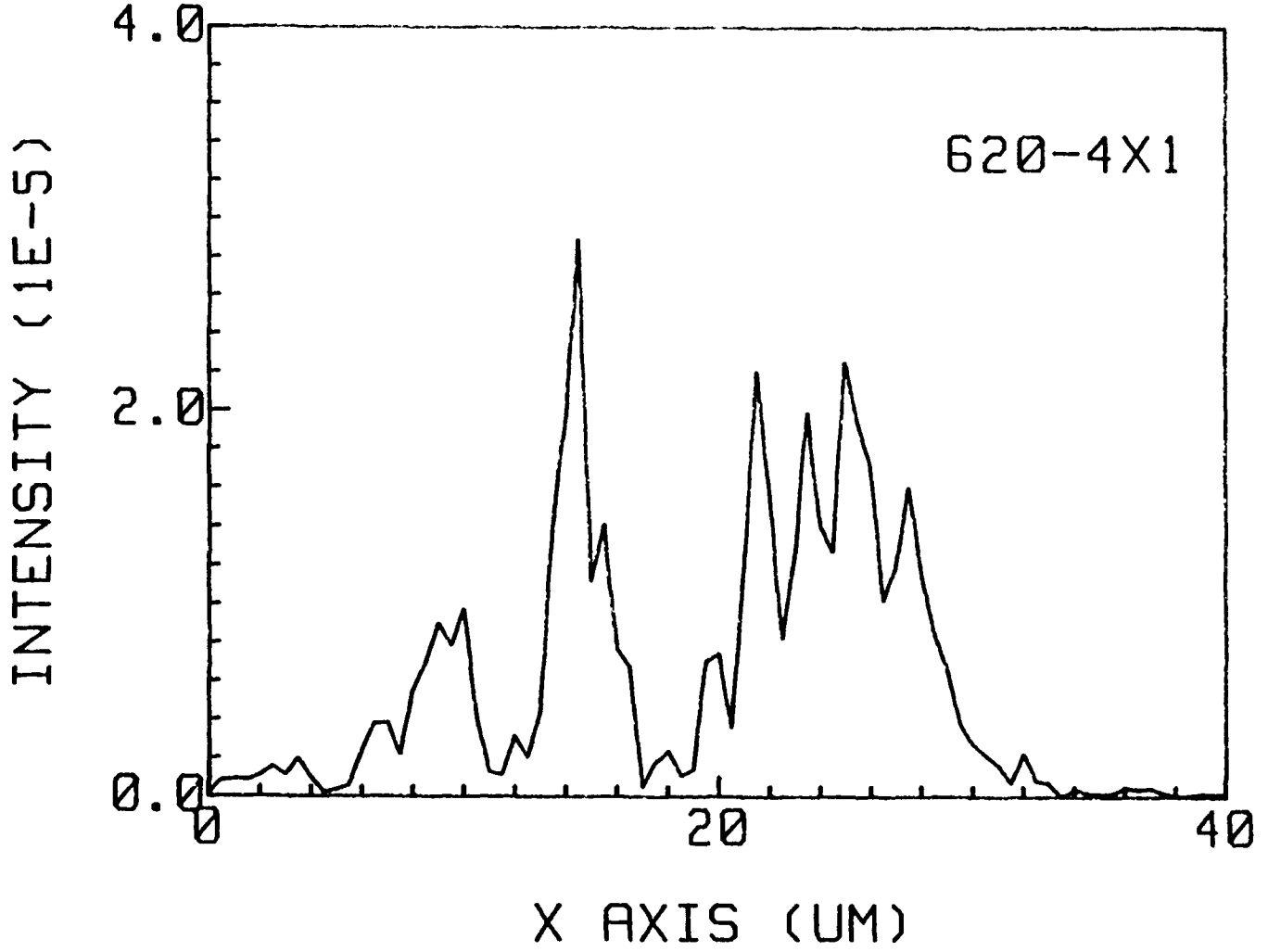

Figure 5.28 Near-field pattern of rectangular waveguide (sample 4) in horizontal direction (TE).

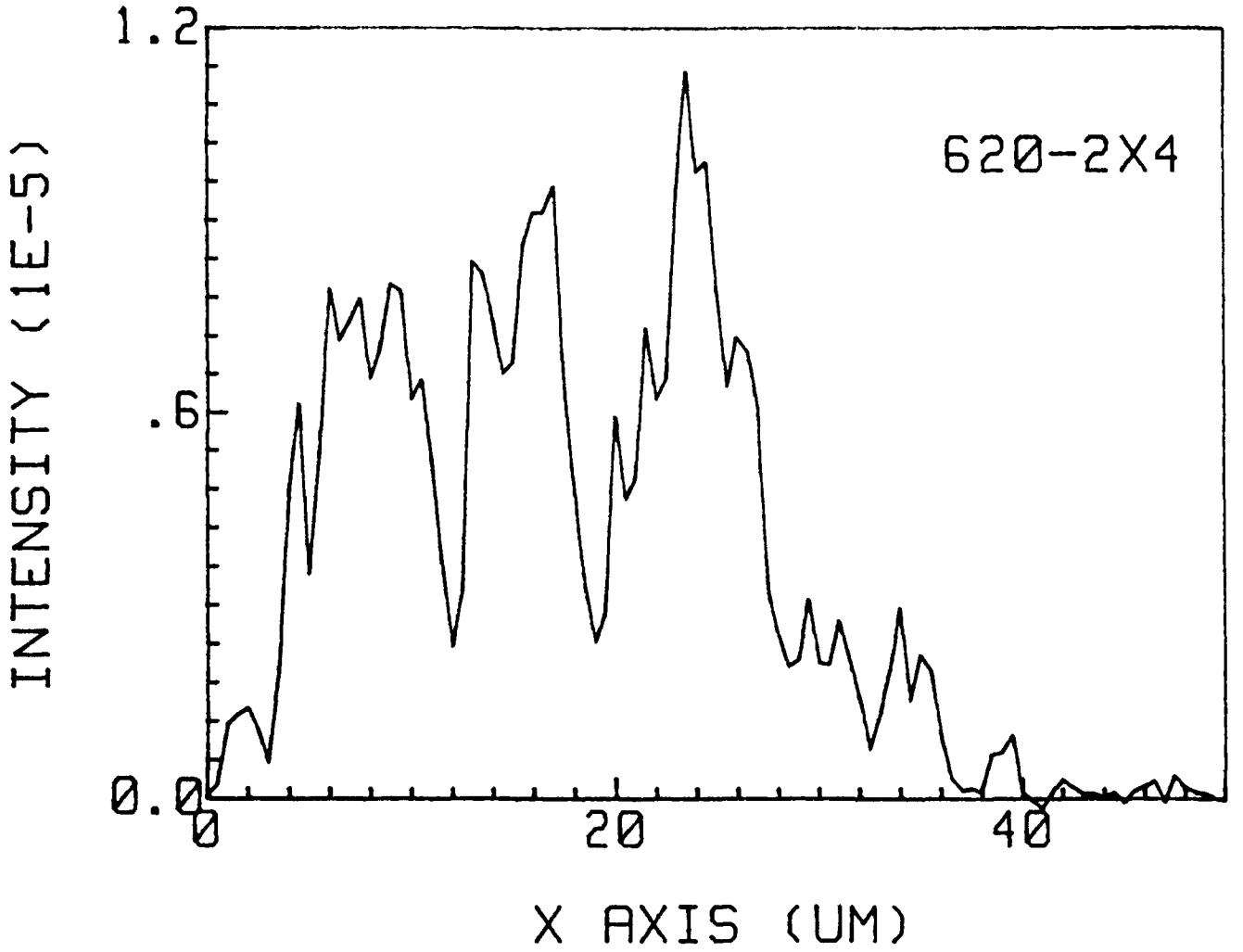

Figure 5.29 Near-field pattern of rectangular waveguide (sample 5) in horizontal direction (TE).

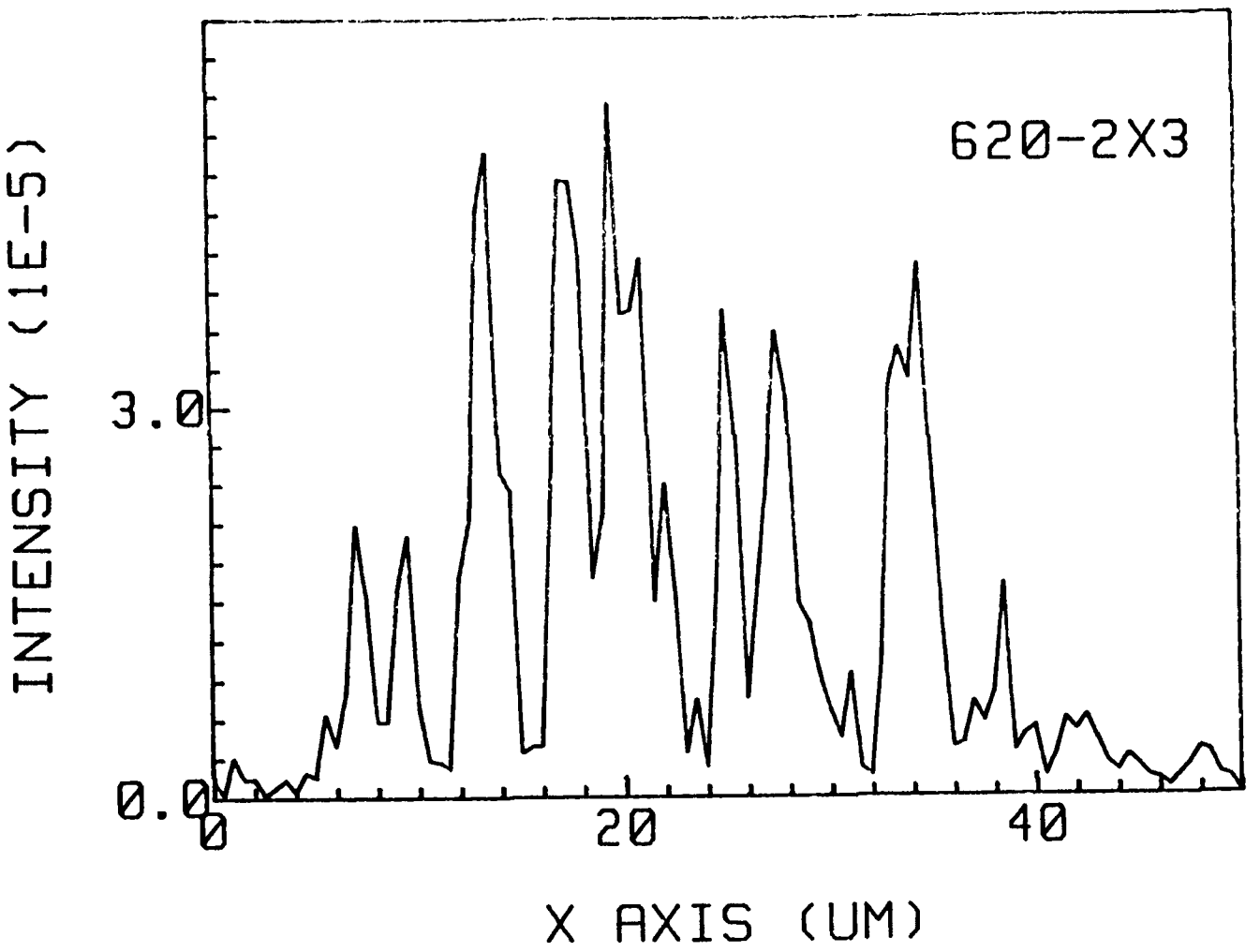

Figure 5.30 Near-field pattern of rectangular waveguide (sample 5) in horizontal direction (TM).

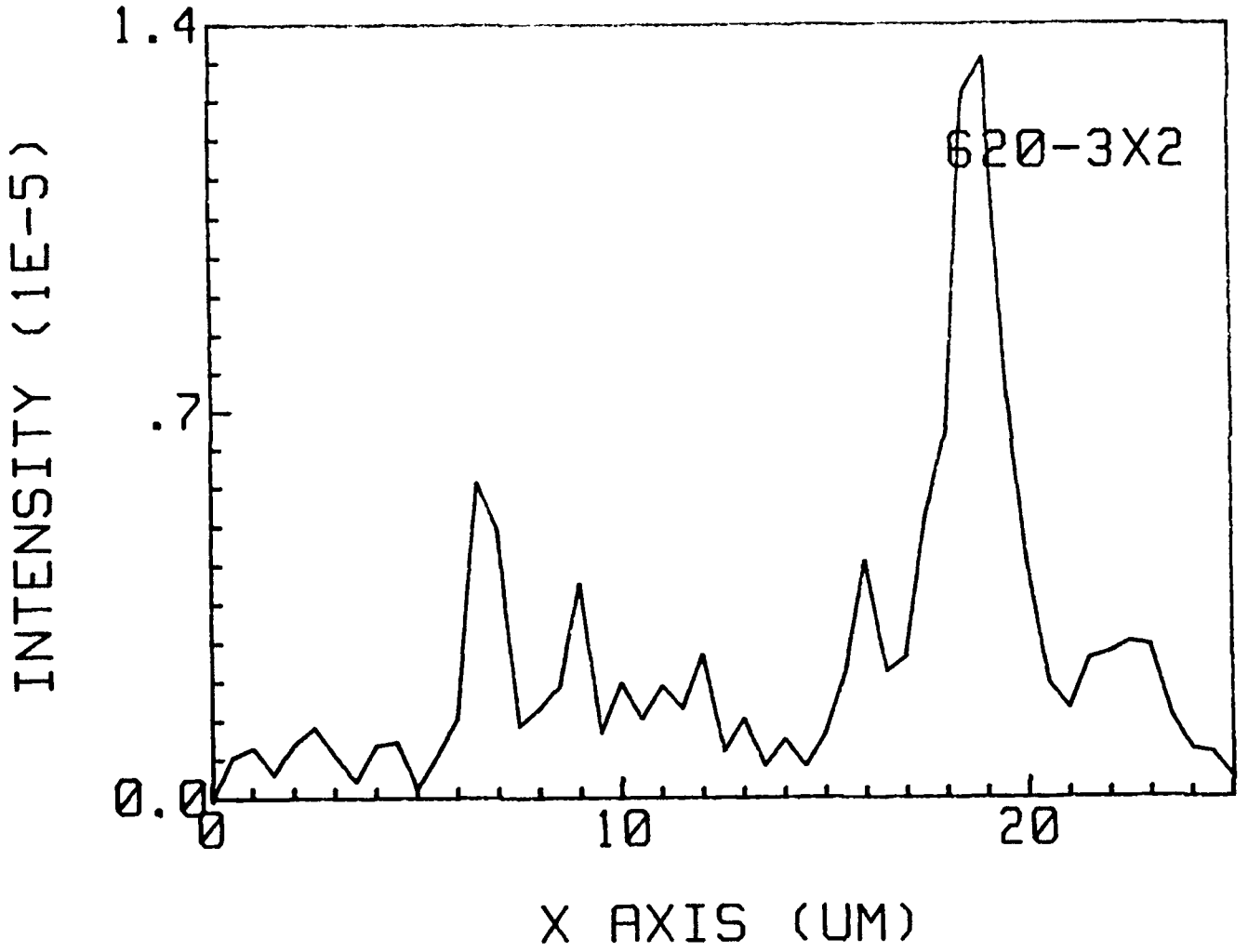

Figure 5.31 Near-field pattern of grating waveguide (sample 2) in horizontal direction (TE).

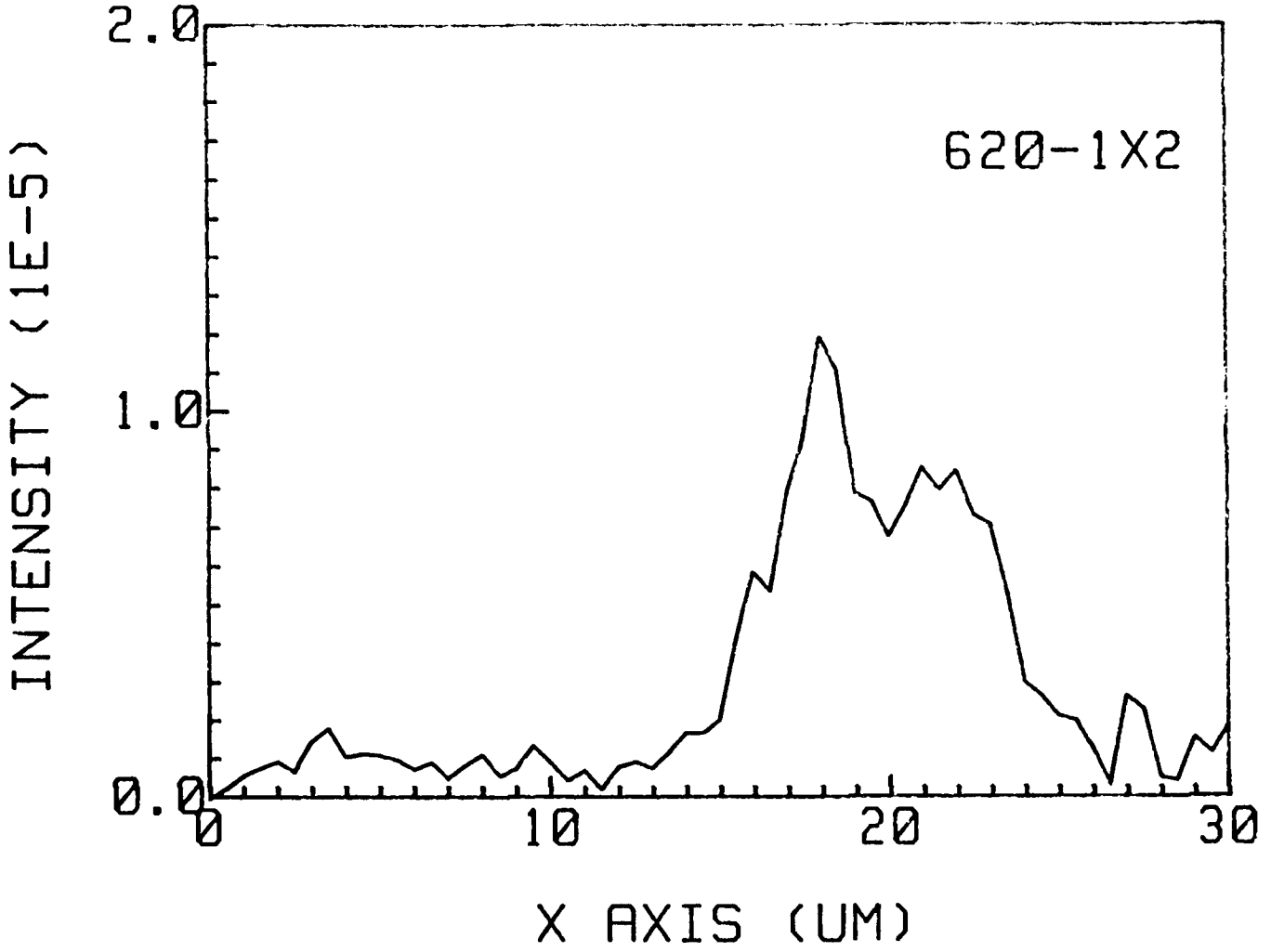

Figure 5.32 Near-field pattern of grating waveguide (sample 3) in horizontal direction (TE).

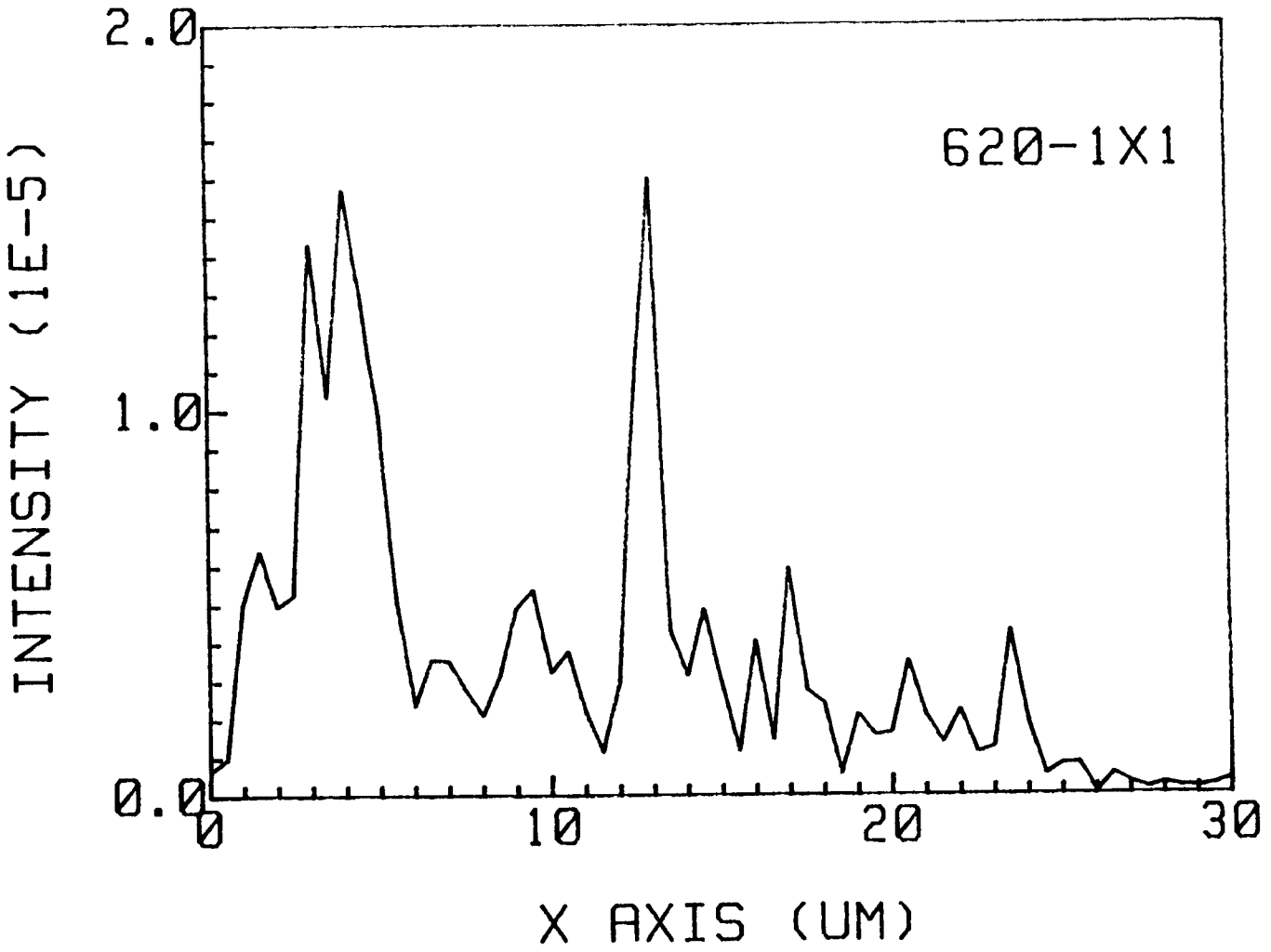

Figure 5.33 Near-field pattern of grating waveguide (sample 3) in horizontal direction (TM).

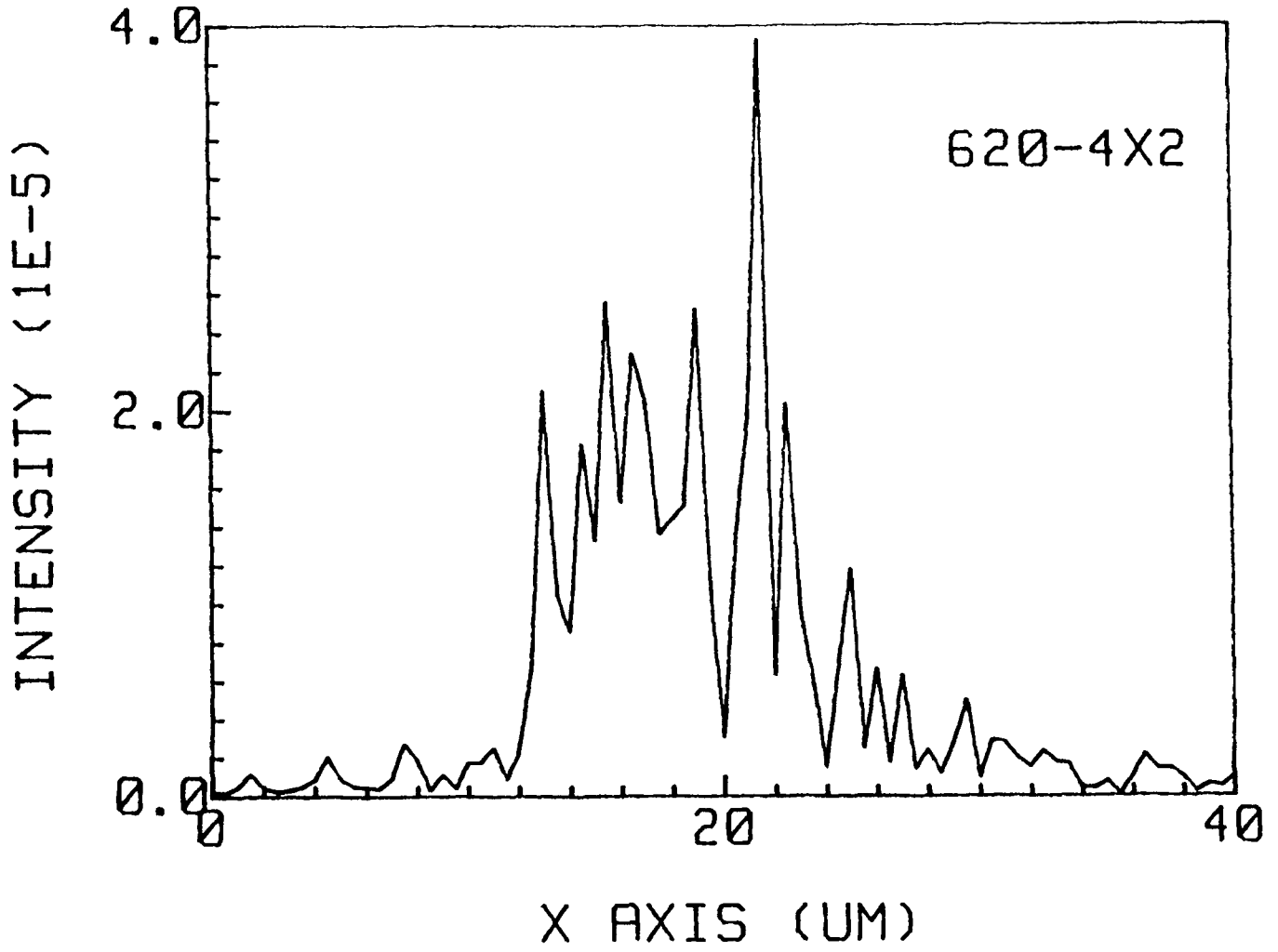

Figure 5.34 Near-field pattern of grating waveguide (sample 4) in horizontal direction (TE).

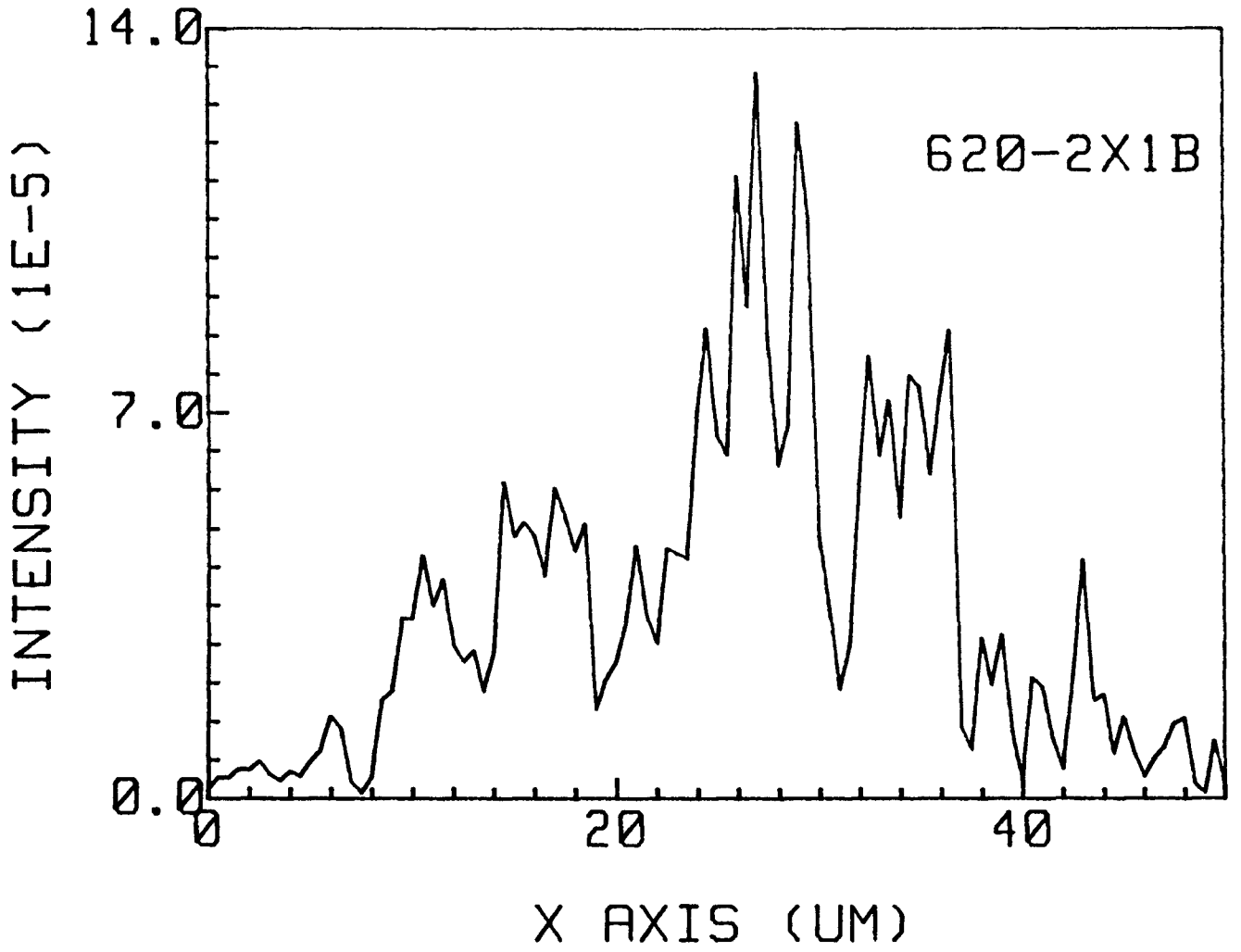

Figure 5.35 Near-field pattern of grating waveguide (sample 5) in horizontal direction (TE).

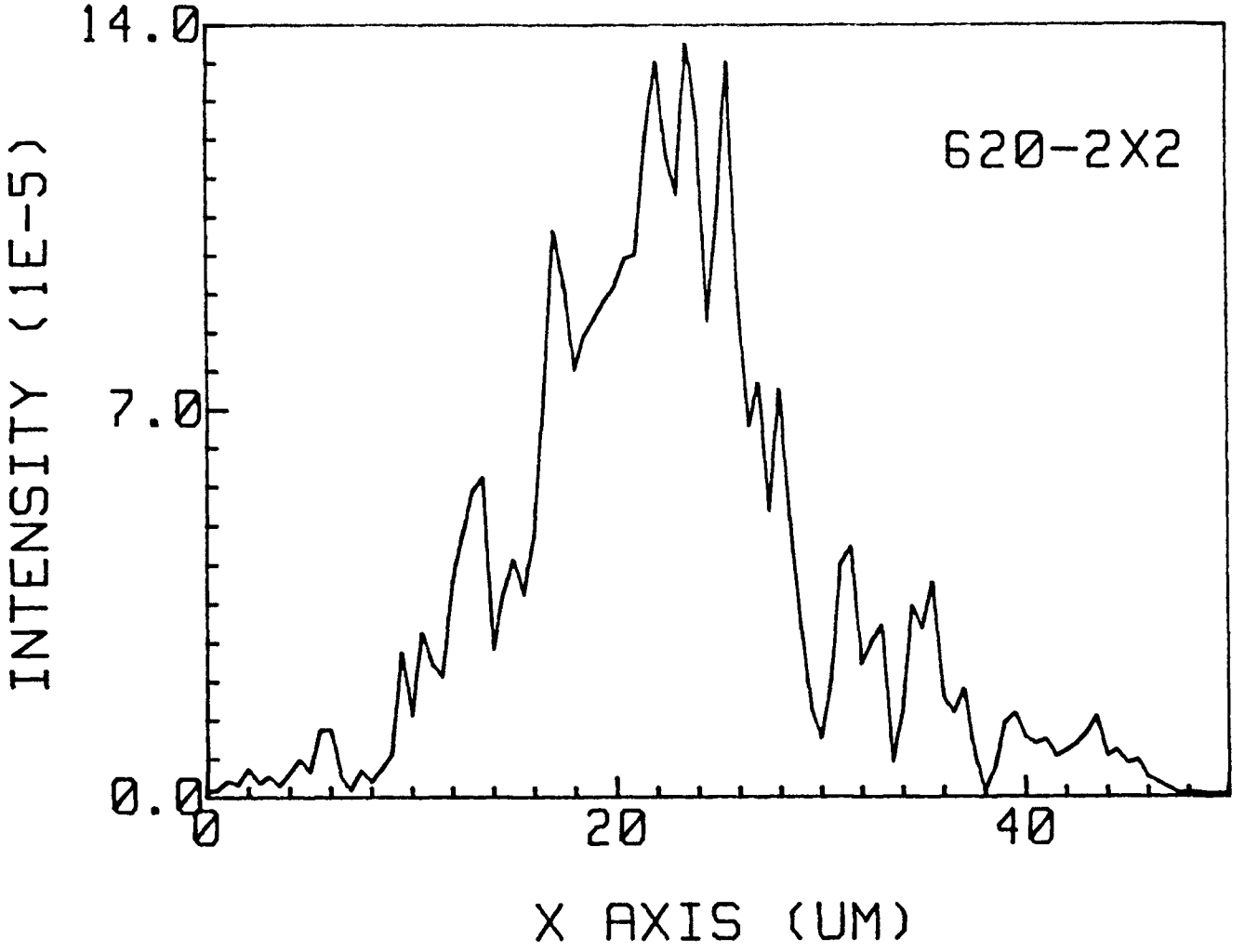

Figure 5.36 Near-field pattern of grating waveguide (sample 5) in horizontal direction (TM).

CHAPTER 6

CONCLUSIONS AND SUGGESTIONS

We have fabricated, analyzed and tested Bragg waveguides for optical integrated circuits. These waveguides have been shown to have good confinement and, to certain extent, mode selectivity based on the periodicity of the confining structures.

Suggested future work:

1. To further investigate the profile of refractive index of waveguide with ablated metal on glass.
2. For plasma polymerization use RF power supply instead of AC power supply to increase the efficiency of deposition.
3. By means of prism coupler, measure and calculate the effective mode index for each selective excited mode of our thin and thick silver-clad waveguides. Then use the theory of grating waveguides to calculate the best confining conditions of confinement.
4. Improve the resolution of the Laser pattering technique to achieve smaller grating pitch.

APPENDIX A

COMPUTER PROGRAMS

```
10    CLEAR SCREEN
20    PRINT "*************************************************************************
*************"
30    PRINT "THIS PROGRAM IS DESIGNED TO:"
40    PRINT "1. RECORD THE DATA WHICH COME FROM THE SR510 LOCK-IN APLIFIER VIA GP
IB INTERFACE"
50    PRINT "2. PLOT THE GRAPH FOR YOUR DBAT FILE"
60    PRINT "3. CHECK YOUR DBAT FILE"
70    PRINT "4. DATA ENTRY TO CREATE YOUR DBAT FILE"
80    PRINT "5. RECORDE THE DATA WHICH COME FROM THE SPECTROMETER"
90    PRINT "6. RATIO TWO DATA "
100   PRINT "7.QUIT"
110   PRINT
120   PRINT "                                                ------ WEI ZHONG  1992.3
"
130   PRINT "*************************************************************************
************"
140   PRINT " PLEASE MAKE YOUR CHOISE. (1, 2, 3, 4, 5, 6, 7)"
150   INPUT Ch
160   IF Ch=1 THEN GOTO 250
170   IF Ch=2 THEN GOTO 1600
180   IF Ch=3 THEN GOTO 860
190   IF Ch=4 THEN GOTO 1260
200   IF Ch=5 THEN GOTO 2500
210   IF Ch=6 THEN GOTO 3150
220   IF Ch=7 THEN GOTO 3630
230   GOTO 150
240!---------------------------------------- RECORDER DATA--------
250    PRINT "   THE MAXIMUM DATA OF THIS PROGRAM HAS BEEN SET TO 500"
260    DIM X(1:500),Y(1:500),X2(1:500),Y2(1:500)
270    DIM A(1:500),B(1:500),P(1:500),Q(1:500)
280    BEEP
290    INPUT "PLEASE INPUT YOUR START POINT OF X AXIS",S
300    INPUT "PLEASE INPUT YOUR END POINT OF X AXIS",E
310    INPUT "PLEASE INPUT YOUR INCREMENT OF X AXIS",M
320    INPUT "PLEASE INPUT THE WAITING TIME (SECOND) YOU NEED BEWEEN TWO DATA",T1
330    N=INT((E-S)/M+.5)
340    PRINT "START"
350    ASSIGN @Path TO 723
360    FOR I=1 TO N+1 STEP 1
370    WAIT T1
380    G=0
390    FOR J=1 TO 2
400    OUTPUT @Path;"Q"
410    ENTER @Path;C
420    WAIT .1
430    G=G+C
440    NEXT J
450    Y(I)=G/2
460    X(I)=S+(I-1)*M
470    PRINT X(I),Y(I)
480    BEEP
490    NEXT I
500    ASSIGN @Path TO *
510    BEEP
520    Xmax=-1.0E+308
530    Ymax=-1.0E+308
540    Xmin=1.0E+308
550    Ymin=1.0E+308
560    FOR I=1 TO N+1 STEP 1
570    IF X(I)>Xmax THEN Xmax=X(I)
580    IF X(I)<Xmin THEN Xmin=X(I)
```

```
590   IF Y(I)>Ymax THEN Ymax=Y(I)
600   IF Y(I)<Ymin THEN Ymin=Y(I)
610   NEXT I
620   PRINT "YOUR DATA X-AXIS RANGE IS FROM";S;"TO";E;",INCREMENT IS ";M
630   PRINT "YOUR DATA Y-AXIS RANGE IS FROM";Ymin;"TO";Ymax;",TOTAL";N+1;"DATA"
640   PRINT "DO YOU WANT TO SAVE THE DATA(Y OR N)?"
650   INPUT A$
660   IF A$="Y" THEN GOTO 730
670   IF A$="N" THEN GOTO 690
680   GOTO 640
690   INPUT "DO YOU WANT TO MEASURE AGAIN?(Y OR N)",F$
700   IF F$="Y" THEN GOTO 290
710   IF F$="N" THEN GOTO 10
720   GOTO 690
730   PRINT 'INPUT THE FILE NAME TO SAVE THE DATA"
740   ENTER 2;File$
750   ON ERROR GOTO 830
760   CREATE BDAT File$,1
770   ASSIGN @Path_2 TO File$
780   FOR I=1 TO N+1 STEP 1
790   OUTPUT @Path_2;X(I),Y(I)
800   NEXT I
810   ASSIGN @Path_2 TO *
820   GOTO 690
830   PRINT 'DUPLICATE FILE NAME.INPUT FILE NAME AGAIN."
840   GOTO 740
850 !-----------------------------------------------CHECK BDAT---
860   PRINT "ENTER THE BDAT FILENAME TO BE OPENED."
870   ENTER 2;File1$
880   ON ERROR GOTO 1210
890   ASSIGN @Path_3 TO File1$
900   No6=0
910   FOR I=1 TO 500 STEP 1
920   ENTER @Path_3;A(I),B(I)
930   ON ERROR GOTO 970
940   No6=No6+1
950   PRINT I,A(I),B(I)
960   NEXT I
970   ASSIGN @Path_3 TO *
980 INPUT 'DO YOU WANT TO CORRECT THE DATA? (Y OR N)",As3$
990 IF As3$= Y' THEN GOTO 1010
1000 IF As3$='N' THEN GOTO 1100
1010 INPUT "WHICH ONE? (GIVE NUMBER)",No3
1020 PRINT
1030 PRINT "WRONG :',No3,A(No3),B(No3)
1040 INPUT "ENTER CORRECT DATA. (X,Y)",Cx1,Cy1
1050 A No3)=Cx1
1060 B(No3)=Cy1
1070 PRINT
1080 PRINT "RIGHT:",No3,A(No3),B(No3)
1090 GOTO 980
1100  INPUT 'DO YOU WANT TO SAVE?(Y OR N)",As4$
1110  IF As4$="N' THEN GOTO 1200
1120  INPUT "ENTER FILE NAME TO SAVE.",File2$
1130  CREATE BDAT File2$,1
1140  ON ERROR GOTO 1230
1150  ASSIGN @Path TO File2$
1160   FOR I=1 TO No6 STEP 1
1170   OUTPUT @Path;A(I),B(I)
1180   NEXT I
1190   ASSIGN @Path TO *
1200   GOTO 10
1210   PRINT "CAN'T FIND IT."
1220   GOTO 860
1230   PRINT "DUPLICATE FILE NAME, INPUT AGAIN."
1240   GOTO 1130
```

```
1250!-------------------------------------------------DATA ENTRY---
1260 INPUT "HOW MANY PAIR OF DATA DO YOU WANT TO INPUT?",No1
1270 PRINT "X-AXIS=","  Y-AXIS="
1280 FOR I=1 TO No1 STEP 1
1290 INPUT P(I),Q(I)
1300 NEXT I
1310 PRINT "No.","X","Y"
1320 FOR I=1 TO No1 STEP 1
1330 PRINT I,P(I),Q(I)
1340 NEXT I
1350 INPUT "DO YOU WANT TO CORRECT THE DATA? (Y OR N)",As$
1360 IF As$="Y" THEN GOTO 1380
1370 IF As$="N" THEN GOTO 1450
1380 INPUT "WHICH ONE? (GIVE NUMBER)",No2
1390 PRINT
1400 PRINT No2,P(No2),Q(No2)
1410 INPUT "ENTER CORRECT DATA. (X,Y)",Cx,Cy
1420 P(No2)=Cx
1430 Q(No2)=Cy
1440 GOTO 1350
1450 INPUT "INPUT THE FILE NAME TO SAVE",File3$
1460 CREATE BDAT File3$,1
1470 ON ERROR GOTO 1560
1480 ASSIGN @Path TO File3$
1490 FOR I=1 TO No1 STEP 1
1500 PRINT I,P(I),Q(I)
1510 OUTPUT @Path;P(I),Q(I)
1520 NEXT I
1530 ASSIGN @Path TO *
1540 WAIT 3
1550 GOTO 1580
1560 PRINT "DUPLICATE FILE NAME.  INPUT FILE NAME AGAIN'
1570 GOTO 1450
1580  GOTO 10
1590!-------------------------------------------------PLOT----
1600  GINIT
1610  GRAPHICS ON
1620  PRINTER IS CRT
1630  PRINT "PLASE ENTER THE DBAT FILE NAME"
1640  ENTER 2;File4$
1650  ON ERROR GOTO 2480
1660  ASSIGN @Path_1 TO File4$
1670  N2=0
1680  FOR I=1 TO 500 STEP 1
1690  ENTER @Path_1;X2(I),Y2(I)
1700  ON ERROR GOTO 1740
1710  PRINT X2(I),Y2(I)
1720  N2=N2+1
1730  NEXT I
1740  X2max=-1.0E+308
1750  Y2max=-1.0E+308
1760  X2min=1.0E+308
1770  Y2min=1.0E+308
1780  FOR I=1 TO N2 STEP 1
1790  IF X2(I)>X2max THEN X2max=X2(I)
1800  IF X2(I)<X2min THEN X2min=X2(I)
1810  IF Y2(I)>Y2max THEN Y2max=Y2(I)
1820  IF Y2(I)<Y2min THEN Y2min=Y2(I)
1830  NEXT I
1840  ASSIGN @Path_1 TO *
1850  PRINT "YOUR DATA X-AXIS RANGE IS FROM";X2min;"TO";X2max
1860  PRINT "YOUR DATA X-AXIS RANGE IS FROM";Y2min;"TO";Y2max
1870  PRINT "DATA POINT=",N2
1880  INPUT "PLEASE INPUT YOUR GRAPH'S TITLE',T1$
1890  INPUT "PLEASE INPUT YOUR GRAPH'S X-AXIS LABEL",X$
1900  INPUT "PLEASE INPUT YOUR GRAPH'S Y-AXIS LABEL",Y$
```

```
1910  INPUT "PLEASE SELECT YOUR GRAPH'S X-AXIS RANGE (XXX, XXX)",Xs,Xe
1920  INPUT "PLEASE SELECT YOUR GRAPH'S Y-AXIS RANGE (XXX,XXX)",Ys,Ye
1930  INPUT "PLEASE SELECT THE NUMBER OF TICKS FOR X-AXIS.(MULTIPLE OF 10)",Tx
1940  INPUT "PLEASE SELECT THE NUMBER OF TICKS FOR Y-AXIS.(MULTIPLE OF 10)",Ty
1950  Kx=(Xe-Xs)*10/Tx
1960  Ky=(Ye-Ys)*10/Ty
1970  R=Ky/Kx
1980  GOTO 2020
1990  GINIT
2000  GRAPHICS ON
2010  PLOTTER IS 705,"HPGL"
2020  CLEAR SCREEN
2030  FOR I=-.3 TO .3 STEP .1
2040  MOVE 60+I,100
2050  LORG 6
2060  LABEL T1$
2070  NEXT I
2080  CSIZE 5.0,.55
2090  LORG 5
2100  MOVE 65,18
2110  LABEL x$
2120  MOVE 90,80
2130  LABEL File4$
2140  DEG
2150  LORG 5
2160  LDIR 90
2170  MOVE 8,60
2180  LABEL Y$
2190  PEN 1
2200  VIEWPORT 30,110,30,90
2210  FRAME
2220  WINDOW Xs,Xe,Ys,Ye
2230  AXES Kx/10,Ky/10,Xs,Ys,10,10,3
2240  CLIP OFF
2250  CSIZE 5.0,.5
2260  LDIR 0
2270  LORG 6
2280  FOR I=Xs TO Xe STEP Kx
2290  MOVE I,Ys
2300  LABEL USING "#,DDD.      ";I
2310  NEXT I
2320  LORG 8
2330  FOR I=Ys TO Ye STEP Ky
2340  MOVE Xs-.05,I
2350  LABEL USING "#,DDD.DDDDD ";I
2360  NEXT I
2370  PENUP
2380  FOR I=1 TO N2 STEP 1
2390  IF X2(I)>Xe THEN 2420
2400  PEN 1
2410  PLOT X2(I),Y2(I)
2420  NEXT I
2430  INPUT "DO YOU WANT TO PLOT? ( Y OR N )",P1$
2440  IF P1$="Y" THEN GOTO 1990
2450  INPUT "AFTER YOU FINISH CHECKING ENTER 'E' TO QUIT",F12$
2460  IF F12$="E" THEN GOTO 1580
2470  GOTO 2450
2480  PRINT "CAN'T FIND IT"
2490  GOTO 1630
2500!---------------------------------------- SPECTROMETER/RECORDER--
2510 CLEAR SCREEN
2520 PRINT "PLEASE USE THE BURST TRIGGER SCAN MODE. "
2530 PRINT "SET 'START POS', 'END POS' AND 'INC' ON THE CD2 CONTROL PANEL"
2540  PRINT "    THE MAXIMUM DATA OF THIS PROGRAM HAS BEEN SET TO 500"
2550  BEEP
2560  INPUT "PLEASE INPUT YOUR START POS",S
```

```
2570  INPUT "PLEASE INPUT YOUR END POS",E
2580  INPUT "PLEASE INPUT YOUR INCREMENT",M
2590  INPUT "PLEASE INPUT THE WAITING TIME (SECOND) YOU NEED BEWEEN TWO DATA",T1
2600  N=INT((E-S)/M+.5)
2610  PRINT "START"
2620  ASSIGN @Path TO 723
2630  FOR I=1 TO N+1 STEP 1
2640  WAIT T1
2650  G=0
2660  FOR J=1 TO 2
2670  OUTPUT @Path;"Q"
2680  ENTER @Path;C
2690  WAIT 1
2700  G=G+C
2710  NEXT J
2720  Y(I)=G/2
2730  X(I)=S+(I-1)*M
2740  PRINT X(I),Y(I)
2750  BEEP
2760  OUTPUT @Path;"X6,";S
2770  WAIT .1
2780  OUTPUT @Path;"X6,";0
2790  NEXT I
2800  ASSIGN @Path TO *
2810  BEEP
2820  Xmax=-1.0E+309
2830  Ymax=-1.0E+309
2840  Xmin=1.0E+309
2850  Ymin=1.0E+309
2860  FOR I=1 TO N+1 STEP 1
2870  IF X(I)>Xmax THEN Xmax=X(I)
2880  IF X(I)<Xmin THEN Xmin=X(I)
2890  IF Y(I)>Ymax THEN Ymax=Y(I)
2900  IF Y(I)<Ymin THEN Ymin=Y(I)
2910  NEXT I
2920  PRINT "YOUR DATA X-AXIS RANGE IS FROM";S;"TO";E;",INCREMENT IS ";M
2930  PRINT "YOUR DATA Y-AXIS RANGE IS FROM";Ymin;"TO";Ymax;",TOTAL";N+1;"DATA"
2940  PRINT "DO YOU WANT TO SAVE THE DATA(Y OR N)?"
2950  INPUT A$
2960  IF A$="Y" THEN GOTO 3030
2970  IF A$="N" THEN GOTO 2990
2982  GOTO 2940
2990  INPUT "DO YOU WANT TO MEASURE AGAIN?(Y OR N)",F$
3000  IF F$="Y" THEN GOTO 2560
3010  IF F$="N" THEN GOTO 10
3020  GOTO 2990
3030  PRINT "INPUT THE FILE NAME TO SAVE THE DATA"
3040  ENTER 2;File$
3050  ON ERROR GOTO 3130
3060  CREATE BDAT File$,1
3070  ASSIGN @Path_2 TO File$
3080  FOR I=1 TO N+1 STEP 1
3090  OUTPUT @Path_2;X(I),Y(I)
3100  NEXT I
3110  ASSIGN @Path_2 TO *
3120  GOTO 2990
3130  PRINT "DUPLICATE FILE NAME.INPUT FILE NAME AGAIN."
3140  GOTO 3040
3150!-----------------------------------------------RATIO BDAT---
3160 CLEAR SCREEN
3170 PRINT " YOU CAN USE THIS PROGRAM TO GET Y1 / Y2.  X1(I), Y1(I) COME FROM FI
LE1. X2(I),Y2(I) COME FROM FILE2. X1(I), X2(I) HAVE TO BE EQUAL."
3180 PRINT
3190  PRINT "ENTER THE BDAT FILENAME1 TO BE OPENED."
3200  ENTER 2;File1$
3210  ON ERROR GOTO 1210
```

```
3220  ASSIGN @Path1 TO File1$
3230  N1=0
3240  PRINT "I","  X1","Y1"
3250  WAIT .2
3260  FOR I=1 TO 500 STEP 1
3270  ENTER @Path1;A(I),B(I)
3280  ON ERROR GOTO 3320
3290  N1=N1+1
3300  PRINT I,A(I),B(I)
3310  NEXT I
3320  ASSIGN @Path13 TO *
3330  PRINT "ENTER THE BDAT FILENAME2 TO BE OPENED."
3340  ENTER 2;File2$
3350  ON ERROR GOTO 1210
3360  ASSIGN @Path2 TO File2$
3370  N2=0
3380  PRINT "I","X2","Y2"
3390  WAIT .2
3400  FOR I=1 TO 500 STEP 1
3410  ENTER @Path2;P(I),Q(I)
3420  ON ERROR GOTO 3460
3430  N2=N2+1
3440  PRINT I,P(I),Q(I)
3450  NEXT I
3460  ASSIGN @Path2 TO *
3470  PRINT "I","X  ","Y1/Y2"
3480  WAIT .3
3490  FOR I=1 TO N1 STEP 1
3500  IF P(I)<>A(I) THEN PRINT "WARNIG: A<>C"
3510  X(I)=A(I)
3520  Y(I)=B(I)/Q(I)
3530  PRINT I,X(I),Y(I)
3540  NEXT I
3550  INPUT "ENTER FILENAME TO SAVE.",File3$
3560  CREATE BDAT File3$,1
3570  ASSIGN @Path3 TO File3$
3580  FOR I=1 TO N1 STEP 1
3590  OUTPUT @Path3;X(I),Y(I)
3600  NEXT I
3610  ASSIGN @Path3 TO *
3620  GOTO 10
3630  CLEAR SCREEN
3640  END
```

APPENDIX B

PLASMA POLYMERIZATION

B.1 Theory of Plasma Polymerization

Another method for the deposition of polymer film involves a plasma polymerization process. In plasma polymerization, an electrical discharge is created in a vapor containing low-weight organic molecules called monomers. The discharge causes an ionization and fragmentation of the monomers and a subsequent rebounding of the fragments into a much larger two- or three- dimensional structure. When a substrate such as glass is introduced into the discharge, the polymer is deposited on its surface. Plasma polymerized organic films have several features distinct from conventional polymer films. In general, plasma polymerized polymer are highly crosslinked, insoluble, and pinhole free as well as heat resistant. In addition, no catalyst is required in this polymerization technique.

B.1.1 Mechanism of Polymer Formation in a Glow Discharge

A glow discharge plasma can be defined as a region of relatively low pressure and low temperature gas in which a degree of ionization in a quasineutral state is sustained by the presence of energetic electrons.

By examining the discussions of mechanisms which have been proposed, two major approaches to explaining plasma polymerization may be discerned [B.1]. In the first

approach, which is called plasma-induced polymerization, polymerization is assumed to take place on an electrode or other solid substrate as a result of monomer adsorption and the subsequent bombardment of the monomer by ions and radicals produced in the plasma. The second approach, which can be called plasma polymerization, assumes that free radials or ionic species are produced in the gas phase and that these may interact among themselves or with the monomer to produce active species of larger molecular weight, i.e., oligomers. The formation of a film occurs when both the original species and the oligomers diffuse to the substrate surface where they can react further. The processes involved can be represented schematically, as in Fig. B.1 [B.2].

It seems reasonable to believe that both approach to explaining plasma polymerization have merit and that one may predominate over the other depending upon the condition and apparatus used for polymerization. The same conclusion may be drawn for the choice of active species.

In contrast to conventional polymerization, i.e., molecular polymerization, polymer formation in glow discharge may be characterized as elemental or atomic polymerization. That is, in glow discharge polymerization, the molecular structure of a monomer is not retained, and the original monomer molecules serve as the source of elements which will be used in the construction of large molecules. Therefore, glow discharge polymerized styrene is

not polystyrene. Also, glow discharge polymerized benzene is not polybenzene, but glow discharge polymers of styrene and of benzene are very much alike.

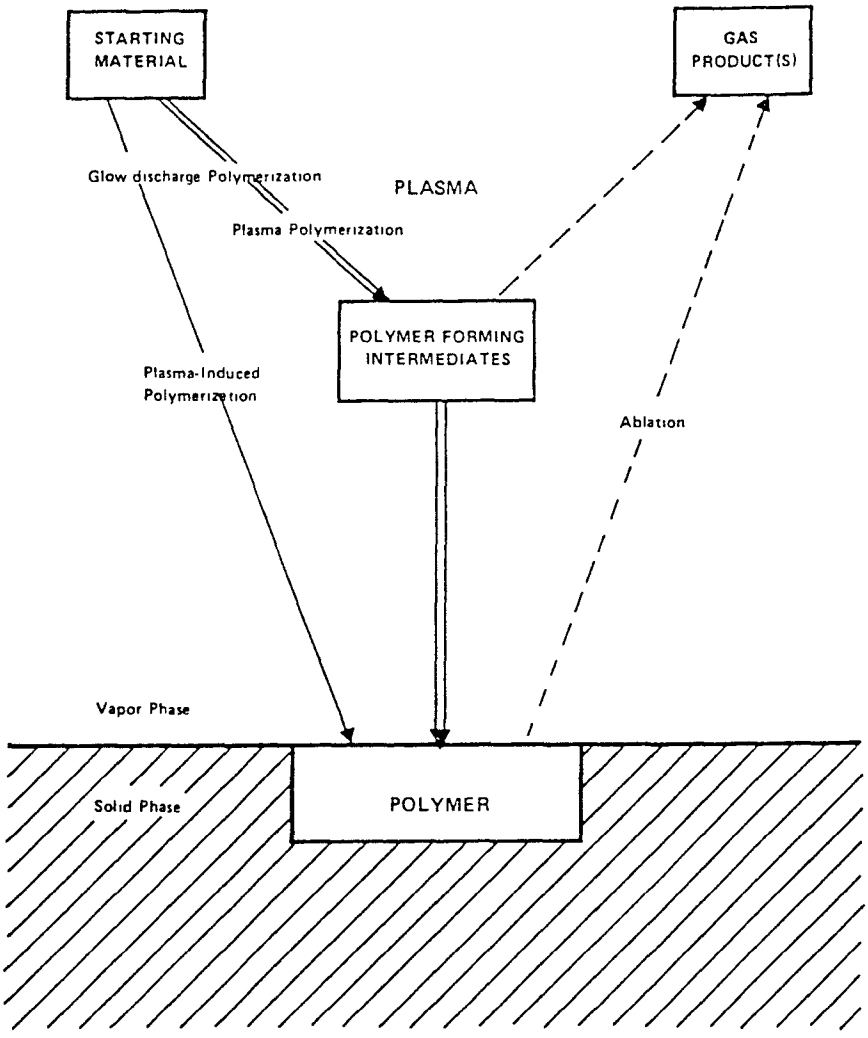

Figure B.1 Overall mechanism of glow discharge polymerization.

A polymer formed by glow discharge polymerization cannot be identified by the starting material since the molecular structure of the starting material is not retained in the polymer structure. This leads to another important point-- the glow discharge polymerization or polymer formed by glow discharge of a starting material are highly dependent on the system or conditions under which the polymer is formed.

B.1.2 Processing Factors of Glow discharge Polymerization

a. Modes of Electric Discharge

Electric power source with frequencies in the 0 (dc) to gigahertz (microwave) range can be used for glow discharge polymerization. The use of a low frequency electric power source (up to about the audio frequency range) require internal electrodes. With high frequencies, external electrodes or a coil also can be used. Typical combinations of discharge modes and reactor design are shown schematically in Fig. B.2.

b. Flow Rate

The flow rate in most cases of glow discharge polymerization simply refers to the feeding-in rate of the starting materials into the total vacuum system, and it does not necessarily mean the rate at which the starting material is fed to the region of the system where polymerization occurs.

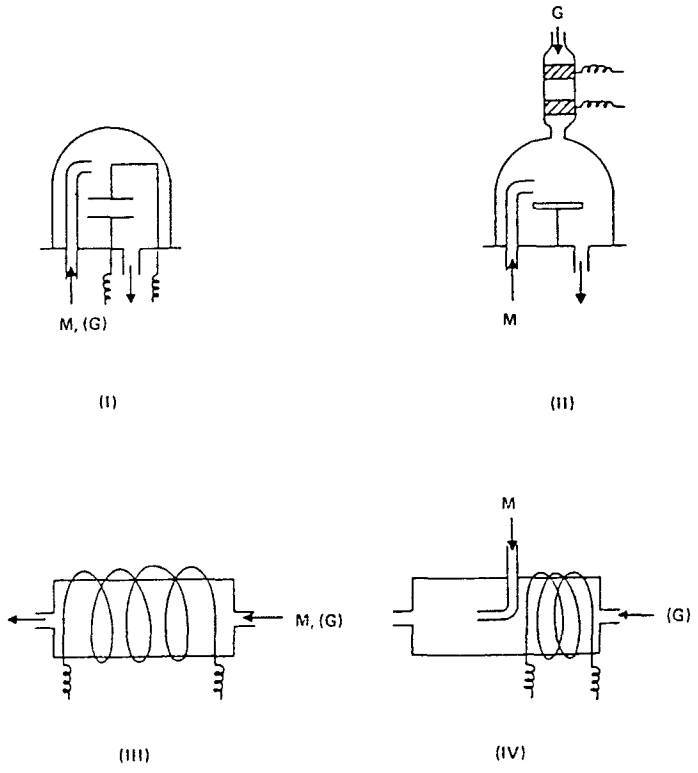

Figure B.2 Schematic representation of some typical arrangements of electric discharge, flow of starting material M, (and carrier gas G), and the location of polymer deposition.

c. System Pressure

The system pressure is perhaps the most misunderstood and ill-treated parameter of glow discharge polymerization. Efficient glow discharge polymerization is an excellent pump Fig. b.3.[B.3]. The initial pressure at a given flow rate is dependent on the pumping rate of the system as shown by the two lines representing systems with without liquid nitrogen.

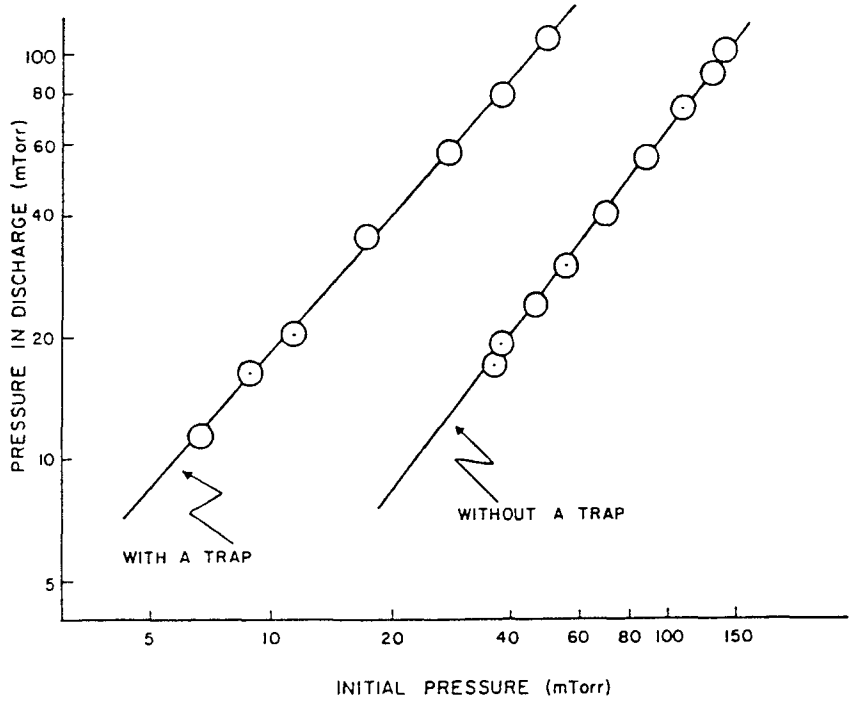

Figure B.3 The dependence of system pressure in the discharge on the initial system pressure, for glow discharge polymerization of ethlene.

d. Discharge Power

The significance of discharge power in glow discharge polymerization is quite different from that for nonpolymer-forming plasmas. In essence, (the absolute value of) discharge power itself cannot be considered as an independent variable of the operation, since a certain level of discharge power in a given set of discharge conditions for one starting material could not even initiate a glow discharge with another starting material under otherwise identical conditions. The discharge power necessary for glow

discharge polymerization depends on both the molecular weight and chemical structure of the compounds.

The best first-order approach to dealing with this situation is to use the parameter given by W/FM, where W is the power input, F the flow rate given in cubic centimeters (STP) per minute, and M the molecular weight of starting material [B.4]. The parameter W/FM represents the power input per unit mass of the starting material. The parameter W/FM does not contain terms of that describe the geometric factor of and flow pattern within a reactor, and consequently, the absolute value cannot be used in general cases. However, it is a useful parameter to describe glow discharge polymerization of different starting materials in a polymerization reactor.

e. Geometrical Factor of Reactor

1. Bypass Ratio of Flow

Not all staring materials fed into a glow discharge polymerization reactor are utilized in the polymer formation. The bypass ratio represents the portion of flow which does not contribute to glow discharge polymerization. Consequently, the higher the bypass ratio of a reactor is, the lower the conversion of the starting material to the polymer. Clearly, this ratio depends on the ratio of the volume occupied by discharge to the total volume.

2. Relative Position of Energy-Input and Polymer Deposition

In glow discharge polymerization which utilizes internal electrodes either the substrate is placed directly on an electrode surface or in the space between the electrodes.

3. Relative Location of the Feed-In of the starting Material and Flow Pattern

The location where the starting material is introduced is very important for polymer deposition. This factor is less obvious in a system with internal electrodes (e.g., in a bell jar).

B.2 EXPERIMENT

B.2.1 System Setup for Plasma Polymerization

The plasma polymerization system of our experimental setup is shown in Fig. B.4. It is composed of:

(1) a glass vacuum chamber

(2) a pair of internal electrodes

(3) vacuum pumps (mechanical pump and diffusion pump)

(4) AC power supply

(5) monomer container

(6) carrier gas cylinder

(7) instrumentation, including: flow meters, pressure meter, T.C gauge, ionization gauge and needle valves, etc.

The two parallel electrodes are made of stainless steel plate. Their size is 4.5 inch by 4.5 inch. The top one has many small holes, so the carrier gas and monomer can go through it, to enter the space between electrodes.

The AC power supply can provides maximum ac voltage 1000 V (maximum ac current is 15 mA). Fig. B.5 shows the electric circuit for the AC power supply.

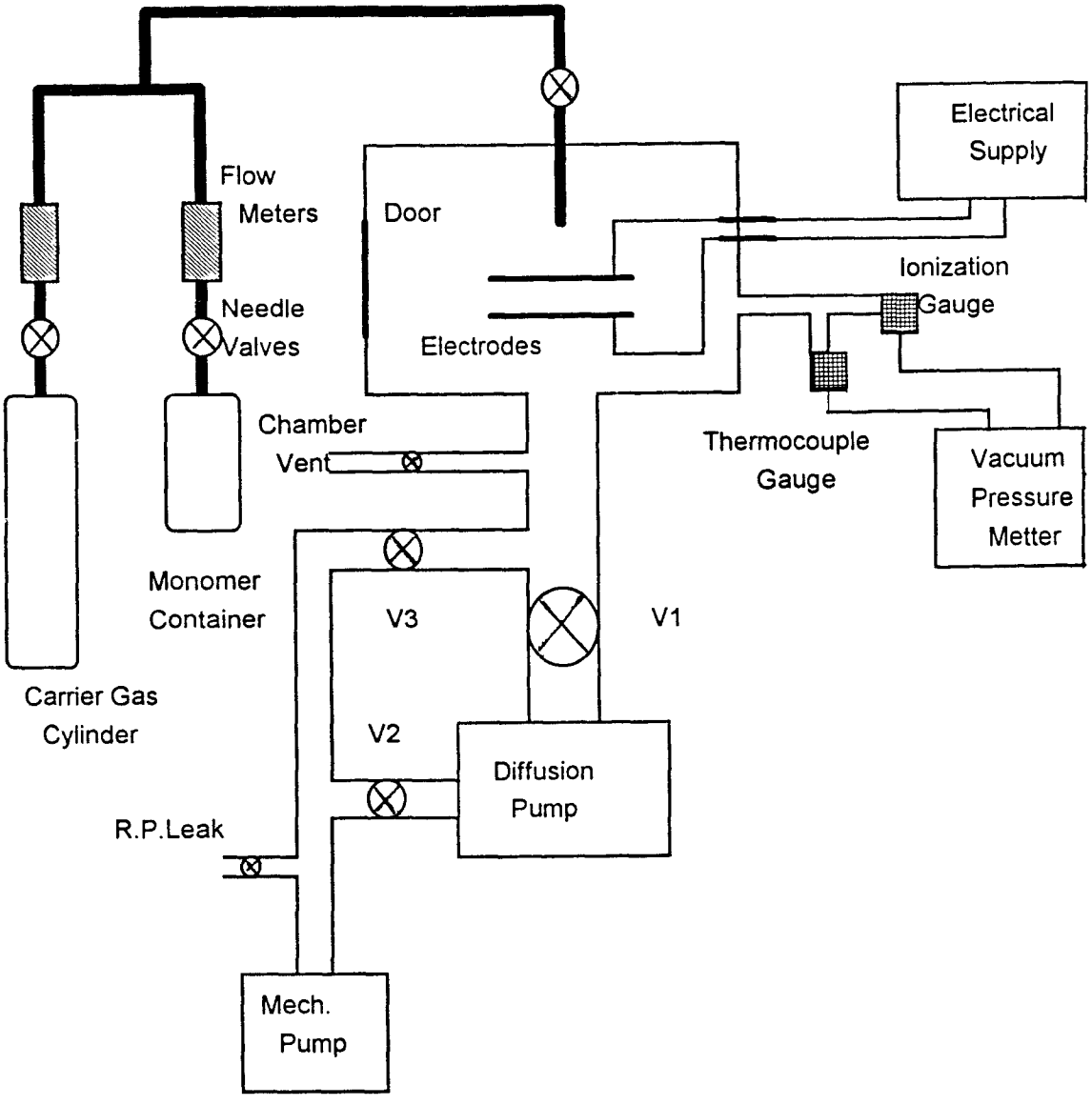

Figure B.5 Schematic representation of plasma polymerization system.

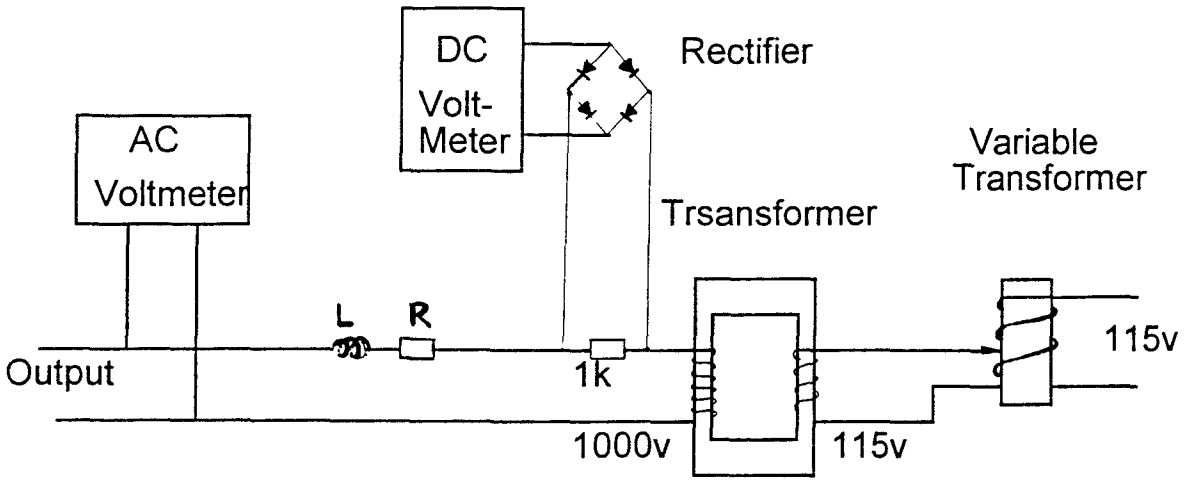

Figure B.6 Electric circuit of AC power supply

B.2.2 Polymer Deposition and Film Measurement

In this experiment, the plasma polymerization of MMA (Methyl Methacrylate) has been studied. In order to achieve higher polymer film deposition rate and high quality film, we adjusted some process parameters like system pressure, flow rate, discharge power and the distance between two electrodes.

a. Substrate Preparation

The corning 2947 micro-slices (7.5cm by 2.5cm by 0.1cm) were used as the substrate in our experiment. The contaminations on the specimen surface were removed by cleaning using ultrasonic cleaner: 5 min in Acetone;

5 min in Methanol;

10 min in deionized water, twice.

After the cleaning the samples were dried in oven of 120°C for 1 hour.

Prior to the plasma polymerization process, the cleaned glass substrates were weighed using analytical scale (0.1 mg accuracy).

b. Monomer Preparation

A small amount of methyl ether of hydroquinone (MEHQ) is added to methyl methacrylate monomer to prevent polymerization during shipment and storage. Inhibited monomer remains liquid and free of polymers for long periods at room temperature and still longer times under refrigeration. But the inhibitor has to be removed before polymerization. Inhibitor may be removed by passing it through a column packed with De-hibit 100 resin which is a macro-reticular resin which absorbs the MEHQ. Prior to use the resin it is pretreated by passing 4 column volumes of dilute NaCl (approximately 4% by weight) and then rinsed with deionized water followed by 2.5 bed volumes of methanol. The monomer is then passed through a column at a rate of 4 bed volumes/hr. Once the inhibitor is removed, the monomer must be used promptly or it may be stored in the dark for a few days at 4°C or bellow. Unless kept cold, unhibited monomers may polymerize spontaneously on standing. An air space should be maintained over the monomer at all times during storage to maintain stability since oxygen acts as inhibitor.

We used an aluminum foil to wrap the monomer container to prevent monomer color change.

c. Plasma Polymer Deposition

When substrate and monomer are ready we can start the plasma polymer deposition by following the procedure:

1. Use aluminum foil sheet to cover the lower electrode and put substrate on it. Close the door of vacuum chamber.
2. Use mechanical pump to pump the diffusion pump, glass chamber and the gas pipe. Use Vacuum pressure meter to monitor the vacuum condition.
3. When the vacuum better than 50 militorr, turn on the diffusion pump its cooling fan.
4. After 0.5-1 hr the vacuum can reach 2 * 10^{-5} Torr. Turn off the diffusion pump, close the main valve and put a little carrier gas Ar (or N2) inside (around 200 millitorr).
5. Close valve 1 and open bypass valve to certain degree.
6. Adjust needle valve for monomer and carrier gas, until the wanted vacuum pressure and flow ratio is obtained.
7. Put certain AC power into chamber and initiate the stable plasma discharge.
8. After finishing deposition, vent the chamber and take the sample out.
9. Use mechanical pump to pump the system again, then close all the vales, turn off mechanical pump and cooling fan, if diffusion pump is already cool.

d. Measurement

Weigh the specimen again to measure the weight increase. Calculate the average deposition rate. Examine the film quality and uniformity. If the film was deposited on silicon wafer, we can use Ellipsometry method to get the refractive index and the thickness distribution of polymer film.

We chose 1.19 g/cm^3 for the density of PMMA, 1.10 g/cm^3 for the density of polystrene [4.1].

B.3 EXPERIMENT RESULTS OF PLASMA POLYMERIZATION

B.3.1 Processing Factors

Polymer film formed by glow discharge is highly dependent on the system and the conditions under which the polymer is formed.

a. Carrier Gas

At beginning, we do the glow discharge polymerization of MMA without carrier gas. We find that it requires high AC voltage to initial the plasma glow. Also the electrical current is lower.

at system pressure P=220 millitorr; AC voltage V=600 v
the current I=5.3mA

After we put the carrier gas N_2, the intensity of plasma is getting stronger. It only need 250 v to initial the plasma.

at P= 220 millitorr; MMA : N_2=1 : 1; V=300v

the current can be 15mA

The deposition rate is increased 70%, from 0.17um/hr to 0.28um/hr.

The present of the inert gas can change the properties of the plasma as well as the structure of the film. We also compared different carrier gases, Ar with N_2. We found that Ar can create higher concentrations of free radicals and have stronger sputtering ability at high flow rate [B.5].

b. AC Deposition Power

When pressure and flow rate are held constant the deposition rate generally increase with power (power density) and becomes independent of power at high value. If we use the high power, the deposited film tends to become brittle and discolored. Normally, we chose power of 6W for MMA, 2 W for styrene. Styrene is more likely getting yellowish.

c. The Frequency of Power Supply

In our experiment we find the deposition rate of conductive substrate is much higher than the deposition rate of insulating substrate. Under same deposition condition:

system pressure=560mTorr;

flow of MMA=39 cc/min;

flow of N_2=13.5cc/min;

power=500v*8.5mA=4.25w

For 1 hour the thickness we got on micro-slice is 0.42 um. For only 15 min we can have a 2.2 um thick polymer film on aluminum foil. The rate is 20 times higher.

For frequencies below 1 kH_Z, The discharge is still basically of a dc-type and each electrode really acts as cathode and anode alternatively. The time during which the insulator charge up is much less than half the period of the AC supply, so most of the time the glow discharge will be off. The conventional mains frequency (60 H_Z) was found to be not effective for insulating substrate.

For our system the highest deposition rate of PMMA is 0.42 um/hr, the highest deposition rate of polystyrene is 0.55 um/hr. Also we can not deposit thick films by using AC power supply. The deposition rate is getting lower and lower. For three hours we only get PMMA films of 0.59 um (average thickness), polystyrene films of 0.82 um (average thickness).

d. Electrodes

Because of the charging of insulating film, we have to clean the electrodes after operation for several times. Otherwise, the plasma is getting weak, we have to increase the voltage to get enough power. We can use Aluminum foil to cover the electrodes and change it each time.

Before cleaning: P=250mTorr, V=720v; I=2mA

After cleaning: P=250mTorr, V=500v; I=4.5mA

During the deposition, the temperature of electrodes is increased, it will cause increasing of film ablation and reduce the deposition rate. The experimental data prove it. under same condition:

P=550mTorr, N_2:MMA=1.5:1, Power=5.5w

the deposition rate:
for continuous deposition--- 0.42 um/hr.
for deposition of every 5 min stop for 5 min---0.67 um/hr

e. Pressure

The deposition rate rises at first and tends to saturate at increased pressure (power and flow rate being held constant).

f. Flow Rate and Flow Ratio of Carrier Gas to Monomer

If we plot the deposition rate vs flow rate at a power and pressure held constant, at first we have a monotonic rise because the polymerization rate is limited by the supply of fresh monomer. At high flow rates the deposition rate decreases as the residence time of the monomer is lowered and even activated species may be prevented from reaching the substrate by being drawn away and pumped out. A maximum occurs where competing processes are balance.

Also, at first by increasing the flow ratio (carrier gas: monomer) we can get higher deposition rate. When the ratio is too high, the deposition rate will be lower.

Because at that time the monomer is insufficient and the sputtering effect is very strong.

When we put the plastic plate into the chamber for deposition. We found it lost weight after first one hour. Then started to glow up. But deposition rate is lower than that on glass.

B.3.2 Properties of Deposition Films

The films of plasma polymerized MMA and styrene are amorphous, pinhole-free, and highly cross-linked. they have superior thermal stability, high melting points, and low solubility.

Using ellipsometry method we get the refractive index of the film deposited on silicon wafer.

n=1.511 for glow discharge polymerized MMA

n=1.603 for glow discharge polymerized styrene

They are higher than the indices of conventional polymer films.

n=1.492 (n_D) for PMMA

n=1.591 (n_D) for polystyrene [4.1]

By inspecting the film, we can see interference color rings which show the uniformity of the deposition film. There are 6 red rings on the polystyrene film which

deposited for three hours. The difference of thickness between center and edge is about 0.9 um. By using ellipsometry we know that the film at edge of the glass is more thicker than the film at center of glass.

Deposition condition:

P=220 millitorr, A_r:styrene=1.6:1, Power=1.1W

Time= 2 hours, substrate----Silicon.

point	thickness
1	3317 A
2	4410 A
3	5692 A

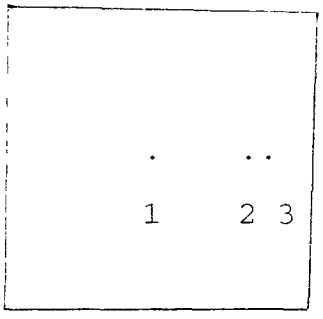

Figure B.7 The point picked up for thickness measurement.

I think, the reason is that the charge at the edge more likely leaked than the charge at the center.

Fig. B.8 shows the transmission of our films at different wavelength.

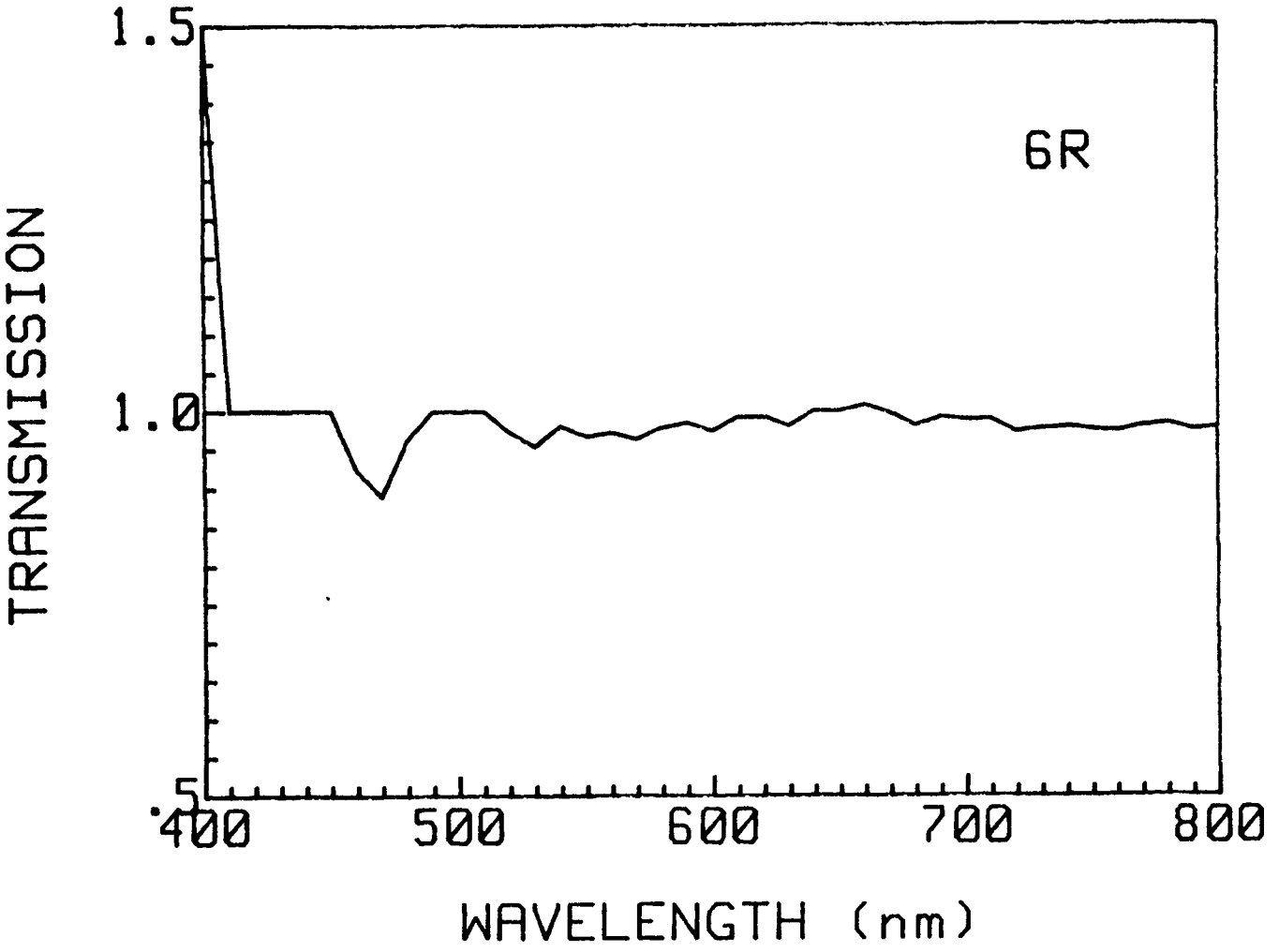

Figure B.8 The transmission of plasma polymerized styrene film (0.8 um thick) at different wavelength.

BIBLIOGRAPHY

1.1 Yeh, P. and A. Yariv "Bragg Reflection Waveguides." Opt. Commun. 19 (1976): 427.

1.2 Yeh, P., A. Yariv and C. S. Hong "Electromagnetic Propagation in Periodic Stratified Media. I. General/ Theory." J. Opt. Soc. Amer. 67 (1977): 423.

1.3 Cho, A. Y., A. Yariv and P. Yeh "Observation of Confined Propagation in Bragg Waveguides." Appl. Phys. Lett. 30 (1977): 471.

1.4 Dupuis, R. D. and P. D. Dapkus "Room Temperature Operation of Distributed Bragg Confinement GaAlAS Lasers Grown by MOCVD." Appl. Phys. Lett. 33 (1978) : 68.

1.5 Ash, E. A. "Grating Surface Wave Waveguides." presented at Int. Microwave Symp., Newport Beach, Calif., May 1970.

1.6 Fox, A. J. "The Grating Guide-A Component for Integrated Optics." Proceedings of the IEEE, May 1974: 644.

1.7 Yeh et al., "Electromagnetic Propagation in Periodic Stratified Media. I. General Teory." J. Opt. Soc. Am., Vol 67 (1977): 433

2.1 Yariv, A. and P. Yeh "Optical Waves in Crystals." John Wiley & Sons, Inc., (1984): 473.

2.2 Kressel, H., M. Ettenberg, J. Wittke, I. Ladan "Laser Diodes and LEDs for Fiber Optical Communications." in Semiconductor Devices, 2nd edition, ed. by H. Kressel, Topics Appl. Phys., Vol. 39 (Springer, Berlin, Heidelberg, New York 1982): 23-25.

2.3 Somekh, S., E. Garmire, A. Yariv, H. Garvin, R. G. Hunsperger "Channel Optical Waveguides and Directional Couplers in GaAs-Imbedded and Ridged." Appl. Opt. 13 (1974): 327.

2.4 Marcatilli, E. A. J. "Dielectric Rectangular Waveguide and Directional Courpler for Integrated Optics." Bell Syst. Tech. J. 48 (1969): 2071.

2.5 Furuta, H., H. Noda and A. Ihaya "Novel Optical Waveguide for Integrated Optics." Appl. Opt. 13 (1974) : 322

2.6 Delano, E. and R. J. Pejus "Progressive Optics", vol. 7, Amsterdam, Lodon: North Holland, 1969, ch2.

2.7 Tıen, P. K. and R. Urich "Theory of Prism-Film Coupler and Thin Film Light Guides." J. Opt. Soc. Amer. 60 (1970): 1325.

3.1 Hunsperger, R. G. "Integrated Optics: Theory and Technology." Second Edition, Springer-Verlag, Berlin, Heidelberg, New York, Tokyo, 1985.

3.2 Allmen, M. von "Laser-beam Interactions with Materials. " Springer-Verlag, Berlin, (1987): 202.

4.1 Kingslake, R. "Applied Optics and Optical Engıneering." Vol 1, Academic Press, New York and London 1965.

4.2 Grebel, H. and P.Chen "Atificial Dielectric Polymeric Waveguide: Metal Embedded Films." J. Opt. Soc. Am. A, Vol. 8 (1991): 615.

B.1 Bell, A. T. "Techniques and Applications of Plasma Chemistry." edited John R. Hollahan, John Wiley & Sons, Inc, New York, London, Sydney, Toronto, (1974): 193.

B.2 Tasuda, H. in "Thin Film Processes", ed. by John L. Vossen and Werner Kern, Academic Press, New York, San Francisco, London, (1978): 365.

B.3 Tasuda, H. and T. Hirotsu "Critical Evaluation of Conditions of Plasma Polymerization." J. Polym. Sci., Polym. Chem. Ed. 16 (1978): 743.

B.4 Morita, S. and S. Hattori "Application of Plasma Polymerization." Pure and Applied Chemistry 57, (1985): 1283.